ULTRA-STABLE OLIGONUCLEOTIDE–NANOPARTICLE CONJUGATES PREPARED BY SILICA REINFORCEMENT METHOD: PROPERTIES AND APPLICATIONS FOR COLORIMETRIC DNA DETECTION

WONG KWUN FUNG JACKY

Ph.D

THE HONG KONG POLYTECHNIC UNIVERSITY

2012

The Hong Kong Polytechnic University

Interdisciplinary Division of Biomedical Engineering

Ultra-Stable Oligonucleotide–Nanoparticle Conjugates Prepared by Silica Reinforcement Method: Properties and Applications for Colorimetric DNA Detection

WONG Kwun Fung Jacky

A thesis submitted in partial fulfillment of the requirements for the degree of Doctor of Philosophy

December 2011

Certificate of Originality

I hereby declare that this thesis is my own work and that, to the best of my knowledge and belief, it reproduces no material previously published or written, nor material that has been accepted for the award of any other degree or diploma, except where due acknowledgement has been made in the text.

_____ (Signed)

Mr. WONG Kwun Fung Jacky (Name of Student)

Abstract

Gold nanoparticles have been widely utilized for molecular diagnosis, drug delivery, and nanostructuring. In particular, colorimetric methods of deoxyribonucleic acid (DNA) detection using oligonucleotide–gold nanoparticle conjugates has received considerable attention for point-of-care and on-site testing. Typically, these conjugates are prepared by chemisorption of monothiol-modified oligonucleotides onto gold nanoparticles' surface. Despite their high stability against salt-induced aggregation, they have limited chemical and thermal stabilities, as well as enzymatic amplification reaction compatibility, which prohibit them from real applications. This thesis describes a new silica reinforcement method designed to address these issues by coating the conjugate with a thin silica layer using (3-mercaptopropyl)trimethoxysilane.

The silica-modified conjugate is simple-to-prepare and exhibits extremely high stability toward dithiothreitol (no noticeable aggregation after 24 h). In addition, the conjugate has high stability against gold core oxidative dissolution by sodium cyanide. These favorable chemical properties are attributed to the entrapment effect offered by the silica layer. Importantly, the silica layer is so thin that the unique sequence-specific hybridization-induced colorimetric detection of conjugate is

preserved. With these properties, a closed-tube colorimetric isothermal amplification reaction (nicking endonuclease-assisted amplification) platform based on the silica-modified conjugate is demonstrated. Aiming at higher sensitivity, the incorporation of silica-modified conjugate into polymerase chain reaction is highly desirable. Compared to the conventional unmodified conjugate, the silica-modified conjugate has significantly higher thermal stability as well as lower non-specific adsorption of Taq DNA polymerase. With these, a closed-tube colorimetric polymerase chain reaction is demonstrated for the first time, the sensitivity of which is comparable with the standard gel electrophoresis technique and avoids carryover contamination due to enzymatic reaction incompatibility of unmodified conjugate (requirement of post-amplification addition of unmodified conjugates for detection). Besides oligonucleotide–gold nanoparticle conjugate, this silica reinforcement method is successfully applied to oligonucleotide–silver nanoparticle conjugate. In fact, it is potentially broadly applicable to other biomolecule/polymer–nanoparticle conjugates. To conclude, this silica coating method not only enables simple, sensitive, and contamination-free DNA analysis for point-of-care and on-site applications, but also holds promise for new medical diagnostic and therapeutic applications.

List of Publications

Journal Articles

J. K. F. Wong, S. P. Yip, and T. M. H. Lee, "Silica-Modified Oligonucleotide–Gold Nanoparticle Conjugate Enables Closed-Tube Colorimetric Polymerase Chain Reaction", *Small*, Vol. 8, 2012, pp. 214–219.

J. K. F. Wong, S. P. Yip, and T. M. H. Lee, "Ultra-Stable Oligonucleotide–Gold and –Silver Nanoparticle Conjugates Prepared by a Facile Silica Reinforcement Method", manuscript submitted to Nano Research (Accepted).

Patent Application

United States provisional patent application for "Ultra-Stable Oligonucleotide–Gold and –Silver Nanoparticle Conjugates Prepared by a Facile Silica Reinforcement Method" filed on 20 July 2011 (Application Number: 61/510,056).

Acknowledgements

I would like to express my gratitude to my supervisor, Dr. Thomas Lee, for his patience, understanding, and encouragement throughout my study. It would not be possible to overcome the hurdles in developing this new coating technique within 5 years without the insightful suggestions from him.

I would like to thank my co-supervisor, Prof. S. P. Yip, for his patience, comment, and kind help in teaching me the concepts and techniques in molecular biology.

I would like to thank many people in the Department of Health Technology and Informatics, especially those in S106b. This work would not have proceeded so smoothly without their support and help.

Last but not least, I would like to thank my family for their unconditional love, support, and encouragement throughout my study.

Table of Contents

List of Figures

List of Abbreviations

AgNP	silver nanoparticle
APTES	(3-aminopropyl)triethoxysilane
APTMS	(3-aminopropyl)trimethoxysilane
ATP	adenosine triphosphate
AuNP	gold nanoparticle
Au–N	gold–amino
Au–S	gold–thiol
bp	base pair
dATP(αS)	2'-deoxyadenosine 5'-O-(l-thiotriphosphate)
dCTP	deoxycytidine triphosphate
dGTP	deoxyguanosine triphosphate
dNTPs	deoxyribonucleoside triphosphates
DNA	deoxyribonucleic acid
dsDNA	double-stranded DNA
DTT	dithiothreitol
FRET	fluorescence resonance energy transfer
GOD	glucose oxidase
HDA	helicase-dependent amplification
LAMP	loop-mediated isothermal amplification
MPTMS	(3-mercaptopropyl)trimethoxysilane
oligo–AgNP	oligonucleotide–silver nanoparticle
oligo–AuNP	oligonucleotide–gold nanoparticle

PBS	phosphate-buffered saline
PCR	polymerase chain reaction
PDGF	platelet-derived growth factor
PEG_6	hexaethylene glycol
RCA	rolling circle amplification
RNA	ribonucleic acid
SAM	self-assembled monolayer
SDA	strand displacement amplification
SNP	single nucleotide polymorphism
SPR	surface plasmon resonance
ssDNA	single-stranded DNA
TEM	transmission electron microscopy
TEOS	tetraethyl orthosilicate
TMOS	tetramethyl orthosilicate
TNT	2,4,6-trinitrotoluene
TTP	5-methyluridine triphosphate
UV–vis	UV–visible

Chapter 1

Introduction

Nanotechnology has received enormous interest thanks to the unique physicochemical properties of nanomaterials. Among the great variety of nanomaterials, gold nanoparticles (AuNPs) have been most extensively studied in biomedical and biology fields because of their well-controlled and simple synthesis as well as easy functionalization/attachment with different molecules (e.g., biomolecule and polymer) [1-3]. Another attractive feature of AuNPs for in vitro molecular diagnostics is the interparticle-distance-dependent color change property, which enables simple visual readout of the presence of a specific target analyte in a sample that is conducive to point-of-care and on-site testing [4-7]. Background information of AuNPs is presented in Section 1.1. Then, colorimetric detection techniques using AuNPs are introduced in Section 1.2. This is followed by colorimetric AuNP-based detection platforms with enzymatic amplification reactions in Section 1.3. Limitations of currently-used approaches are described in Section 1.4. Finally, the objectives of this thesis are stated in Section 1.5.

1.1. Gold Nanoparticles

Since ancient Rome, artisans have stained glass with yellow, red, and purple colors by dissolving different quantities of gold ores into molten glass, thereby forming AuNPs of different sizes. Alchemists prepared red-colored "drinkable" AuNP solution by dissolving gold in aqua regia and claimed to cure different kinds of diseases.

1.1.1. Synthesis Methods

In 1857, Faraday first reported a series of thin film experiments using AuNP solution produced by the reduction of chloroaurate with phosphorus in a two-phase system [8]. Nearly a century later, citrate reduction of chloroauric acid ($HAuCl_4$) in water was introduced by Turkevitch et al. in 1951 [9]. This technique utilized citrate ion ($C_6H_5O_7^{3-}$) as a reducing agent to convert chloroaurate ion ($AuCl_4^-$) into gold atom according to the following equation:

$$4HAuCl_4 + 4C_6H_5O_7Na_3 + 6H_2O \rightarrow 4Au + 4C_6H_8O_7 + 3O_2 + 12NaCl + 4HCl$$

The reaction started with vigorous boiling and stirring of $HAuCl_4$, followed by the addition of sodium citrate. The color of the resulting mixture changed from clear to pink within a minute, and became a wine red color after 5 minutes. The

synthesized AuNPs had a mean diameter of 20 nm.

Later on, Frens refined this method for synthesizing particles of different sizes by adjusting the ratio of trisodium citrate ($C_6H_5O_7Na_3$) and $HAuCl_4$ [10]. The synthesized AuNPs were spherical in shape with mean diameters of 16–150 nm. The color of the AuNPs changed gradually from red to purple with increasing particle size. Citrate-stabilized AuNPs have been the most popular method for preparing AuNPs as they could be easily functionalized/attached/conjugated with different molecules through ligand exchange of the citrate with higher affinity functional groups such as thiol and amino.

The two-phase reaction of Faraday also inspired Brust et al. to develop an alternative synthesis technique. They demonstrated the reduction of $AuCl_4^-$ in toluene by sodium borohydride ($NaBH_4$) in the presence of tetraoctylammonium bromide ($N(C_8H_{17})_4^+Br^-$) as a phase-transfer reagent [11]. AuNPs formed in the process were subsequently immobilized with dodecanethiol ($C_{12}H_{25}SH$) to improve nanoparticle stability. The color of the toluene layer changed from orange to deep brown several seconds after the addition of $NaBH_4$. This method produced both thermally and atmospherically stable AuNPs (1.5–5.2 nm in diameter) with narrow size distribution. The synthesized AuNPs could be isolated and redissolved in

organic solvents without decomposition and irreversible aggregation.

Seeding growth is another approach to obtain AuNPs with controllable size. AuNPs of several nanometers diameter synthesized by the typical citrate reduction were used as a seed solution. $HAuCl_4$ and reducing agent (e.g., ascorbic acid, hydroxylamine, or trisodium citrate) were added into the seed solution to form additional gold on the existing AuNPs, thereby enlarging the diameter [12-15]. AuNPs of desired size and shape could be produced by manipulating the amounts of reactants, temperature, synthesis time, and pH value.

1.1.2. Characteristic Properties

In AuNP synthesis, the formation of nanoparticles is indicated by the color of the reaction mixture. The color is attributed to AuNP's characteristic surface plasmon resonance (SPR) property [1]. AuNPs possess a strong absorption band in the visible light region, which is caused by the collective resonant oscillation of free electrons on AuNP surface. The absorption peak of the SPR band depends on the size of AuNPs. In other words, different sizes of AuNPs exhibit different colors (Figure 1.1). For instance, 13 nm AuNPs have an absorption peak at ~520 nm and appear red. The SPR peak shifts to longer wavelength as the particle size increases, with the color

gradually changing to purple for particles larger than 60 nm. On the other hand, the absorption band diminishes greatly for very small AuNPs and eventually disappears for 2 nm AuNPs, which appear colorless. In fact, particle shape, dispersion solvent, and temperature also affect the absorption peak position.

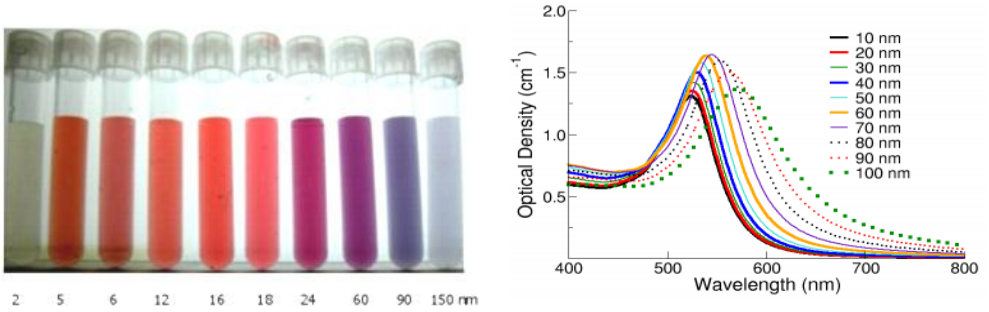

Figure 1.1. Colors (left) and absorption spectra (right) of AuNPs of different sizes (Adapted from [16] and [17]).

More importantly, AuNPs possess interparticle-distance-dependent optical property. When the distance between AuNPs is reduced to less than 2.5 times of their diameter, both red shifting and broadening of the absorption band occur [18]. Take 13 nm AuNPs as an example, they appear red when in monodispersed state. Upon the addition of 0.1 M sodium chloride (NaCl), rapid salt-induced particle aggregation occurs due to charge screening/shielding, and thus the solution color turns purple (Figure 1.2).

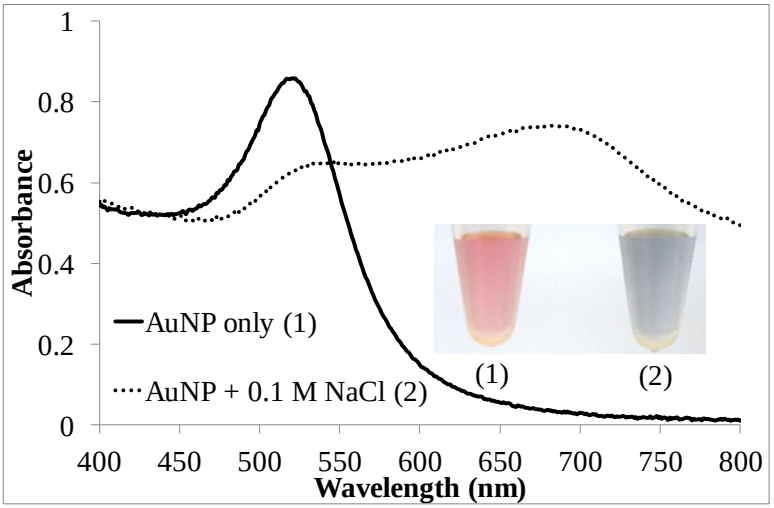

Figure 1.2. Interparticle-distance-dependent optical property of AuNPs.

The characteristic SPR absorption property of AuNPs was employed as an efficient quenching element in fluorescence measurement [19-22]. When an acceptor/quencher dye is brought very close to a fluorescent donor dye, and with the absorption spectrum of the quencher overlaps with the emission spectrum of the donor, fluorescence resonance energy transfer (FRET) occurs, i.e., emission energy from the donor is used to excite the acceptor or is absorbed by the quencher. The energy transfer efficiency is inversely proportional to the fourth power of the distance between donor and acceptor/quencher (up to ~20 nm). Compared to organic quenchers, AuNPs have much higher quenching efficiency.

Other than the physical properties mentioned above, similar to bulk gold,

AuNPs can be conjugated with thiol and amino ligands by chemisorption [23-24]. Gold–thiol (Au–S) linkage is more commonly utilized than gold–amino (Au–N) linkage as the former one has higher affinity. Therefore, thiolated compounds are frequently used as stabilizing and modifying agents to functionalize AuNPs. By immobilizing appropriately selected thiol-containing bifunctional molecules, AuNPs can be further conjugated with other molecules through covalent bonds to form functional hybrid materials.

1.1.3. Utilizations of Gold Nanoparticles

In chemistry, AuNPs are usually employed in catalytic reactions because of their inert nature, large surface-to-volume ratio, and multiple redox states [1]. In the biological field, AuNPs are mainly applied for immunolabeling of biomolecules and cells [25]. Proteins/antibodies are conjugated to AuNPs for locating target antigens so that direct observation of the target can be made with the aid of electron microscopy. The large surface-to-volume ratio and ease of surface functionalization/tailoring allow AuNPs to be used as the reporting component for recognition [2,4,26] and imaging [27-32], carrier for drug delivery [3,33-35], and building block for nanostructuring [5,36]. Most of these applications require

conjugation of a specific molecule onto the AuNP surface, such as oligonucleotide, peptide/antibody, and polymer. A vast majority of the applications utilize oligonucleotide–gold nanoparticle (oligo–AuNP) conjugates due to the programmable nature of deoxyribonucleic acid (DNA) that can perform various functions by simply altering the base sequences of the oligonucleotides.

1.2. Colorimetric Detection Using Gold Nanoparticles

When AuNPs are utilized as a reporting component in recognition platforms, it is preferable to take advantage of their colorimetric property for signal readout. As mentioned in Section 1.1.2, the SPR absorption band of AuNPs is strongly influenced by the interparticle-distance, and hence the solution color. This unique property enables the colorimetric detection of numerous analytes including nucleic acids [37-45], metal ions [44,46-61], small molecules [44,62-73], proteins [44,74-76], and cells [77] directly by the naked eye or a portable colorimeter. Without the utilization of sophisticated instrumentation, this approach is well suited for point-of-care and on-site applications. Crosslinking and non-crosslinking configurations are applied for the detection of different targets.

1.2.1. Crosslinking Aggregation

In this arrangement, oligo–AuNP conjugates are used to analyze the existence of target molecules. The oligonucleotides interact with the targets to effect assembly or disassembly of oligo–AuNP networks, resulting in an observable solution color change.

1.2.1.1. Assembly of Gold Nanoparticles

In the year 1996, Mirkin et al. reported a special phenomenon of oligonucleotide-assisted reversible assembling of oligo–AuNP conjugates [78]. Two sets of oligo–AuNP conjugates with two different oligonucleotides were used. Upon the addition of a linker double-stranded DNA (dsDNA) with overhangs that were complementary to the two AuNP-bound oligonucleotides, aggregation occurred and the solution color changed from red to purple. After several hours, pinkish-grey precipitates were formed. When the temperature was raised to 80 ℃, the precipitates dispersed again (Figure 1.3, left). The periodic assembly and disassembly of the conjugates could be achieved by oscillating the incubation temperature. After one year, the same group demonstrated single-stranded DNA (ssDNA) detection with a detection limit of 10 fmol (Figure 1.3, right) [37]. Interestingly, this crosslink

network had an extraordinarily sharp melting curve which could be used for single nucleotide polymorphism (SNP) analysis. Sequence with a single-base mismatch would have a significantly lower melting temperature than the perfectly complementary target sequence. Therefore, under appropriate temperature control, extremely high specificity could be achieved.

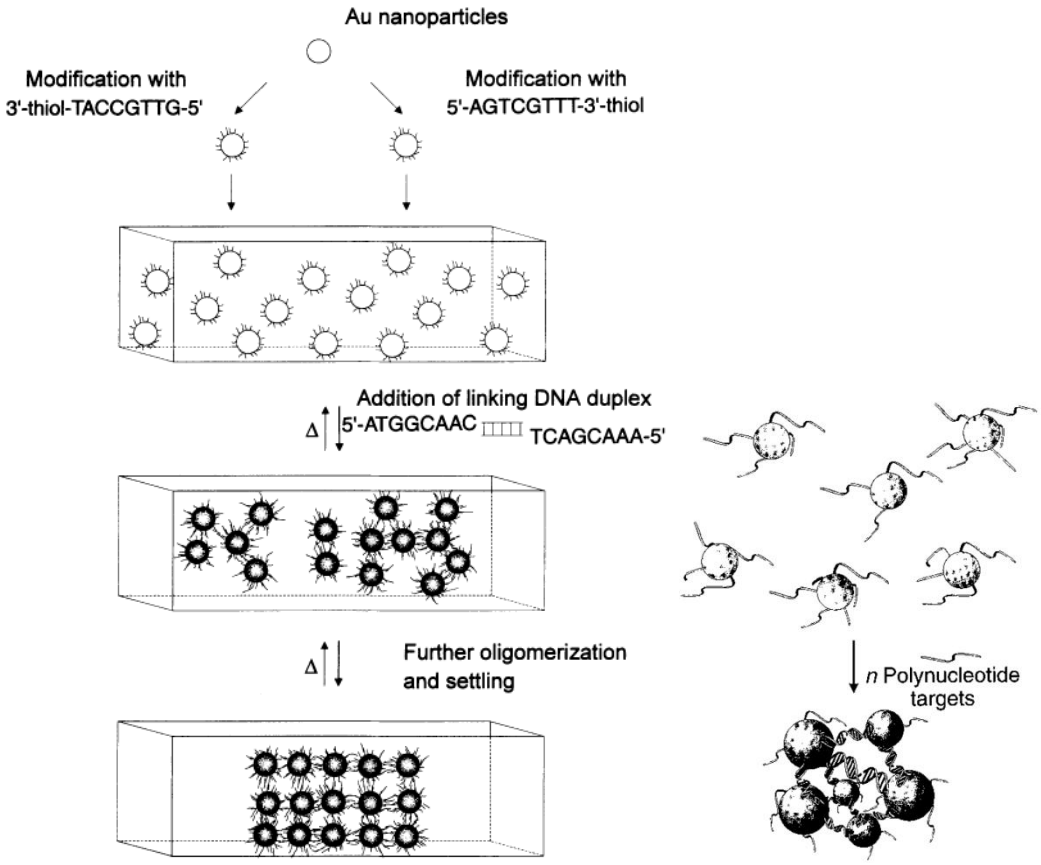

Figure 1.3. Assembly/detection method developed by Mirkin et al. using target of dsDNA with overhangs (left) and ssDNA (right) (Adapted from [37,78]).

Another method that involved crosslinking and connecting the hybridized oligonucleotides between two oligo–AuNP conjugates by ligation was described by Li et al. for SNP detection. [38]. A perfectly matched sequence maintained the crosslink network with purple color even when the temperature was raised above the melting temperature of the conjugates, while mismatch sequences changed from purple to red because ligation did not take place as a result of the mismatch and the conjugates dehybridized at elevated temperature (Figure 1.4).

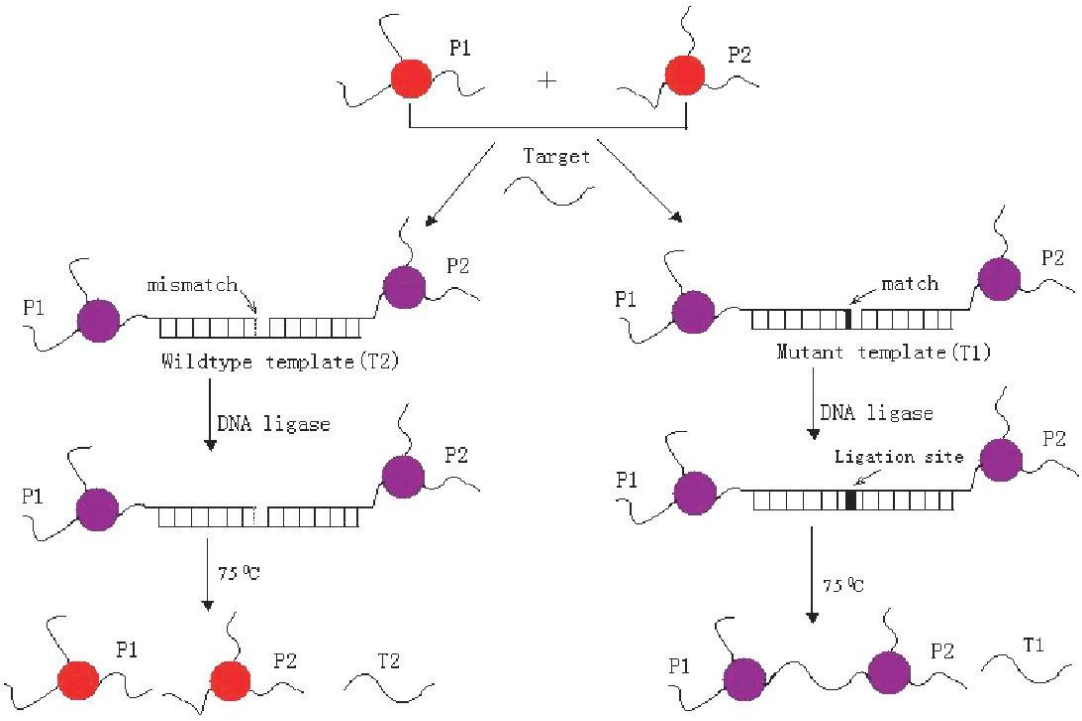

Figure 1.4. SNP discrimination method by target-assisted ligation of two oligo–AuNP conjugates (Adapted from [38]).

The crosslinking method was also applied for the detection of metal ions by using ion-induced DNA hybridization or aptamer [46-48]. Xue et al. introduced a mercury ion (Hg^{2+}) recognition technique with 3 μM sensitivity [46]. Two oligo–AuNP conjugates were partially complementary to a linker sequence and mismatched with thymidine–thymidine base pairing (Figure 1.5). The hybridization could not occur at room temperature unless Hg^{2+} was added to facilitate the thymidine–Hg^{2+}–thymidine interaction, resulting in a red-to-purple color change. A similar approach was reported by Li et al. for the detection of silver ion (Ag^{+}) with a detection limit of 12 nM by cytosine–Ag^{+}–cytosine-induced hybridization [47]. Other than ion-induced mismatch base pairing, recognition of potassium ion (K^{+}) was demonstrated by Zhu et al. with the use of aptamer and nicking endonuclease in 2011 [48]. An aptamer sequence specific to K^{+} and complementary linker sequence were used. Hybridization between the sequences could not occur in the presence of K^{+} because the aptamer had higher affinity to interact with K^{+}. Therefore, nicking endonuclease could not cleave the ssDNA linker, which was then capable of crosslinking two oligo–AuNP conjugates and produced a purple color. Whereas in the absence of K^{+}, the oligo–AuNP conjugates maintained a red color (Figure 1.6).

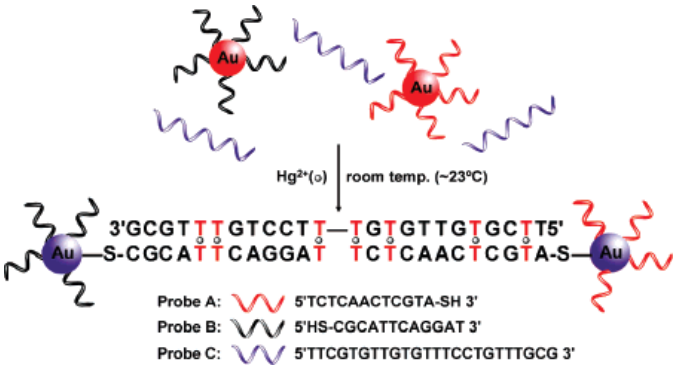

Figure 1.5. Hg^{2+} recognition by target-induced thymidine–thymidine hybridization of two oligo–AuNP conjugates (Adapted from [46]).

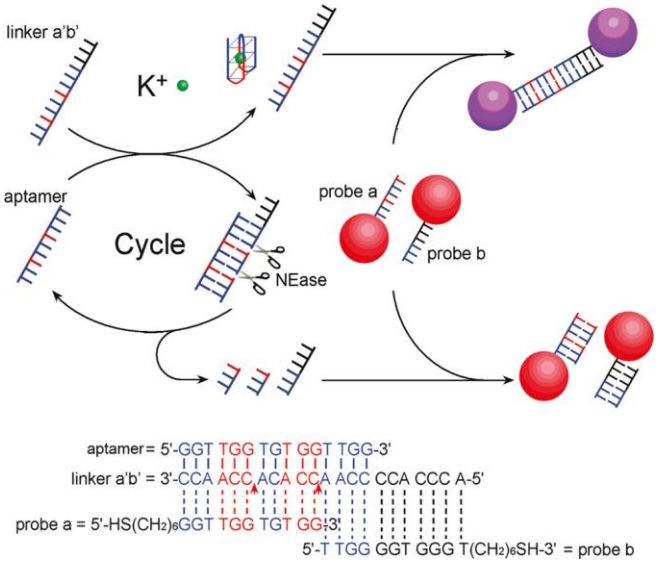

Figure 1.6. K^{+} detection by target-hampered endonuclease cleavage of ssDNA linker for crosslinking oligo–AuNP conjugates (Adapted from [48]).

Recognition of small molecules, proteins, and cells were achieved by using specific aptamer sequences. In 2009, Li et al. employed two oligo–AuNP conjugates

with partial aptamer sequences specific to adenosine [62]. The presence of adenosine brought the two partial aptamer sequences together and resulted in a crosslink network, thereby producing a color change from red to purple (Figure 1.7). The detection limit of this platform was 0.25 mM.

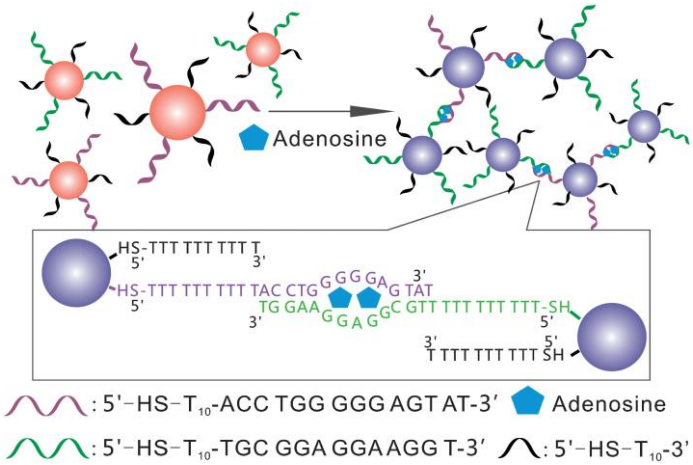

Figure 1.7. Adenosine detection by target-induced hybridization of two oligo–AuNP conjugates immobilized with partial aptamer sequences (Adapted from [62]).

Huang et al. reported a detection method for platelet-derived growth factor (PDGF) by utilizing oligo–AuNP conjugate with PDGF aptamer [74]. PDGF crosslinked the conjugates and resulted in a purple color (Figure 1.8). This method had a sensitivity range of 10–400 nM. It should be noted that too much target would hinder the crosslink formation due to saturated PDGF binding to the aptamer.

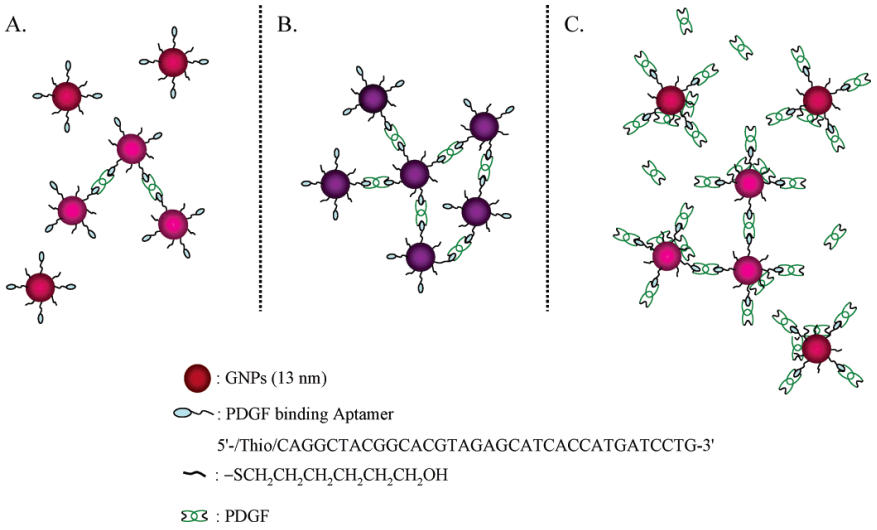

Figure 1.8. Aptamer immobilized oligo–AuNP conjugates for PDGF detection (Adapted from [74]).

Medley et al. demonstrated cancer cell detection by using oligo–AuNP conjugate with aptamer sequence specific to the protein/receptor of the cancer cell [77]. The target cell would have the conjugate accumulated on its surface and appeared purple while non-target cells were colorless (Figure 1.9).

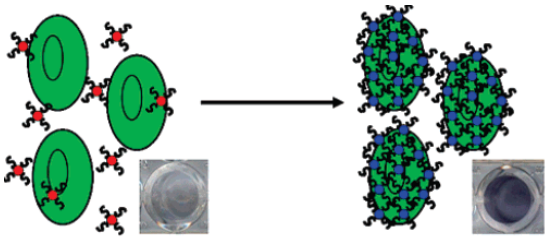

Figure 1.9. Aptamer immobilized oligo–AuNP conjugates for cancer cell recognition (Adapted from [77]).

Mirkin et al. introduced a technique to screen potential triplex DNA binders by using a sandwich system consisted of two oligo–AuNP conjugates with similar sequences and a complementary sequence to the two AuNP-bound sequences [79]. Crosslink network could not be formed as the complementary sequence would only hybridize to one AuNP-bound sequence unless facilitated by a triplex binder (Figure 1.10).

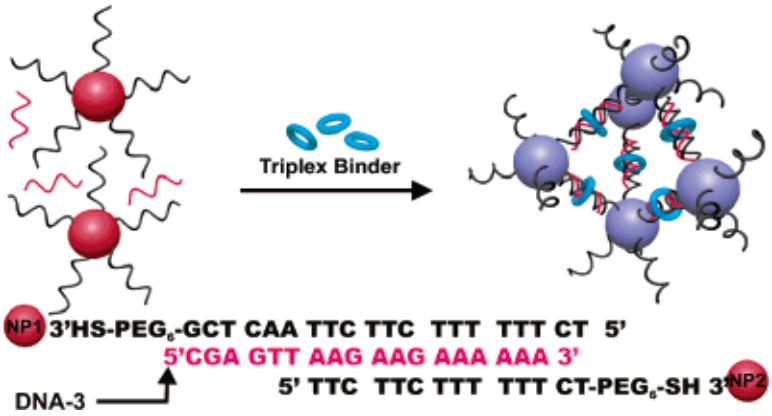

Figure 1.10. Triplex DNA binders screening method by analyte-assisted hybridization between two oligo–AuNP conjugates and a linker ssDNA (Adapted from [79]).

The controllable aggregation property offered by oligo–AuNP conjugates was utilized to construct colorimetric logic gate [80-81]. Bi et al. demonstrated the

settings of several logic gates by using a circular supramolecular DNA structure that consisted of lead ion (Pb^{2+}) and magnesium ion (Mg^{2+}) specific DNAzyme recognition sites [81]. The presence of Pb^{2+} and/or Mg^{2+} triggered the activities of the DNAzymes and the cleaved structure crosslinked an oligo–AuNP conjugate to give a colorimetric output (Figure 1.11).

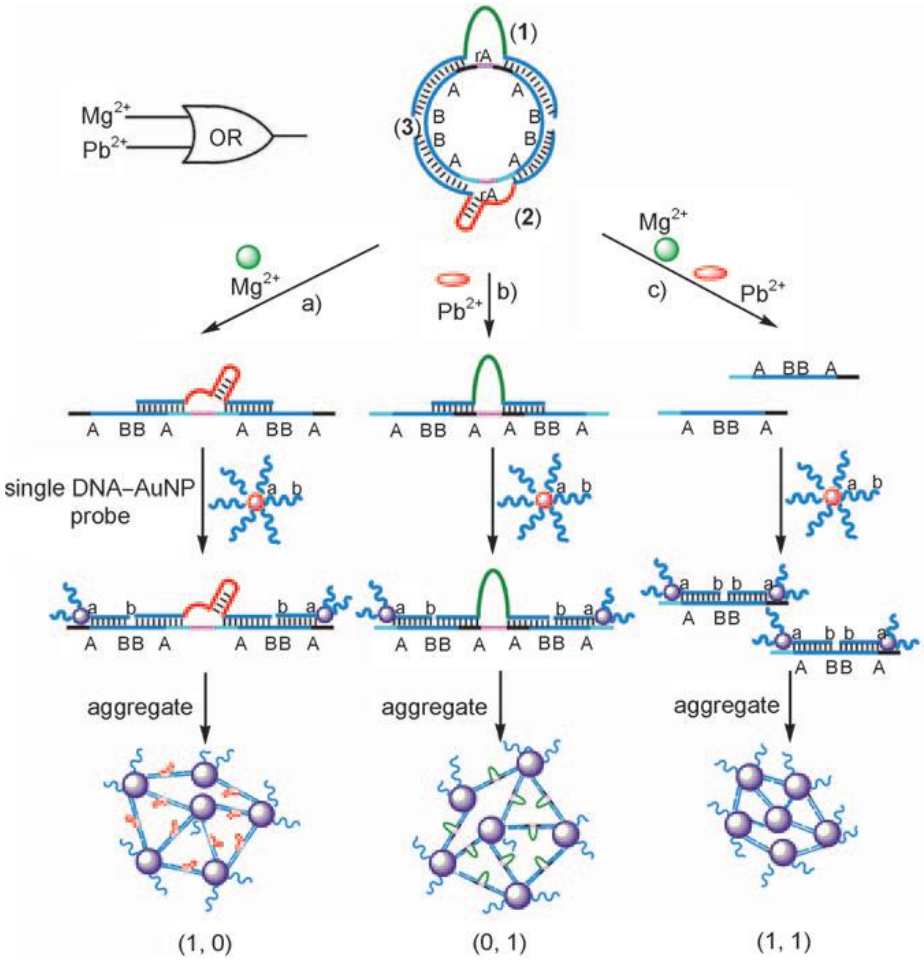

Figure 1.11. Molecular logic gate achieved by oligo–AuNP conjugate along with Mg^{2+} and Pb^{2+} specific DNAzymes (Adapted from [81]).

1.2.1.2. Disassembly of Gold Nanoparticles

In this setting, a crosslink network is constructed prior to detection. The presence of a target analyte would induce disassembly of the network with a concomitant color change from purple to red. Liu and Li incorporated Pb^{2+} specific DNAzyme sequence into a crosslinked network of oligo–AuNP conjugates. The activation of the DNAzyme's activity by Pb^{2+} caused the network to disassemble (Figure 1.12) [49]. The sensitivity of this detection scheme was 0.1 μM.

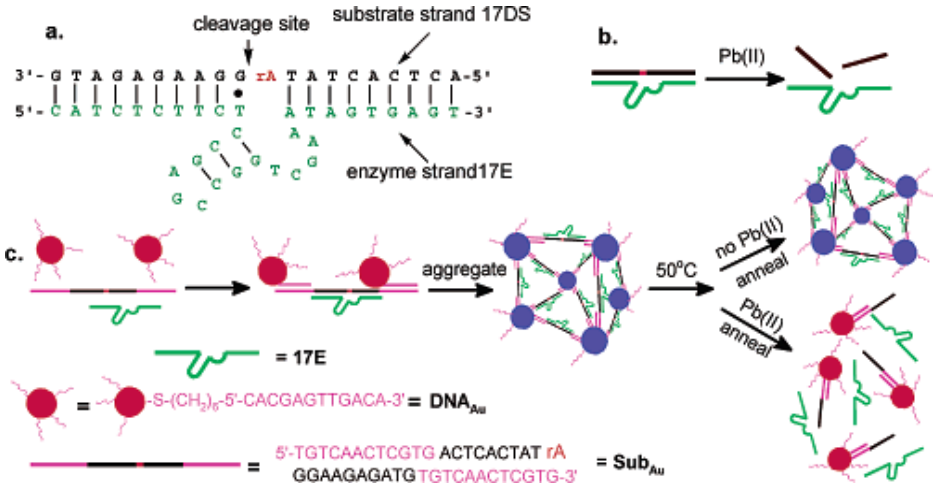

Figure 1.12. Pb^{2+} detection by DNAzyme-assisted disassembly of crosslinked network (Adapted from [49]).

Recognition of metal ions can be achieved by using components that interact specifically to the target ions [50-51]. Mirkin et al. illustrated a method to distinguish

copper ion (Cu^{2+}) with a detection limit of 20 μM by catalytic cyclization of alkyne and azide in the presence of Cu^{2+} [51]. Two oligo–AuNP conjugates were used, with one oligonucleotide having an alkyne group at the 5' end and another one having an azide group at the 3' end. A crosslinked network of the conjugates was formed when hybridized with a complementary linker sequence, which brought the alkyne and azide groups very close to each other. In the presence of Cu^{2+}, cyclization joined the two AuNP-bound sequences together. Therefore, the solution color remained purple even when the temperature was increased to dehybridize the linker sequence. On the other hand, samples without Cu^{2+} appeared red (Figure 1.13).

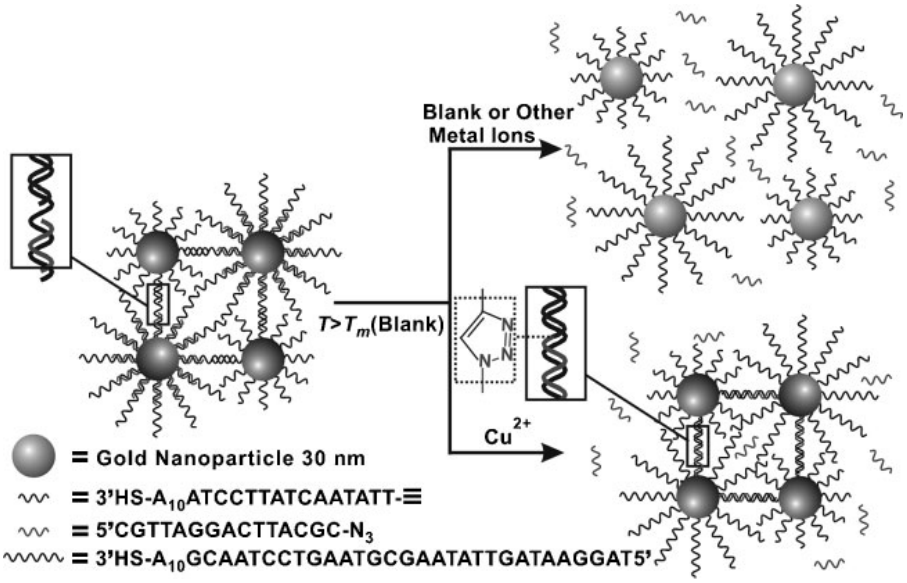

Figure 1.13. Cu^{2+} detection by catalytic cyclization of alkyne- and azide-functionalized oligo–AuNP conjugates (Adapted from [51]).

Similar to the assembly-based crosslink approach, the disassembly of crosslinked structure could be used to recognize small molecules and proteins by utilizing linkers with aptamer sequences [63,75]. Liu and Li reported an adenosine sensor and a cocaine sensor that utilized crosslinked network with aptamer-containing linkers having detection limits of 0.3 mM and 50 μM, respectively [63]. When the target existed, the aptamer sequence interacted with the target and caused dehybridization of the linker with one of the two oligo–AuNP conjugates. Therefore, the solution color changed from purple to red (Figure 1.14).

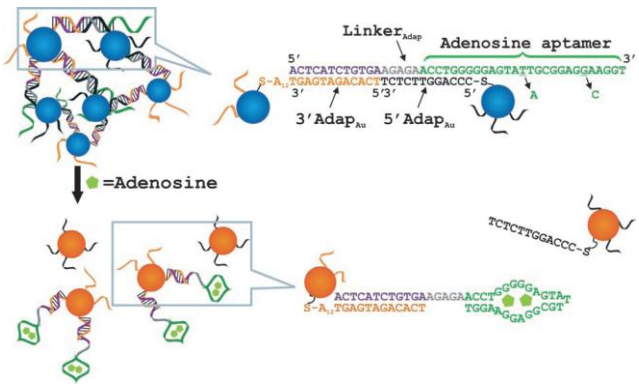

Figure 1.14. Aptamer-based adenosine detection by target-induced disassembly of crosslinked network (Adapted from [63]).

The disassembly arrangement can be applied as a platform for screening of DNA-binding agents and endonuclease inhibitors, as well as for monitoring enzyme

activity [82-85]. In 2006, Mirkin et al. reported a DNA-binding molecules screening system by using crosslinked structure [82]. When DNA-binding molecules were added to the crosslinked structure, they bound to the hybridized portion of the oligo–AuNP conjugates. The crosslinked structure with a strong DNA-binding molecule had a higher melting temperature than a weak DNA-binding molecule. Analysis was performed by increasing the temperature that the weak DNA-binding molecule changed from purple to red at a higher temperature than the strong DNA-binding molecule (Figure 1.15).

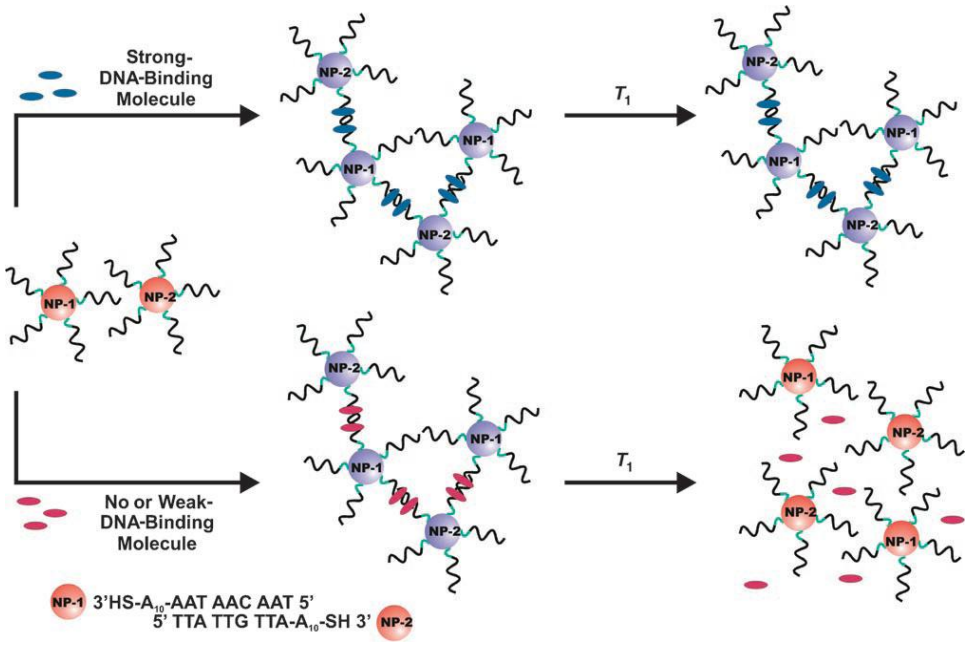

Figure 1.15. Screening of DNA-binding molecules based on melting temperature of crosslinked network (Adapted from [82]).

1.2.2. Non-Crosslinking Aggregation

Salt-induced aggregation property of AuNPs plays an important role in this arrangement. AuNPs are monodispersed due to charge repulsion of the same charge on nanoparticles' surfaces. The charge can be shielded by adding certain amount of opposite charge. This reduces the repulsion between AuNPs and causes aggregation. The SPR absorption band is red-shifted and the solution color changes from red to purple. This salt-induced aggregation is strongly dependent on the amount of surface charge or surface modification such as oligonucleotide and protein.

1.2.2.1. Oligonucleotide-Modified Detection

Oligo–AuNP conjugates were used to recognize nucleic acids and analyze SNP with a non-crosslink approach [39-41]. In 2003, Maeda et al. first demonstrated a DNA detection system by utilizing a single type of oligo–AuNP conjugate [39]. The oligo–AuNP conjugate remained monodispersed and appeared red in 0.5 M NaCl, while it aggregated and became purple in the same solution with perfectly matched complementary sequence (Figure 1.16). This method featured short recognition time (3 min or less) and high specificity (single-base mismatch identification). However, this method suffered from low sensitivity (200 nM), which was ~100 times higher

than the concentration required for the crosslink detection system [37].

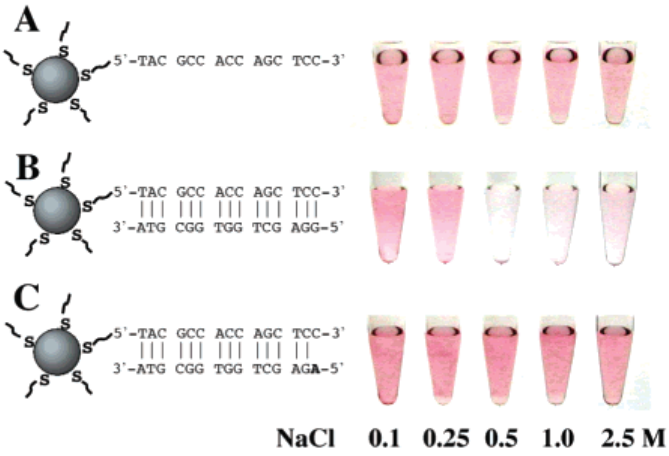

Figure 1.16. DNA detection by non-crosslinked hybridization between oligo–AuNP conjugate and ssDNA target (Adapted from [39]).

Alternative ways were developed for target recognition by manipulating the total charge on oligo–AuNP conjugate or the conformation of the AuNP-bound sequence [52,64-66,86]. Zhao et al. demonstrated a detection platform for sensing adenosine with a detection limit of 10 μM by using an oligo–AuNP conjugate that was hybridized with a long aptamer-containing sequence [64]. The additional negative charge provided by the long sequence stabilized the hybridized oligo–AuNP conjugate and displayed red color with 35 mM magnesium chloride ($MgCl_2$) and 0.3 M NaCl. After the addition of adenosine, dehybridization of the long sequence

occurred due to the binding between the aptamer and adenosine. The unhybridized oligo–AuNP conjugate alone did not have enough charge against salt-induced aggregation and the solution color turned purple within one minute (Figure 1.17).

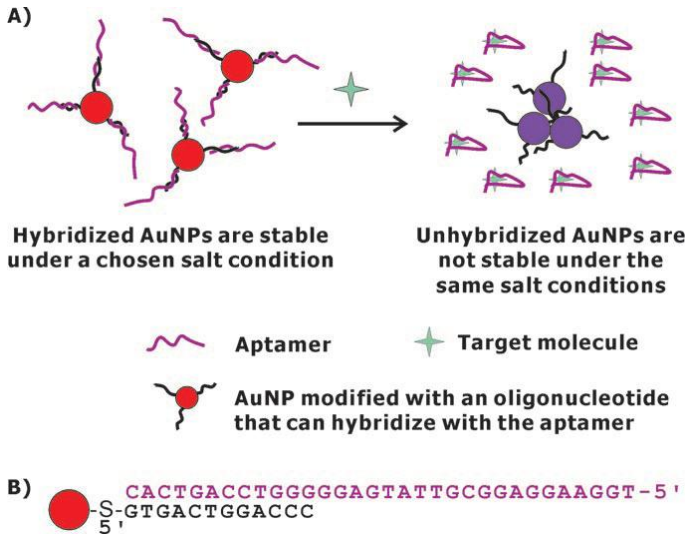

Figure 1.17. Adenosine detection by target-induced charge removal from hybridized oligo–AuNP conjugate with overhanging ssDNA (Adapted from [64]).

The same group also illustrated a method to detect Pb^{2+} and activity of DNase I [52]. Each of the sensing platforms consisted of an oligo–AuNP conjugate hybridized with an oligonucleotide sequence in order to provide a cleavage site. The number of nucleotides on AuNPs, and thus the amount of charge, was reduced by the cleavage action of the target. This caused salt-induced aggregation with the solution

color changing from red to purple (Figure 1.18). The same concept could be applied for screening DNase I inhibitor by using a fixed concentration of DNase I and incubating with different potential inhibitors. A stronger inhibitor would have a slower color change.

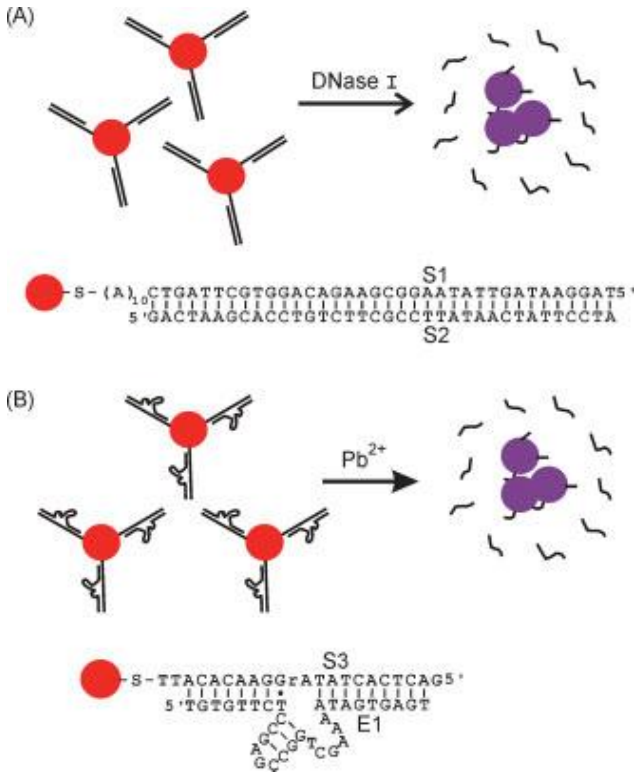

Figure 1.18. DNase I inhibitor screening method and Pb^{2+} detection method by analyte-induced cleavage of hybridized oligo–AuNP conjugate (Adapted from [52]).

Rigid structures formed by the aptamer–target complexes were demonstrated to prevent salt-induced aggregation of oligo–AuNP conjugates [65-66,86]. Chen et al.

reported a scheme to detect adenosine triphosphate (ATP) with sensitivity detection limit of 10 nM [66]. Oligo–AuNP conjugate aggregated under high salt environment and changed to purple color. When ATP interacted with the aptamer, a rigid structure was formed, which served as steric barrier to prevent salt-induced aggregation and the solution color remained red (Figure 1.19).

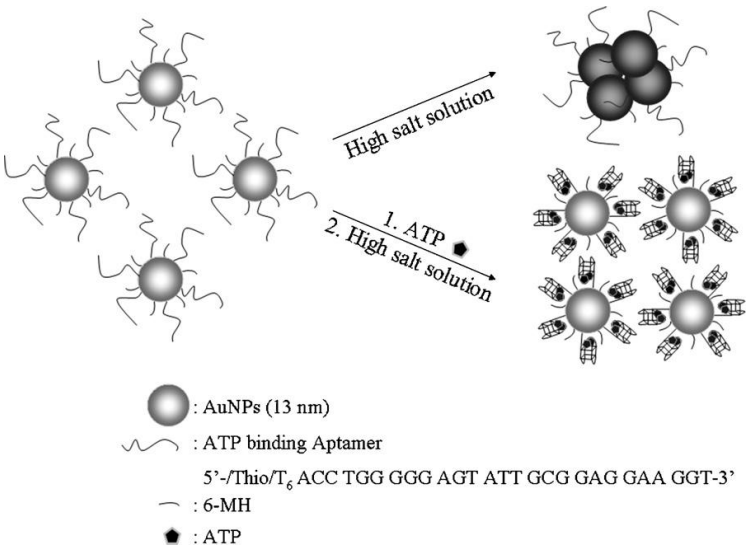

Figure 1.19. ATP detection by target-induced conformation change of aptamer immobilized on oligo–AuNP conjugate (Adapted from [66]).

1.2.2.2. Molecule-Modified Detection

AuNPs modified with a monolayer of molecules were used to detect various ions and small molecules [53-54,67]. Kim et al. demonstrated AuNPs with a

monolayer of 11-mercaptoundecanoic acid could interact with divalent metal ions by an ion-templated chelation process [53]. This resulted in particle aggregation and the solution color changed from red to purple. It should be pointed out that the process was reversible by adding strong metal ion chelator. Jiang et al. reported the use of cysteamine-functionalized AuNPs to recognize 2,4,6-trinitrotoluene (TNT) with a detection limit of 0.5 pM [67]. The thiol group of cysteamine was immobilized to the AuNP surface, while the amino group interacted with TNT by donor–acceptor property. Therefore, the modified AuNPs were aggregated in the presence of TNT and the solution color changed from red to purple (Figure 1.20).

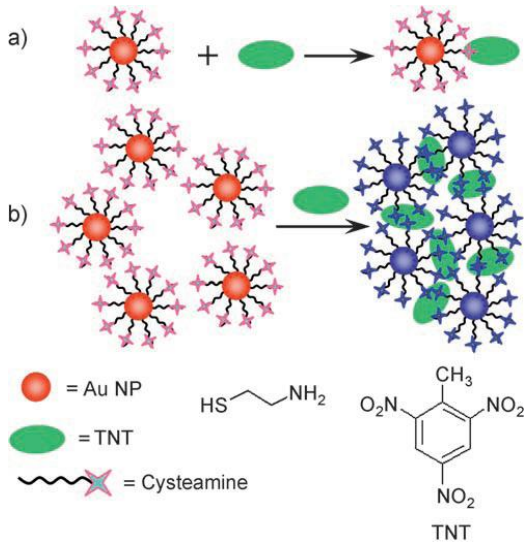

Figure 1.20. Cysteamine-modified AuNP for TNT detection by target–ligand interaction (Adapted from [67]).

Other than chelation and donor–acceptor interaction, the recognition can be achieved by target-induced chemical reaction [68-69]. Mirkin et al. illustrated the detection of nitrite and nitrate by 5-[1,2]dithiolan-3-yl-pentanoic acid [2-(4-amino-phenyl)ethyl]amide and 5-[1,2]dithiolan-3-yl-pentanoic acid [2-(naphthalene-1-yl-amino)ethyl]amide modified AuNPs with (11-mercapto-undecyl)-trimethyl-ammonium co-functionalization to increase the solubility in water [68]. The aniline and naphthalene groups of the two AuNPs were covalently jointed by nitrite or nitrate ion through the formation of an azo linker. The solution color changed from red to colorless (due to rapid precipitation of the aggregates) with sensitivity detection limit of 21.7 μM (Figure 1.21).

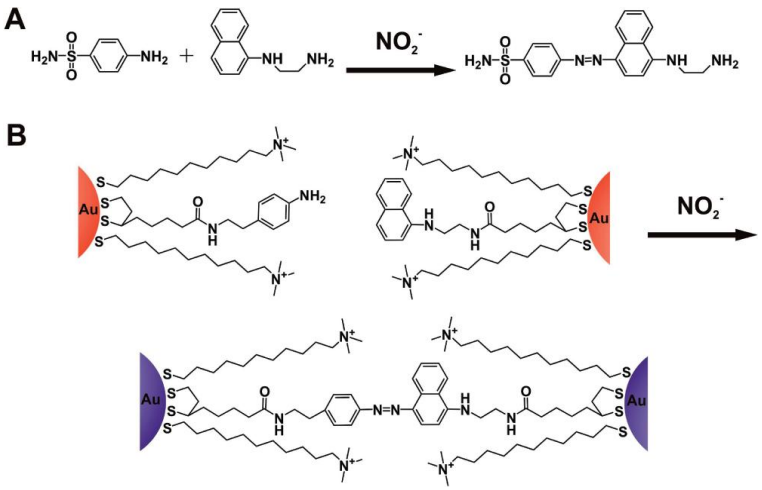

Figure 1.21. Two ligand-modified AuNPs for nitrite and nitrate detection by target-induced crosslinking of the AuNPs (Adapted from [68]).

Colorimetric sensing using molecule modified AuNPs can be triggered by displacement of the AuNPs' surface stabilizer [55-56,70-71,87]. Lin et al. reported using Tween 20-stabilized AuNPs to detect Ag^{+} and Hg^{2+} with 0.1 and 0.1 μM detection limits, respectively [55]. The citrate-stabilized AuNPs were coated with Tween 20 as an additional stabilizer in order to keep them monodispersed at high salt concentration. Citrate ion could reduce Hg^{2+} and Ag^{+} into mercury and silver metals that were deposited on the AuNP surface. The deposition caused the removal of Tween 20 from the AuNP surface, thereby triggering salt-induced particle aggregation (Figure 1.22).

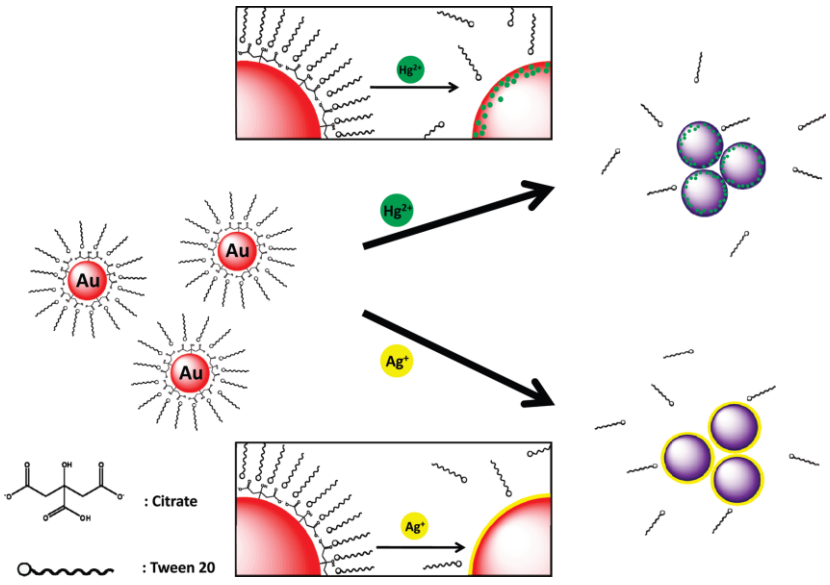

Figure 1.22. Hg^{2+} and Ag^{+} detection by target-induced dissociation of stabilizer from AuNP surface (Adapted from [55]).

Jung et al. demonstrated a high-throughput screening method for palladium-catalyzed coupling reactions of aryl iodides [87]. ATP-stabilized AuNPs were stable toward high salt concentration, but aggregated when exposed to iodide ion (I^-). I^- was released from the palladium-catalyzed coupling reaction of aryl iodide, which in turn destabilized the AuNP colorimetric probe (Figure 1.23).

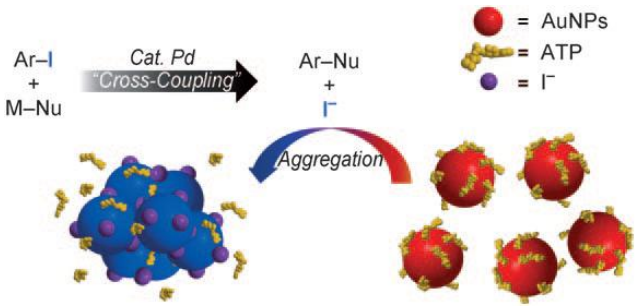

Figure 1.23. Screening method for palladium-catalyzed coupling reaction of aryl iodide by reaction product-induced AuNP aggregation (Adapted from [87]).

1.2.2.3. Unmodified Detection

Bare AuNPs, or more precisely citrate-stabilized AuNPs, can also be used for the detection of various analytes. Li and Rothberg demonstrated a DNA detection method with a detection limit of 4.3 nM by utilizing different binding affinities of ssDNA and dsDNA toward AuNPs [42]. Amino groups of nucleobases could be

absorbed onto the AuNP surface by Au–N linkage, which allowed binding of ssDNA onto AuNPs. The negative charge of the sugar-phosphate backbone of ssDNA stabilized the particles against salt-induced aggregation. In contrast, the nucleotide bases of dsDNA were not accessible due to base pairing, and thus did not bind to AuNPs. Detection of specific ssDNA target sequence could be achieved by adding a complementary ssDNA probe, followed by the addition of AuNPs and salt. Purple color was observed for the probe–target hybrid whereas red color was observed for the unhybridized probe (Figure 1.24). The same group also used the same method to recognize ribonucleic acid (RNA) without major modification [43].

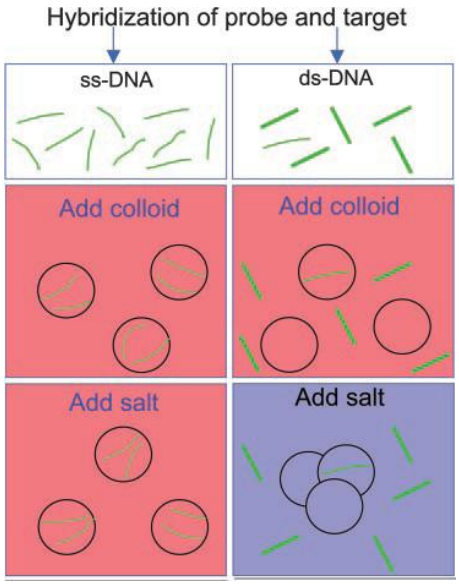

Figure 1.24. DNA detection based on preferential binding of ssDNA than dsDNA onto AuNP, followed by salt-induced aggregation (Adapted from [42]).

Jiang et al. illustrated a technique to examine glucose concentration in rat brain by employing the enhanced salt-tolerant property of AuNPs with adsorbed ssDNA [72]. Glucose oxidase (GOD), iron(II) ion (Fe^{2+}), and ssDNA were added to a glucose sample. GOD would convert glucose into hydrogen peroxide (H_2O_2). Then, H_2O_2 and Fe^{2+} would undergo the Fenton reaction to generate hydroxyl radicals that cleaved the ssDNA. Unlike intact ssDNA, the cleaved ssDNA could not stabilize AuNPs against salt-induced aggregation. Therefore, different colors were observed for different glucose concentrations (Figure 1.25).

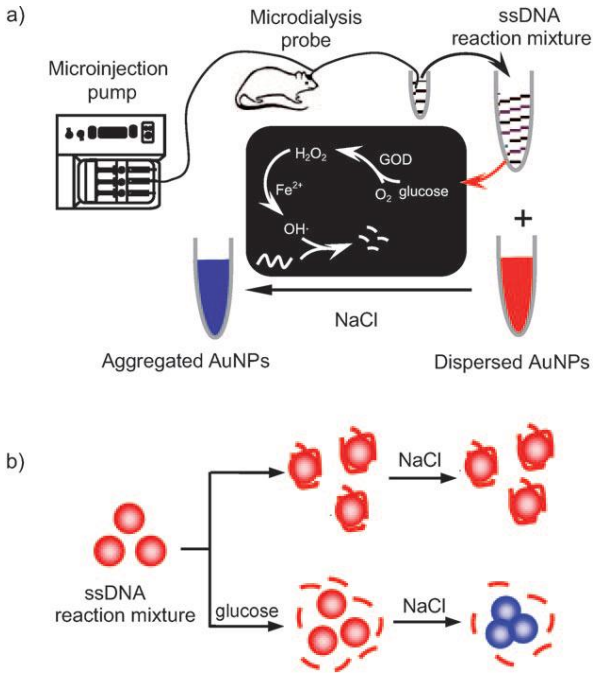

Figure 1.25. Salt-induced AuNP aggregation controlled by glucose-induced cleavage of ssDNA (Adapted from [72]).

Wang et al. reported a Pb^{2+} recognition method with a detection limit of 3 nM using a double-stranded DNAzyme sequence [57]. The presence of Pb^{2+} activated the DNAzyme to cleave the substrate strand. This in turn released a short ssDNA that stabilized AuNPs against salt-induced aggregation (Figure 1.26).

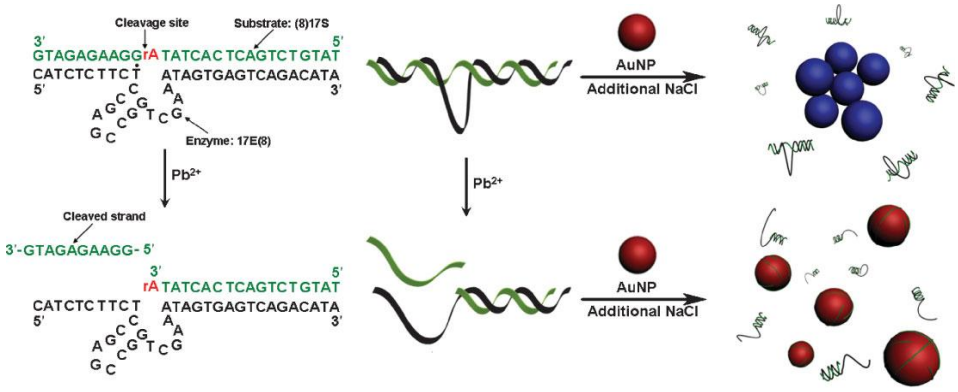

Figure 1.26. Salt-induced AuNP aggregation controlled by Pb^{2+}-induced cleavage of DNA substrate (Adapted from [57]).

The conformation of ssDNA can also influence the binding affinity toward AuNPs [58,73]. Wang et al. reported an aptamer-based detection method for K^+ with a detection limit of 1 mM [58]. The aptamer adopted a rigid G-quartet structure when bound with K^+, which significantly lowered the affinity of single-stranded aptamer toward AuNP surface, and thus the solution color changed from red to purple upon the addition of salt (Figure 1.27).

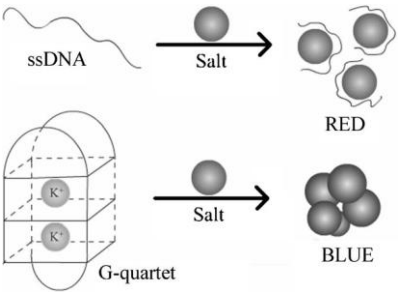

Figure 1.27. Salt-induced AuNP aggregation controlled by target–aptamer interaction for K^+ detection (Adapted from [58]).

Xia et al. demonstrated a general detection approach for different targets by utilizing bare AuNPs, single-stranded functional DNA molecules (i.e., ssDNA for DNA detection and aptamer for ions, small molecules, and protein detection), and positively charged conjugated polyelectrolyte [44]. In the absence of the targets, these single-stranded functional DNA molecules were adsorbed onto the AuNPs surface. Subsequently, the addition of the positively charged conjugated polyelectrolyte sequestered the single-stranded functional DNA molecules from the AuNP surface, leading to particle aggregation. For DNA detection, the hybridization of a complementary target resulted in dsDNA that could stabilize AuNPs under low salt concentration. Importantly, the positively charged conjugated polyelectrolyte could not efficiently sequester dsDNA, so the solution color remained red (Figure 1.28). The same happened for the aptamer–target complex.

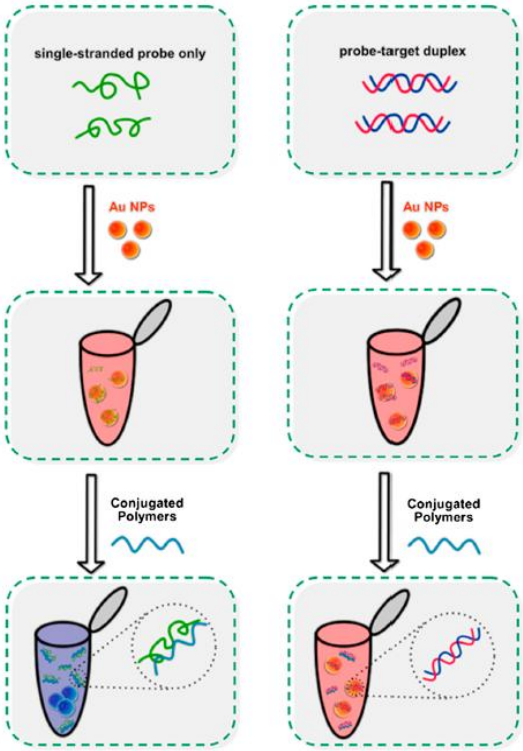

Figure 1.28. Conjugated polymer-induced aggregation for ssDNA-bound AuNP but not dsDNA-bound AuNP (Adapted from [44]).

Jiang et al. reported a screening method for β-lactamase (Bla) inhibitor [88]. A 2-(4-mercaptophenyl) acetic acid coupled 1,2-bis(2-aminoethoxy) ethane linker was connected to the 3'-position of cephalosporin. Bla would cleave this linker to release a fragment containing thiol and positively charged amino end groups. This fragment bound to AuNP via Au–S linkage and the amino group interacted electrostatically with the negatively charged citrate ions on AuNP surface, resulting in aggregation and color change from red to purple (Figure 1.29).

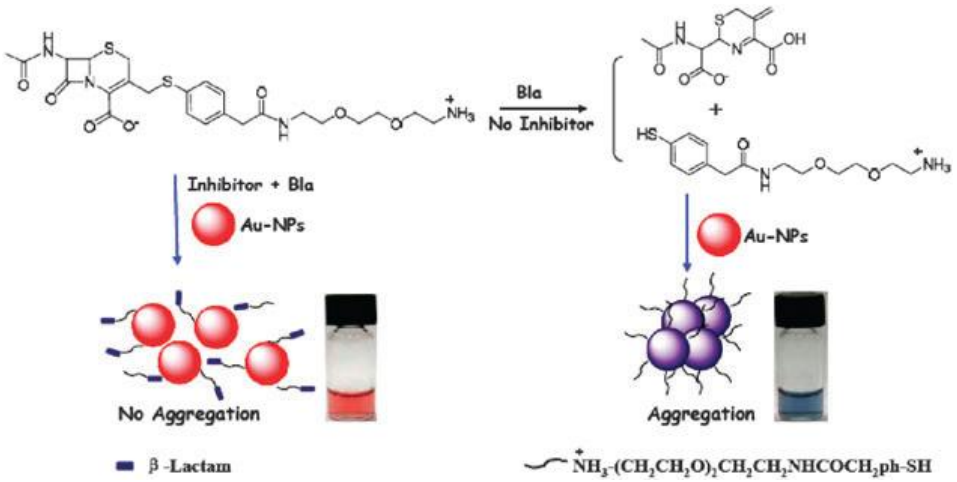

Figure 1.29. Screening method for Bla inhibitor by Bla-induced cleavage of a linker for AuNP aggregation (Adapted from [88]).

1.3. Gold Nanoparticle-Based Colorimetric Enzyme Assisted Amplification

For the colorimetric nucleic acid recognition schemes with AuNPs presented above (Section 1.2), the low sensitivity (nanomolar detection limit) and short synthetic target (i.e., oligonucleotide target) used are not conducive to real applications. To address this issue, efforts have been made to apply these schemes for the detection of different enzymatic amplification reaction products.

A standard method for nucleic acid amplification is the polymerase chain reaction (PCR). Sensitive and specific methods of product detection are highly desired (details of PCR technique are presented in Section 4.1). Li and Rothberg

demonstrated a DNA detection system for indentifying PCR product and performing SNP analysis [89]. PCR product was mixed with a detection probe, followed by heating (dehybridization of the PCR product) and incubating the mixture below the melting temperature of the probe (formation of probe–target hybrid). After that, AuNPs were introduced to the mixture. The hybridized probe could not bind to the AuNPs and caused the mixture color changed from red to purple after the addition of salt (Figure 1.30). SNP analysis was possible by controlling the hybridization temperature. At the melting temperature of the probe, perfectly matched PCR product appeared purple while mismatched ones appeared red as the unhybridized probe bound to the AuNPs and stabilized against salt-induced aggregation.

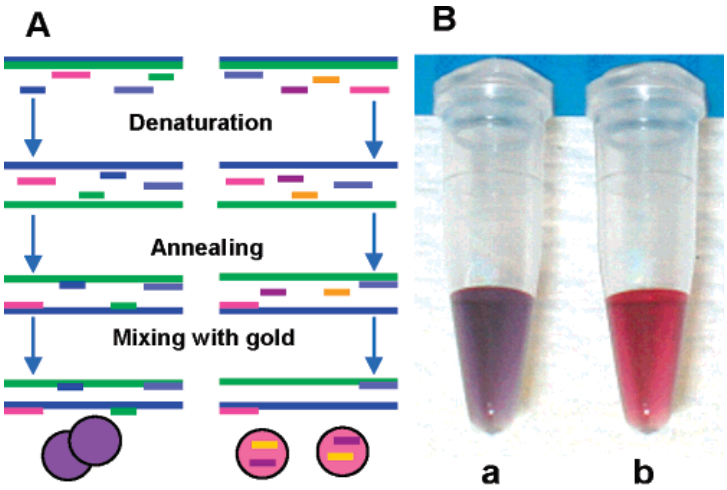

Figure 1.30. AuNP aggregation controlled by hybridization state between DNA probes and PCR product for DNA detection (Adapted from [89]).

Maeda et al. utilized the non-crosslink platform they developed (Section 1.2.2.1) to detect SNP of PCR product by a single-base extension [90]. An oligo–AuNP conjugate was allowed to hybridize with the extended sequence. Aggregation occurred and the solution color turned purple only when the extended sequence was perfectly complementary to the AuNP-bound sequence (Figure 1.31).

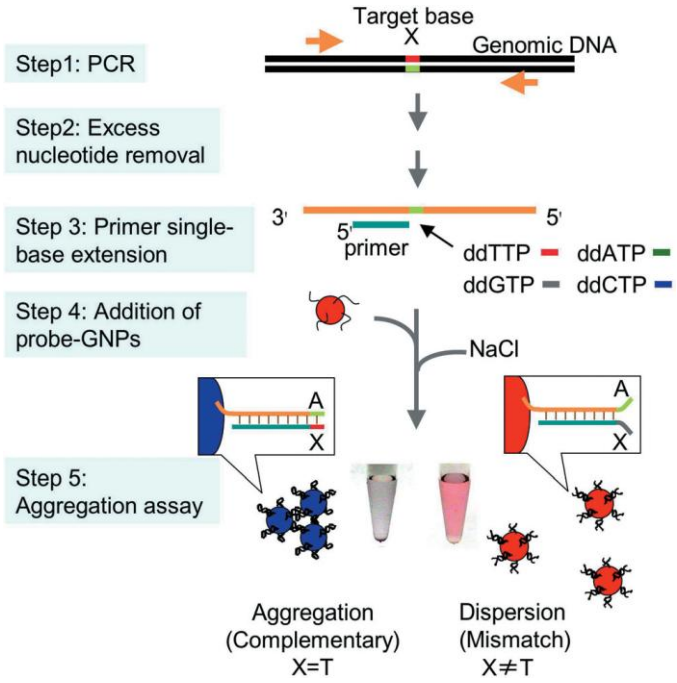

Figure 1.31. Oligo–AuNP conjugate aggregation controlled by single-base extension product for SNP analysis (Adapted from [90]).

Jyoti et al. reported using a crosslink method to detect a 149 base pair (bp) PCR product with a detection limit of 10^6 copies [91]. The PCR product was mixed with

two oligo–AuNP conjugates, followed by dehybridization of the PCR product and annealing at 37 °C. The conjugates hybridized to both ends of the PCR product, forming a crosslinked structure and hence the solution color changed from red to purple (Figure 1.32).

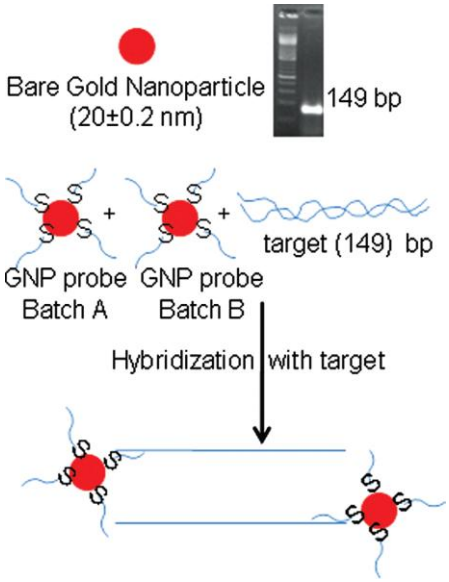

Figure 1.32. Crosslinking of two oligo–AuNP conjugates controlled by hybridization of the conjugates and PCR product for DNA detection (Adapted from [91]).

Jung et al. illustrated a detection method for PCR product with bare AuNPs and without additional detection sequence [92]. A primer with thiol modification at 5' end was used to amplify a specific target sequence. After PCR, AuNPs were added

and the thiolated amplicon/unused thiol-labeled primer was chemisorbed onto the AuNPs. The amplicon provided enough charge to stabilize the AuNPs against salt-induced aggregation and the solution color appeared red, while the primer alone (no target sequence) turned purple (Figure 1.33). The sensitivity of the platform could be adjusted by changing the incubation time and salt concentration. A detection limit of 100 copies was achieved.

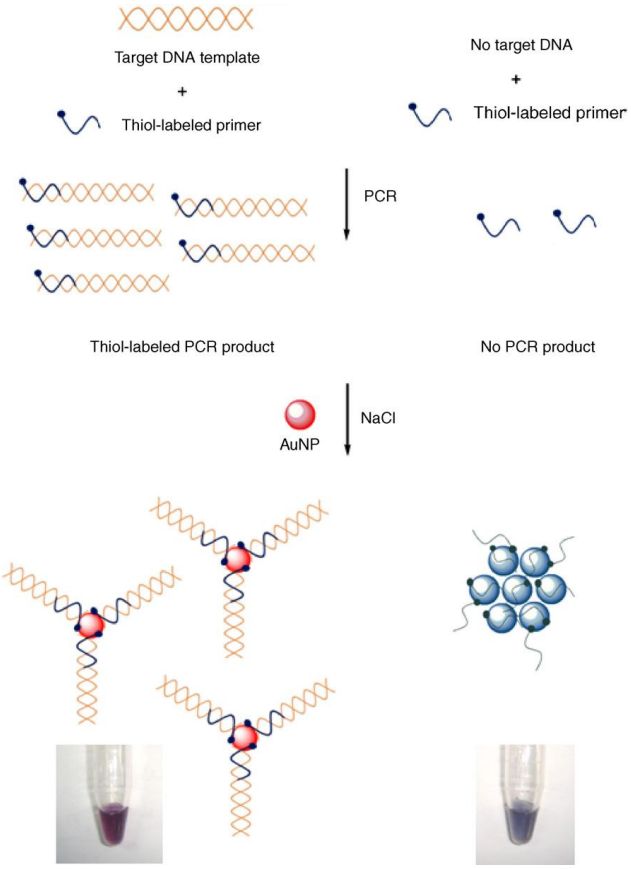

Figure 1.33. Salt-induced AuNP aggregation controlled by PCR product length for DNA detection (Adapted from [92]).

Other than PCR product detection, AuNPs were also applied for isothermal amplification reaction products [93-94]. Tan et al. demonstrated an isothermal method with a detection limit of 100 fM [93]. A target sequence was hybridized with an amplification template containing two target complementary sequences and separated by a nicking endonuclease cleavage site. By nicking and extension reactions, the target sequence was exponentially amplified. Meanwhile, the target and amplified sequences hybridized with a translation template to generate a reporter ssDNA (again by nicking and extension). The generated reporter was applied to crosslink two oligo–AuNP conjugates for colorimetric detection (Figure 1.34).

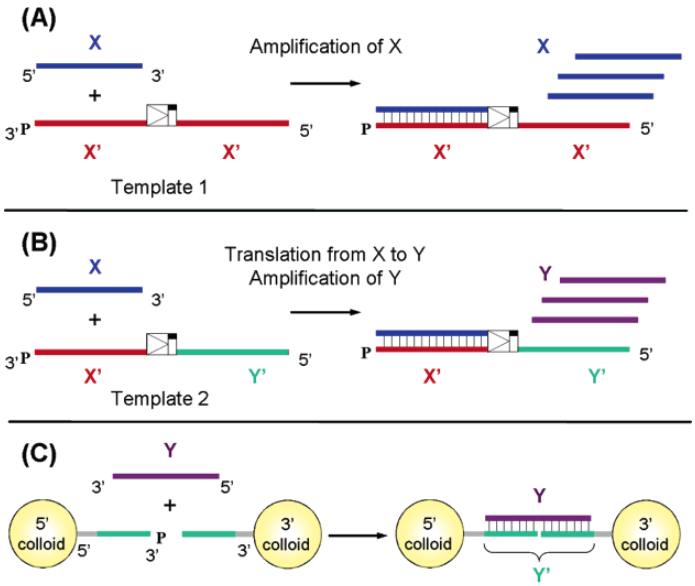

Figure 1.34. Crosslinking of two oligo–AuNP conjugates by target-induced synthesis of ssDNA linkers for DNA detection (Adapted from [93]).

Li et al. reported a rolling circle amplification (RCA) method to accomplish SNP detection by target-controlled formation of amplification template with a detection limit of 70 fM [94]. An initially-open circular probe hybridized with a target sequence, followed by ligation of the probe to form a circular template for RCA. The use of DNA polymerase together with restriction endonuclease produced short ssDNA reporter, which in turn crosslinked two oligo–AuNP conjugates to give a purple-colored result (Figure 1.35). The circular probe/template had phosphorothioate modification to resist its cleavage by the restriction endonuclease.

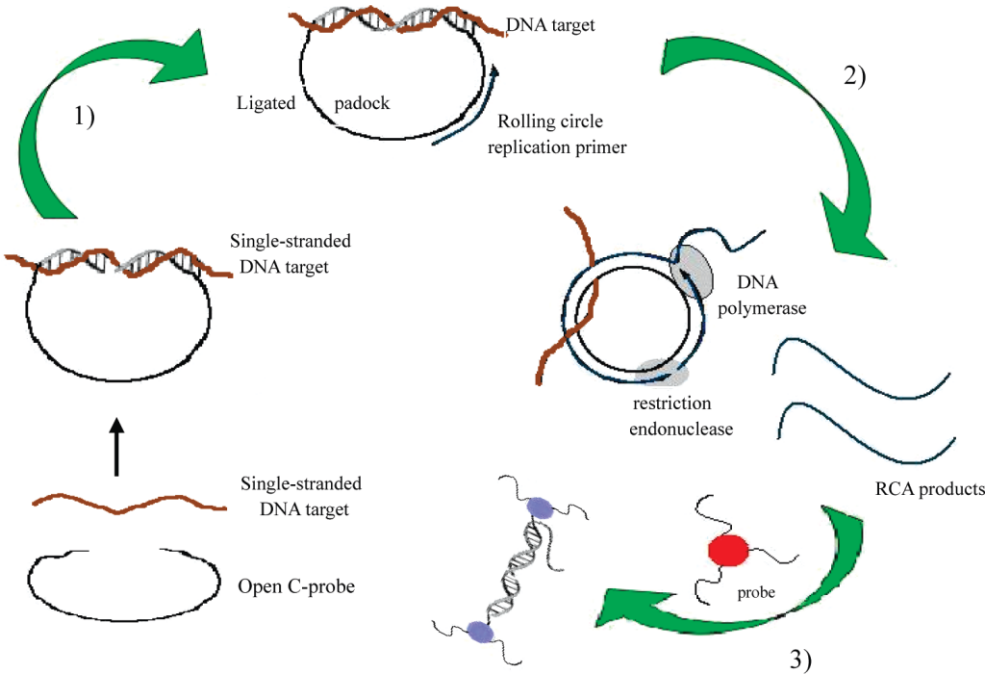

Figure 1.35. DNA detection by target-induced synthesis of ssDNA linker for crosslinking two oligo–AuNP conjugates (Adapted from [94]).

Xu et al. illustrated a DNA recognition approach by utilizing nicking endonuclease (without polymerase) and achieved a detection limit of 10 pM [95]. A linker ssDNA, which was complementary to a target sequence and contained a nicking endonuclease site, was used. The nicking endonuclease cleaved the linker when hybridized with the target. At an appropriate temperature, the cleaved linker dehybridized from the target and the latter was recycled to cleave more linkers. The cleaved linker could not form crosslink structure with two oligo–AuNP conjugates and hence the solution color remained. In the absence of the target, the linker formed crosslink with the two conjugates and the solution color turned purple (Figure 1.36).

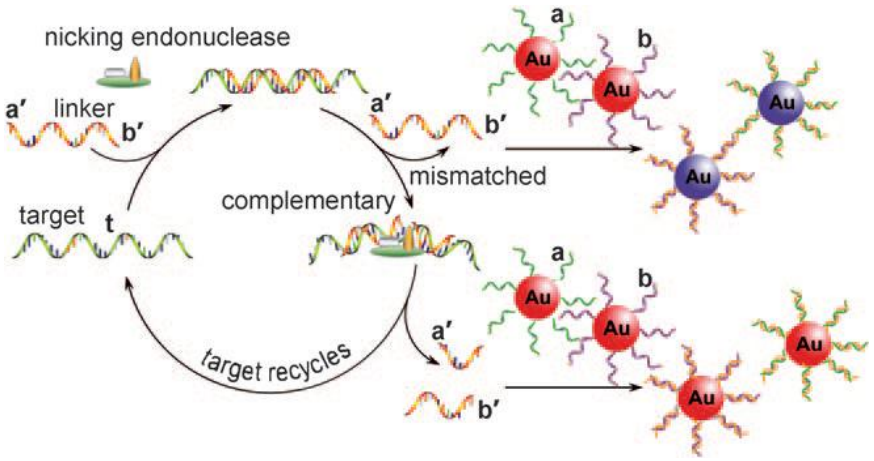

Figure 1.36. DNA detection by target-controlled cleavage of ssDNA linker for crosslinking two oligo–AuNP conjugates (Adapted from [95]).

1.4. Challenges of Gold Nanoparticle-Based Colorimetric Enzyme Assisted Amplification

AuNP-based colorimetric detection of nucleic acid with high sensitivity can be achieved by using enzymatic amplification technique. Nevertheless, multi-step approach (i.e., post-amplification addition of AuNP detection probe(s)) is adopted in previously reported schemes. This is because the reaction conditions result in destabilization/irreversible aggregation of AuNPs, in particular the presence of high concentration of enzyme stabilizer (dithiothreitol (DTT) or 2-mercaptoethanol (2-ME)) and elevated temperature, details are presented in Section 2.1). Besides, enzyme is absorbed/chemisorbed onto AuNP surface via Au–N/Au–S linkage, which inhibits the enzymatic amplification reaction (details are presented in Section 3.1 and Section 4.1). Moreover, the colorimetric property of AuNPs is influenced by the steric and electrostatic stabilization effects of the adsorbed enzyme. The post-amplification open-tube analysis step poses a high risk of carryover contamination. To address these issues, a new AuNP colorimetric detection probe, which possesses high chemical and thermal stabilities as well as excellent compatibility with enzymatic reaction, is highly desired.

1.5. Objectives of the Study

The main objective of this study is to develop an ultra-stable oligo–AuNP conjugate that enables enzymatic reaction and colorimetric detection to be carried out in a closed-tube manner. With this, a simple, highly sensitive, and carryover contamination-free DNA detection is demonstrated.

The ultra-stable oligo–AuNP conjugate is prepared by a new silica reinforcement technique, i.e., coating the conventional conjugate with a silica layer. Chemical and thermal stabilities of the silica-modified oligo–AuNP conjugate are studied in detail (Chapter 2). It should be noted that the conditions for testing chemical and thermal stabilities are targeted for isothermal amplification reaction and PCR. In addition, the effect of the silica coating on the unique hybridization-induced color change property of the oligo–AuNP conjugates is investigated.

Closed-tube colorimetric DNA detection platforms for isothermal amplification reaction and PCR are designed and optimized in Chapter 3 and Chapter 4, respectively. In particular, the effect of the silica coating on enzymatic amplification efficiency is investigated.

To demonstrate that the silica reinforcement method is broadly applicable to other oligo–nanoparticle conjugates, silica-modified oligonucleotide–silver

nanoparticle (oligo–AgNP) conjugate is prepared. Its chemical stability and colorimetric property are examined in Chapter 5.

Chapter 2

Properties of Silica-Modified Oligonucleotide–Gold Nanoparticle Conjugate

The work described in this chapter was done with the aim of developing a new silica-modified oligo–AuNP conjugate that remains stable in DTT and/or at elevated temperature, as well as preserves the hybridization-induced color change property. A brief literature review on oligo–AuNP conjugates' chemical and thermal stabilities as well as previous strategies to enhance their stabilities is given in Section 2.1. The preparation procedures and characterization experiments for the silica-modified oligo–AuNP conjugate are detailed in Section 2.2. Results and discussion are presented in Section 2.3, and a brief summary is provided in Section 2.4.

2.1. Introduction

The most common method to prepare oligo–AuNP conjugates is by chemisorption of monothiol-modified oligonucleotide onto AuNP surface. It should be noted that the chemisorbed oligonucleotide is susceptible to ligand exchange reaction by thiol-containing small molecules (e.g., DTT and 2-ME), which are

included in many enzymatic reaction buffers. When a significant portion of the oligonucleotides are displaced from the AuNP surface, particle aggregation occurs and thus the solution color turns purple. In 10 mM DTT, this happens within a few minutes. Besides, some enzymatic reactions are performed at elevated temperature (e.g., PCR), and the thermal energy is sufficient to break the Au–S linkage [96]. As a result of oligonucleotide desorption, the unique hybridization-induced color change property of the conjugate is severely affected. Moreover, enzymes are adsorbed onto the exposed AuNP surface and thus amplification reactions are inhibited.

2.1.1. Gold–Thiol Linkage

To enhance the stability toward DTT, Mirkin et al. prepared oligo–AuNP conjugates with steroid cyclic disulfide and trihexylthiol anchors (Figure 2.1) [97-98]. The standard monothiol-modified oligo–AuNP conjugates were aggregated in 10 mM DTT within a few minutes, while the oligo–AuNP conjugates with steroid cyclic disulfide and trihexylthiol anchors remained stable up to 2 and 8 h, respectively (Figure 2.1d). The results revealed that the stronger linkage offered by the multiple anchors made the oligo–AuNP conjugates more resistant to displacement reaction.

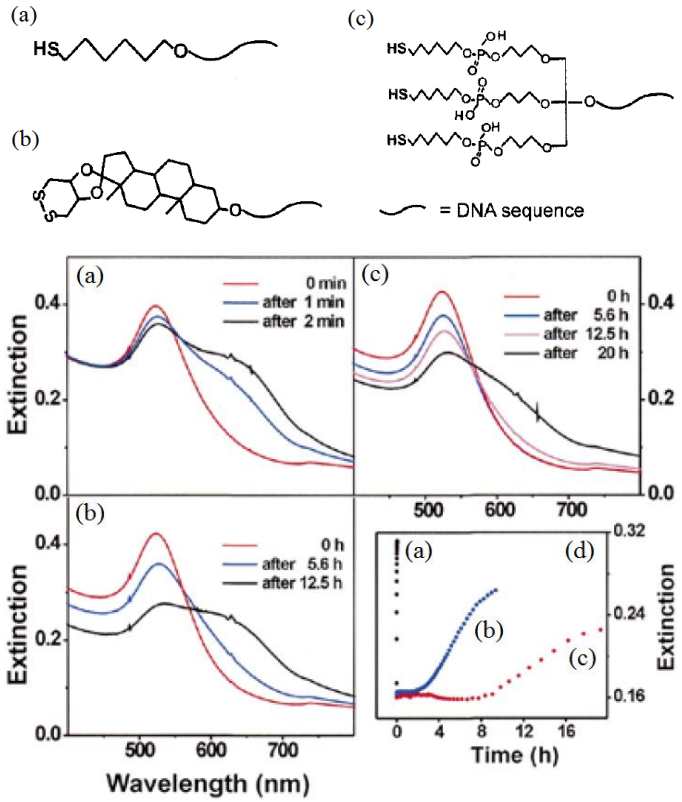

Figure 2.1. The oligonucleotides modified with (a) monohexylthiol, (b) dithiane epiandrosterone, and (c) trihexylthiol anchors, as well as the corresponding UV–vis spectra when incubated with 10 mM DTT. (d) Plots of the absorbance at 600 nm as a function of time for (a–c) (Adapted from [98]).

Nevertheless, these disulfide- and trithiol-modified oligonucleotides were expensive because their syntheses required non-standard phosphoramidites with low coupling yields. In view of this, Graham et al. reported the synthesis of thioctic acid-modified oligonucleotide via treatment of standard 3′-amino-modifier C7

controlled pore glass solid support with N-hydroxysuccinimidyl ester of thioctic acid (Figure 2.2) [99]. Liu et al. reported the synthesis of dithiocarbamate-modified oligonucleotide by means of reaction between amino-modified oligonucleotide and carbon disulfide (Figure 2.3) [100]. The thioctic acid- and dithiocarbamate-modified oligo–AuNP conjugates had similar stability as the steroid cyclic disulfide-modified oligo–AuNP conjugate, but not as good as the trithiol-modified conjugate.

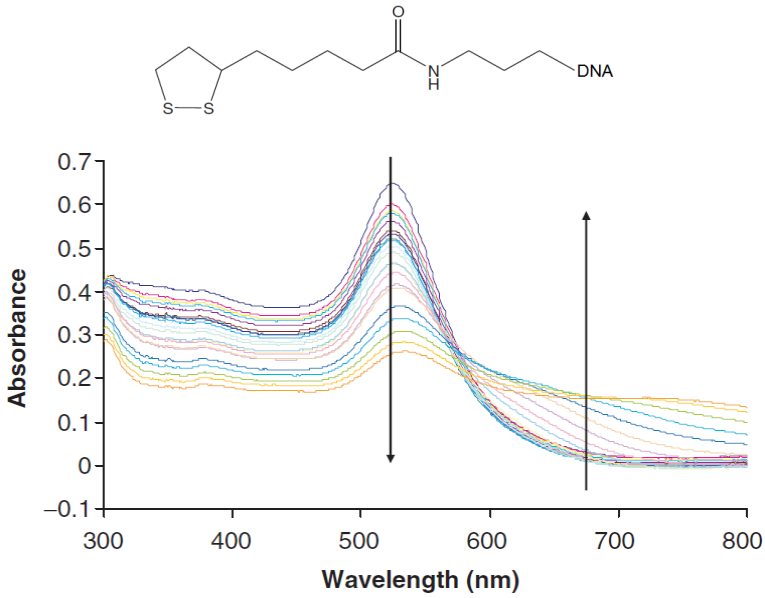

Figure 2.2. Thioctic acid-modified oligonucleotide and UV–vis spectra of thioctic acid-modified oligo–AuNP conjugate in 10 mM DTT at 10 min intervals (Adapted from [99]).

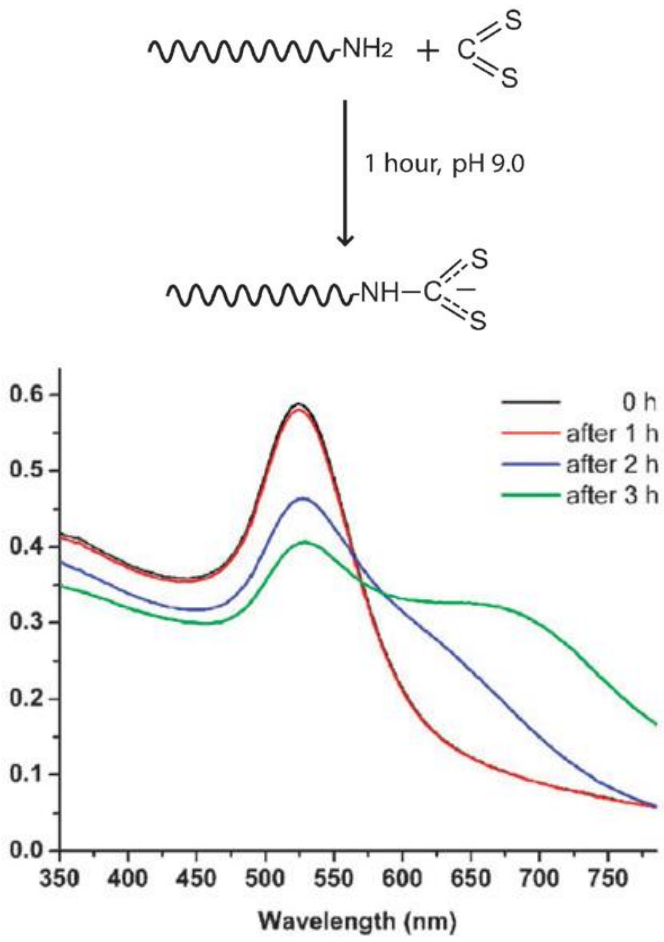

Figure 2.3. Preparation of dithiocarbamate-modified oligonucleotide and UV–vis spectra of thioctic acid-modified oligo–AuNP conjugate in 10 mM DTT (Adapted from [100]).

For the dithiocarbamate-modified oligo–AuNP conjugate, reversible hybridization-induced aggregation property was demonstrated. Two sets of dithiocarbamate-modified oligo–AuNP conjugates were incubated in 10 mM DTT for 1 h, followed by hybridization with a complementary sequence. Red shift of the

SPR absorption peak was observed. After heating at 90 °C for 5 min to effect dehybridization, the SPR absorption peak returned to the original monodispersed position.

2.1.2. Covalent Linkage

Another strategy to reduce desorption of oligonucleotides is to covalently attach oligonucleotides onto silica-coated AuNP surface. Silica coating is attractive because the conjugation chemistries have been extensively studied and documented. However, it is difficult to introduce a silica layer directly onto AuNP surface due to the vitreophobic nature of gold. Different approaches were reported for synthesizing silica layer on AuNP surface [101-106]. Liz-Marzán et al. demonstrated a coating technique by treating AuNP with (3-aminopropyl)trimethoxysilane (APTMS), followed by the addition of sodium silicate to form a silica layer (Figure 2.4) [101]. This process required precise control of APTMS concentration in the initial step, as well as the pH after the addition of sodium silicate in order to prevent AuNP aggregation and the self nucleation of silica, respectively. The thickness of the silica layer could be further enlarged from ~3 nm to ~100 nm by typical alkaline hydrolysis method.

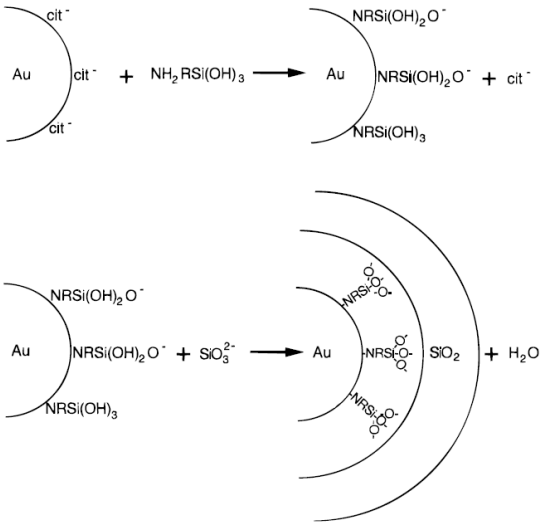

Figure 2.4. Au@SiO_2 synthesis method by immobilization and condensation of silane agents (Adapted from [101]).

Another coating strategy was introduced by Graf et al. that a poly(vinylpyrrolidone) (PVP) layer was adsorbed onto AuNP surface prior to alkaline hydrolysis with tetraethyl orthosilicate (TEOS) (Figure 2.5) [102]. This method was simple in operation as standard alkaline hydrolysis process could be directly applied to the PVP-adsorbed AuNPs without causing aggregation. The synthesized product had a silica shell with minimum thickness of ~10 nm for various diameters of AuNPs.

Some researchers focused on synthesizing silica-coated AuNPs with thin and uniform silica layer [105-106]. AuNP coated with ~1.5 nm thick of silica was

reported by Kang et al. in 2008 [105]. A thiol-terminated imidazolium ion was synthesized to form a self-assembled monolayer (SAM) on AuNP surface, followed by incubation with partially acidified tetramethyl orthosilicate (TMOS) at pH 6 for 1 h (Figure 2.6). UV−vis spectra indicated the formation of silica shell would cause a slight red shift in AuNP's SPR absorption peak.

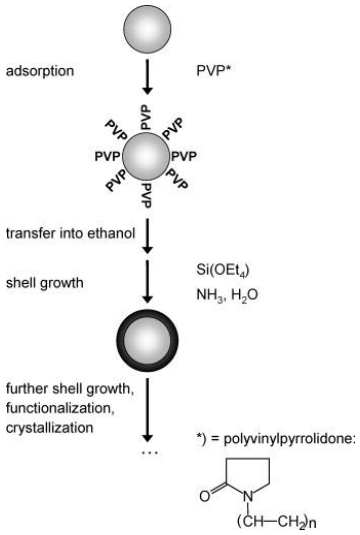

Figure 2.5. Au@SiO_2 synthesis method by PVP conjugation and TEOS condensation (Adapted from [102]).

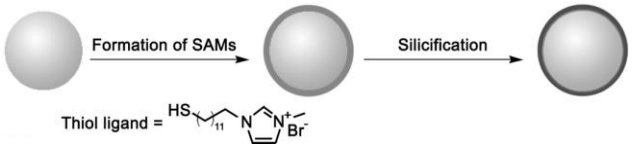

Figure 2.6. Au@SiO_2 synthesis method by ligand immobilization with imidazolium ion and TMOS condensation (Adapted from [105]).

It is important to note that the distance-dependent optical property of AuNP is greatly influenced by the silica layer. Previous study showed that oligonucleotide-functionalized thick silica-coated AuNPs did not experience any color change upon the hybridization of a complementary sequence [107]. Nonetheless, UV−vis spectrum exhibited a decrease in SPR absorption peak after the hybridization due to precipitation of the crosslinked structure and was recovered when heated at 70 °C.

Jana and Ying demonstrated a technique for synthesizing thin silica-coated AuNP, which could then be covalently functionalized with biomolecules [108]. AuNPs of 3–4 nm diameter were synthesized in toluene in the presence of (3-mercaptopropyl)trimethoxysilane (MPTMS). The as-synthesized silica-coated AuNPs were reacted with 2-aminoethyl-aminopropyltrimethoxysilane to introduce amino group on the silica layer surface. Conjugation of amino-modified aptamer or antibody was accomplished by a homobifunctional N-hydroxysuccinimide linker. In their work, strip-based analysis with gold/silver enhancement for protein detection was performed rather than direct colorimetric detection.

Considering all the above points (Section 2.1), it is highly desirable to develop a simple and low-cost method to prepare oligo–AuNP conjugates with excellent

chemical and thermal stabilities. Herein, a thin silica layer is formed onto monothiol-modified oligo–AuNP conjugate by a simple treatment with MPTMS, which entraps and thus reinforces the Au–S linkage. Chemical and thermal stabilities as well as hybridization-induce color change property of the silica-modified oligo–AuNP conjugates are examined.

2.2. Materials and Methods

2.2.1. Materials and Instrumentation

Hydrochloric acid (HCl), nitric acid (HNO_3), $HAuCl_4$, sodium citrate tribasic dihydrate ($C_6H_5O_7Na_3 \cdot 2H_2O$), DL-DTT, sodium phosphate dibasic heptahydrate ($Na_2HPO_4 \cdot 7H_2O$), sodium phosphate monobasic monohydrate ($NaH_2PO_4 \cdot H_2O$), NaCl, 2-ME, MPTMS, potassium chloride (KCl), potassium phosphate monobasic (KH_2PO_4), sodium cyanide (NaCN), and magnesium chloride ($MgCl_2$) were purchased from Sigma-Aldrich (St. Louis, MO, USA). 10× PCR buffer was purchased from Invitrogen (Carlsbad, CA, USA). Nitrocellulose membrane (0.8 μm) was purchased from Millipore (Billerica, MA, USA). All oligonucleotides were purchased from Integrated DNA Technologies (Coralville, IA, USA) and were HPLC-purified. Desalting column (illustra™ MicroSpin G-25) was purchased from

GE Healthcare (Piscataway, NJ, USA). Copper grids (300 mesh) for transmission electron microscopy (TEM) were purchased from Sigma-Aldrich. All reagents were used as received. All solutions were prepared with ultrapure water (18.2 MΩ·cm) from a Milli-Q Advantage A10 System (Millipore).

UV–vis spectra were measured using an Ultrospec™ 2100 pro UV/visible spectrophotometer (GE Healthcare). TEM images were taken using a JEOL JEM-2010F TEM with field emission source (JEOL, Japan). Centrifugation was performed with an Eppendorf Microcentrifuge 5415 D (Eppendorf, Germany). Shaking was performed with a Thermomixer compact (Eppendorf). Real-time fluorescence measurement was carried out using an Applied Biosystems 7500 Real-Time PCR System (Applied Biosystems, Carlsbad, CA, USA). Heating was done in a GeneAmp® PCR System 9700 (Applied Biosystems).

2.2.2. Synthesis of 15 nm Gold Nanoparticles

The synthesis of AuNPs was based on the protocol described by Natan et al. with minor modifications [109]. All glassware and magnetic stir bar used in the AuNP synthesis were cleaned with aqua regia (mixture of concentrated HCl and HNO_3 in a volume ratio of 3:1; CAUTION: aqua regia is harmful and highly corrosive, and must

be handled with care in a fume hood), rinsed with water, and dried in an oven. A solution of $HAuCl_4$ (30 mL, 0.01 wt%) was boiled under reflux with vigorous stirring. Then, $C_6H_5O_7Na_3$ (3 mL, 1 wt%) was added quickly. The solution color changed from pale yellow to deep red within minutes. Heating and stirring were continued for 10 min, followed by cooling to room temperature under stirring, and then the solution was filtered through the nitrocellulose membrane. UV−vis spectrum of the as-prepared AuNPs was measured. According to the method reported by Haiss et al., the size and concentration of AuNPs could be determined from the absorbance data [110]. By calculating the ratio of the absorbance at the SPR peak ($A_{SPR,AuNP}$) to the absorbance at 450 nm ($A_{450,AuNP}$), the size of the AuNPs used in this work was determined to be ~15 nm. The concentration of the AuNP solution (c_{AuNP}, in M) was determined by the following equation:

$$c_{AuNP} = A_{450,AuNP}/\varepsilon_{450,AuNP} \qquad \text{[Eq. (2.1)]}$$

where $\varepsilon_{450,AuNP}$ is the molar extinction coefficient of the 15 nm AuNPs at 450 nm (i.e., $2.18 \times 10^8\ M^{-1}cm^{-1}$).

2.2.3. Preparation of Oligonucleotide–Gold Nanoparticle Conjugate

The preparation of the oligo–AuNP was based on the protocol described by Mirkin et al. with minor modifications [111]. Thiol-modified probe (without or with hexaethylene glycol (PEG_6) spacer), 5′-HS-$(CH_2)_6$-GCAATAAACTCAACAGGAG CAG-3′ and 5′-HS-$(CH_2)_6$-$(OCH_2CH_2)_6$-GCAATAAACTCAACAGGAGCAG-3′, was treated with DTT (0.1 M) in sodium phosphate (0.2 M, pH 8.2) for 30 min. This activated capture probe solution (i.e., with disulfur linkage cleaved) was purified by passing through a desalting column according to the manufacturer's instructions. Immediately afterward, the purified capture probe (1.75 μM) was mixed with the AuNPs (3.5 nM). They were incubated for 16 h, and then aged with NaCl (0.3 M) and sodium phosphate (10 mM, pH 7.4) for 24 h. Next, the solution was centrifuged at 13,200 rpm for 30 min to remove excess capture probe. The supernatant was discarded and the red oily precipitate (i.e., oligo–AuNP conjugate) was redispersed in sodium phosphate (10 mM, pH 7.4). The solution was centrifuged again and redispersed in water. UV–vis spectrum of the as-prepared oligo–AuNP was measured and the particle concentration was determined by the following equation:

$$c_{\text{oligo–AuNP}} = c_{\text{AuNP}} \times (A_{\text{SPR,oligo–AuNP}}/A_{\text{SPR,AuNP}}) \quad \text{[Eq.(2.2)]}$$

To determine the immobilized oligonucleotide density, a 3′-FAM-labeled probe

was used. The oligo–AuNP conjugate (2.5 nM) was treated with 2-ME (12 mM) in NaCl (0.3 M) and sodium phosphate (10 mM, pH 7.4) for 24 h under shaking at 1,400 rpm to release the capture probe from the AuNP surface, followed by centrifugation (13,200 rpm for 30 min) and fluorescence measurement of the collected supernatant. The amount of the immobilized capture probe was determined with reference to a standard curve and the immobilized oligonucleotide density (i.e., number of oligonucleotide strands per AuNP, $n_{\text{total,oligo–AuNP}}$) was calculated accordingly.

2.2.4. Preparation of Silica-Modified Oligonucleotide–Gold Nanoparticle Conjugate

The oligo–AuNP conjugate (1 nM) was mixed with MPTMS (0.1 mM) (i.e., AuNP:MPTMS ratio of $1:10^5$), unless otherwise specified. The mixture was shaken at 1,400 rpm for 24 h, supplied with sodium phosphate (10 mM, pH 7.4) and centrifuged at 13,200 rpm for 30 min. The supernatant was removed and the red oily precipitate (i.e., silica-modified oligo–AuNP conjugate) was redispersed in sodium phosphate (10 mM, pH 7.4). The solution was centrifuged again and redispersed in water.

UV−vis spectrum of the as-prepared silica-modified oligo−AuNP conjugate was measured and the particle concentration was determined by the following equation:

$$c_{\text{modified oligo–AuNP}} = c_{\text{AuNP}} \times (A_{\text{SPR,modified oligo–AuNP}}/A_{\text{SPR,AuNP}}) \quad \text{[Eq.(2.3)]}$$

To determine the oligonucleotide density of the silica-modified oligo−AuNP conjugate, the fluorescently labeled oligo−AuNP was used. The supernatant of the MPTMS-treated oligo−AuNP was collected after the first round centrifugation and fluorescence measurement was performed to determine the amount of capture probe displaced after the silica coating step. By subtracting the displaced amount from the immobilized amount, the oligonucleotide density of the silica-modified oligo−AuNP ($n_{\text{total,modified oligo–AuNP}}$) was obtained.

2.2.5. Transmission Electron Microscopy Characterization

20 μL of AuNP, oligo−AuNP, and silica-modified oligo−AuNP conjugates (2.5 nM) were applied to copper grids and left dry at room temperature. Images were recorded on TEM operated at 200 kV.

2.2.6. Chemical Stability Test

Stability tests of the oligo–AuNP and silica-modified oligo–AuNP conjugates (2.5 nM) were performed in phosphate-buffered saline (1× PBS: 137 mM NaCl, 2.7 mM KCl, 4.3 mM $Na_2HPO_4{\cdot}7H_2O$, and 1.4 mM KH_2PO_4, pH 7.4) with DTT (10 mM) or NaCN (2 mM). UV–vis spectra and solution colors were recorded at different time intervals. Fluorescence characterization of the oligonucleotide desorption in DTT was performed using 3′-FAM-labeled unmodified and silica-modified oligo–AuNP conjugates. The supernatants were collected for fluorescence measurement to determine the amounts of desorbed probe at the end of the 2-h treatment ($n_{\text{desorbed,2h}}$). The amounts of probe desorbed from the conjugates at different incubation times (in terms of the total immobilized amount, n_{total}, i.e., $n_{\text{total,oligo–AuNP}}$ for the oligo–AuNP conjugate and $n_{\text{total,modified oligo–AuNP}}$ for the silica-modified oligo–AuNP conjugate) was determined by the following equation:

$$\%_{\text{desorbed,t}} = (F_t/F_{2h}) \times (n_{\text{desorbed,2h}}/n_{\text{total}}) \times 100\% \qquad \text{[Eq. (2.4)]}$$

where $\%_{\text{desorbed,t}}$ is the percentage of desorbed probe at time t, and F_t and F_{2h} are the fluorescence readings at time t and 2-h, respectively.

2.2.7. Synthesis pH Test

The silica layer was synthesized at pH 5–7 with 0.5 intervals. The protocol was described in Section 2.2.4 except with the addition of phosphate buffer (1 mM) at the beginning of the reinforcement process. Chemical stability tests of the resulting silica-modified oligo–AuNP conjugates were performed as depicted in Section 2.2.6.

2.2.8. Reversible Hybridization Test

The silica-modified oligo–AuNP conjugate (3.125 nM) was incubated in PBS with DTT (10 mM) for 3 h. Then, NaCl (0.5 M) and complementary target (5′-CTGCTCCTGTTGAGTTTATTGC-3′, 0.2 μM) were added, with a final conjugate concentration of 2.5 nM. Hybridization was allowed to proceed for 10 min. Finally, the solution was heated at 94 ℃ for 1 min. UV–vis spectra and colorimetric results were recorded before and after hybridization, as well as after heat denaturation.

2.2.9. Melting Analysis

Melting analysis of the oligo–AuNP conjugate (2.5 nM) was performed in 1× PCR buffer (20 mM Tris-HCl and 50 mM KCl, pH 8.4) with $MgCl_2$ (6 mM) and

complementary target (0.4 μM) after 30 min incubation. Absorbance at 260 nm was recorded under heating (1 ℃/min) from 25–80 ℃. UV–vis spectra and colorimetric results were recorded at 25, 50 and 80 ℃. Similar procedures were used for analyzing the silica-modified oligo–AuNP conjugate with the complementary target concentration and incubation time changed to 0.2 μM and 10 min, respectively. A control experiment without AuNPs was performed (concentrations of the capture probe and target were 0.4 μM).

2.2.10. Thermal Stability Test

Thermal stabilities of the oligo–AuNP and silica-modified oligo–AuNP conjugates were fluorescently characterized using 3′-FAM-labeled probe at different temperature settings. For constant temperature (i.e., 94, 72, or 55 ℃), the sample contained the unmodified or silica-modified conjugate (2.5 nM), 1× PCR buffer, and $MgCl_2$ (6 mM). Fluorescence signal was acquired every 10 min for 2 h. After that, the sample was centrifuged (13,200 rpm for 30 min) and the supernatant was collected for fluorescence measurement to determine the amount of desorbed probe at the end of the 2-h thermal treatment ($n_{desorbed,2h}$). The amount of probe desorbed from the conjugate at different incubation times (in terms of the total immobilized amount,

n_{total}, i.e., $n_{total,oligo–AuNP}$ for the oligo–AuNP conjugate and $n_{total,modified\ oligo–AuNP}$ for the silica-modified oligo–AuNP conjugate) was determined by the following equation:

$$\%_{desorbed,t} = (F_t/F_{2h}) \times (n_{desorbed,2h}/n_{total}) \times 100\% \qquad \text{[Eq. (2.5)]}$$

where $\%_{desorbed,t}$ is the percentage of desorbed capture probe at time t, and F_t and F_{2h} are the fluorescence readings at time t and 2-h, respectively. For PCR thermal cycling, the sample contained the unmodified or silica-modified conjugate (2.5 nM), 1× PCR buffer, $MgCl_2$ (6 mM), and dithiothreitol (5 μM). The thermal cycling profile used was identical to that described later in Section 4.2.2. Fluorescence signal was acquired at the extension step of each cycle. After thermal cycling, the sample was centrifuged (13,200 rpm for 30 min) and the supernatant was collected for fluorescence measurement to determine the amount of desorbed probe at the end of PCR ($n_{desorbed,end\ PCR}$). The amount of probe desorbed from the conjugate at different cycle numbers was determined by the following equation:

$$\%_{desorbed,cycle} = (F_{cycle}/F_{end\ PCR}) \times (n_{desorbed,end\ PCR}/n_{total}) \times 100\% \qquad \text{[Eq. (2.6)]}$$

where $\%_{desorbed,cycle}$ is the percentage of desorbed probe at a particular cycle, and F_{cycle} and $F_{end\ PCR}$ are the fluorescence readings at the particular cycle and the end of PCR, respectively.

2.3. Results and Discussion

2.3.1. Physical Properties

TEM images of bare AuNPs, oligo–AuNP and silica-modified oligo–AuNP conjugates are shown in Figure 2.7. The diameter of the synthesized AuNPs was ~15 nm. Particle size determination based on absorption data as suggested by Haiss et al. gave very consistent result [110].

However, the silica layer coated on the AuNP surface could not be seen in the TEM image. This observation was similar to the study reported by Jana and Ying that very thin and amorphous silica layer was indistinguishable from background even with high-resolution TEM [108]. Therefore, UV–vis absorption was used to provide evidence for the existence of an ultra-thin silica layer on the oligo–AuNP conjugate surface. UV–vis spectrum of the as-synthesized AuNPs exhibited an SPR absorption peak at 520 nm. The peak shifted to 522 nm and further increased to 523 nm after conjugation of oligonucleotides and after silica modification, respectively (Figure 2.8). This was consistent with previous studies that the immobilization of oligonucleotides or coating of silica layer onto AuNP surface would result in a red shift of the SPR absorption peak [105].

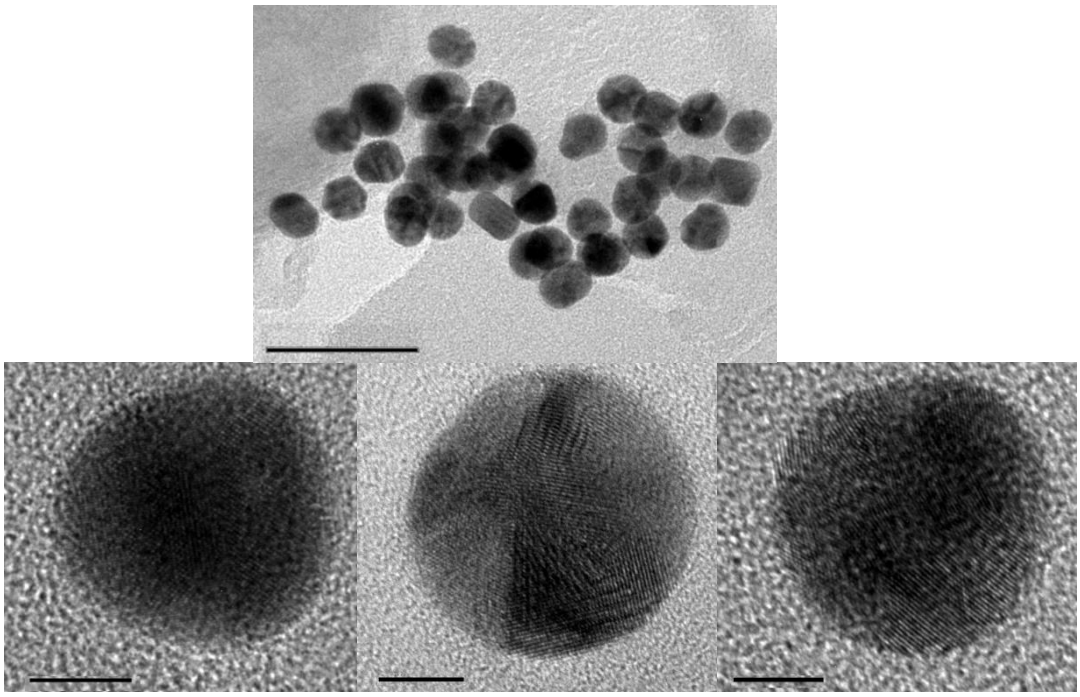

Figure 2.7. TEM images of bare AuNPs (top and bottom left), oligo–AuNP conjugate (bottom middle), and silica-modified oligo–AuNP conjugate (bottom right). Scale bar = 50 and 5 nm for the top and bottom images, respectively.

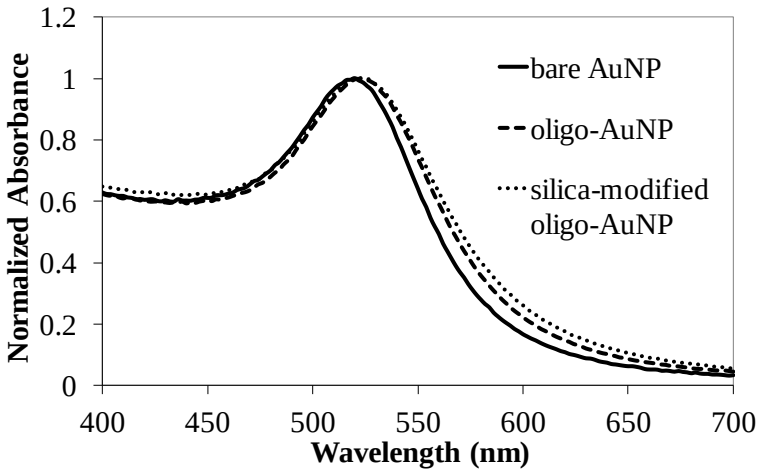

Figure 2.8. UV–vis spectra of bare AuNPs, oligo–AuNP conjugate, and silica-modified oligo–AuNP conjugate.

2.3.2. Chemical Stability

Previous studies indicated ligand exchange reaction between monothiol-modified oligonucleotide and thiol-containing small molecule was the major factor causing the instability of oligo–AuNP conjugates [97-100]. It was hypothesized that the conjugate's stability could be enhanced by introducing a silica layer to physically entrap and reinforce the Au–S linkage between the monothiol-modified oligonucleotide and AuNP surface. In fact, the silica layer might act as a physical barrier to efficiently block the access of the thiol-containing small molecule.

After the addition of 10 mM DTT to the oligo–AuNP conjugate, red shift and broadening of the SPR absorption band were observed, with a moderate decrease in absorbance at 520 nm and a large increase in absorbance at longer wavelengths (600–700 nm, together with a new absorption peak at ~650 nm). The solution color changed from red to purple within a few minutes (Figure 2.9). As expected, the silica-modified oligo–AuNP conjugate was much more stable. After 24-h incubation in 10 mM DTT, the absorption peak dropped by 22% only (no change at longer wavelengths) and the solution remained red (Figure 2.10).

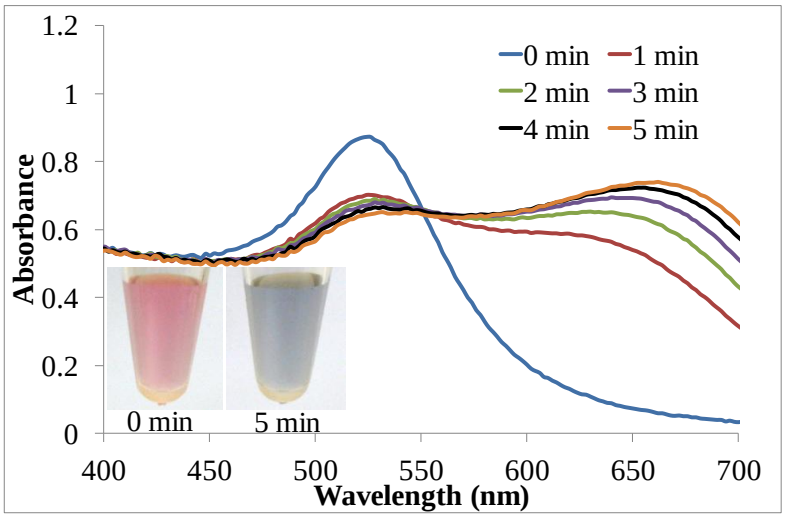

Figure 2.9. UV–vis spectra of the oligo–AuNP conjugate incubated in 10 mM DTT. Insets are photographs showing the colors of the samples at different times.

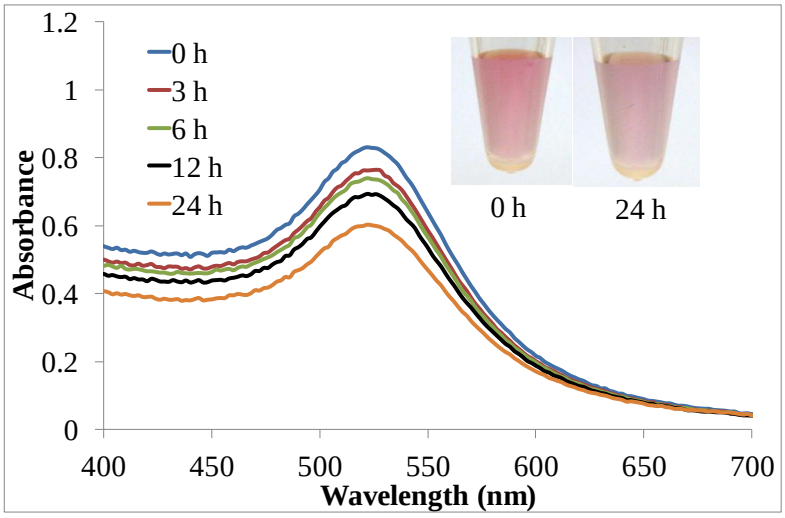

Figure 2.10. UV–vis spectra of the silica-modified oligo–AuNP conjugate incubated in 10 mM DTT. Insets are photographs showing the colors of the samples at different times.

Stability was further enhanced by inserting a PEG_6 spacer next to the thiol group. Absorption spectrum after 24-h incubation with DTT was almost identical as the spectrum recorded at the beginning of the experiment (Figure 2.11). Plots of the absorbance at 600 nm versus incubation time clearly reveal the enormous stability enhancement in DTT of the silica-modified oligo–AuNP conjugate (Figure 2.12). The stability of this conjugate compares favorably to that prepared with disulfide and trithiol linkages, which are stable in 10 mM DTT for 1–3 h and 8 h, respectively [97-100].

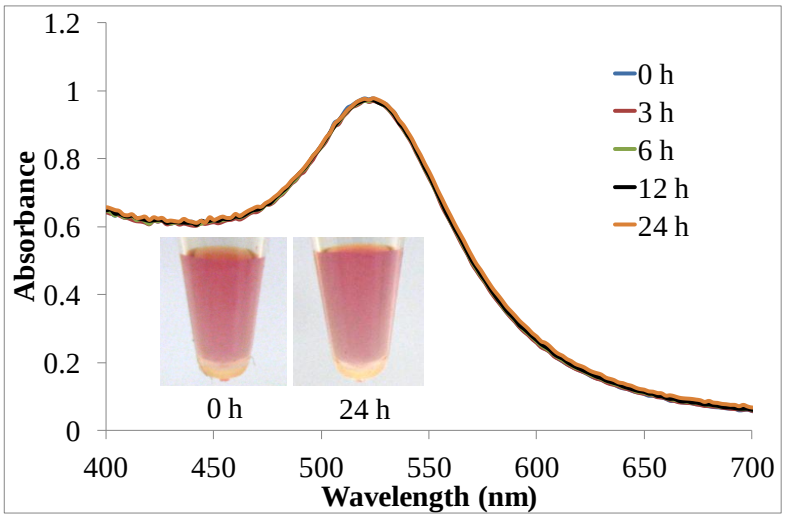

Figure 2.11. UV–vis spectra of the silica-modified oligo–AuNP conjugate (with PEG_6 spacer) incubated in 10 mM DTT. Insets are photographs showing the colors of the samples at different times.

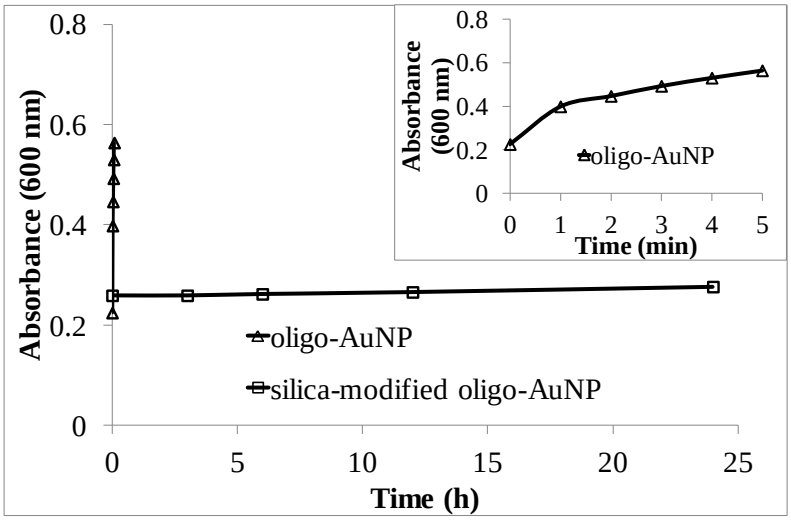

Figure 2.12. Plots of absorbance at 600 nm versus time of the oligo–AuNP and silica-modified oligo–AuNP conjugates. Inset: Expanded view for the oligo–AuNP conjugate.

The above finding suggests that the nature of molecule in close proximity with the AuNP surface would affect the compactness of the formed silica layer and thus the stability against ligand exchange reaction. In terms of the silica layer formation process, MPTMS molecules chemisorbed onto vacant sites on the oligo–AuNP conjugate surface by mercapto groups, followed by hydrolysis and polycondensation of the trimethoxysilyl groups in order to create a silica crosslink network (Figure 2.13). Without the PEG_6 spacer, the bulky size of nucleotides would impede the condensation reaction between MPTMS molecules, resulting in the formation of a

less compact silica network. With the PEG_6 spacer, a compact silica layer was formed, giving better entrapment of the oligonucleotides and, therefore, higher stability against DTT displacement.

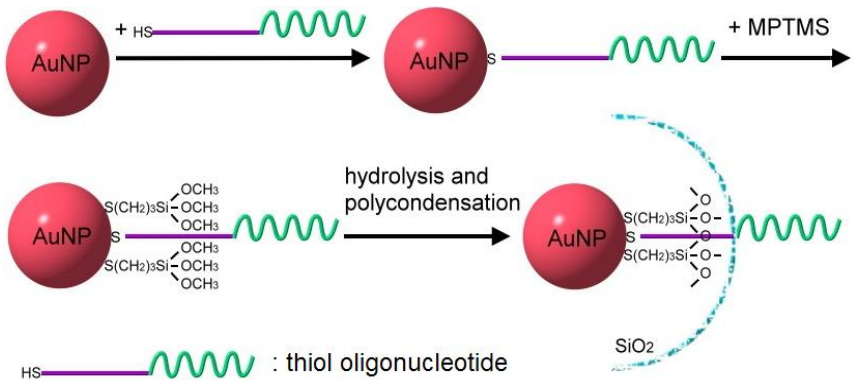

Figure 2.13. Preparation scheme of the silica-modified oligo–AuNP conjugate.

With the PEG_6 spacer, different ratios of AuNP to MPTMS were investigated to determine the optimum ratio for synthesizing the most stable silica-modified oligo–AuNP conjugate (Figure 2.14). Conjugate prepared with AuNP:MPTMS ratio of $1:10^3$ was not stable in 10 mM DTT. After 24-h incubation, AuNP's SPR absorption band disappeared due to serious aggregation and precipitation. UV–vis spectra of the $1:10^4$ and $1:10^6$ conjugates showed slight changes after the DTT treatment. The conjugate prepared with AuNP:MPTMS ratio of $1:10^5$ showed no change in UV–vis spectrum after the DTT treatment. Therefore, the optimum

AuNP:MPTMS ratio for preparing the silica-modified oligo–AuNP conjugate was $1:10^5$.

Liz-Marzán et al. reported that 1,300 silane molecules were required to form a monolayer on a 15 nm AuNP [101]. The silica-modified oligo–AuNP conjugate produced with AuNP:MPTMS ratio of $1:10^3$ could not efficiently entrap the oligonucleotides on the AuNP surface because of the incomplete silica layer. Consequently, analogous to the unmodified oligo–AuNP conjugate, the chemisorbed oligonucleotides were easily displaced by DTT. With AuNP:MPTMS ratio of $1:10^4$, the formed silica layer could entrap the chemisorbed oligonucleotides. Nevertheless, the silica layer was not compact enough that a significant amount of oligonucleotides was displaced after prolonged incubation. A compact silica layer was formed with AuNP:MPTMS ratio of $1:10^5$, offering the oligo–AuNP conjugate with the highest stability against DTT-induced aggregation. At higher ratio (i.e., $1:10^6$), solution-phase polycondensation of the MPTMS molecules might be favored, which hampered their chemisorption onto the AuNPs and the formation of a compact silica layer.

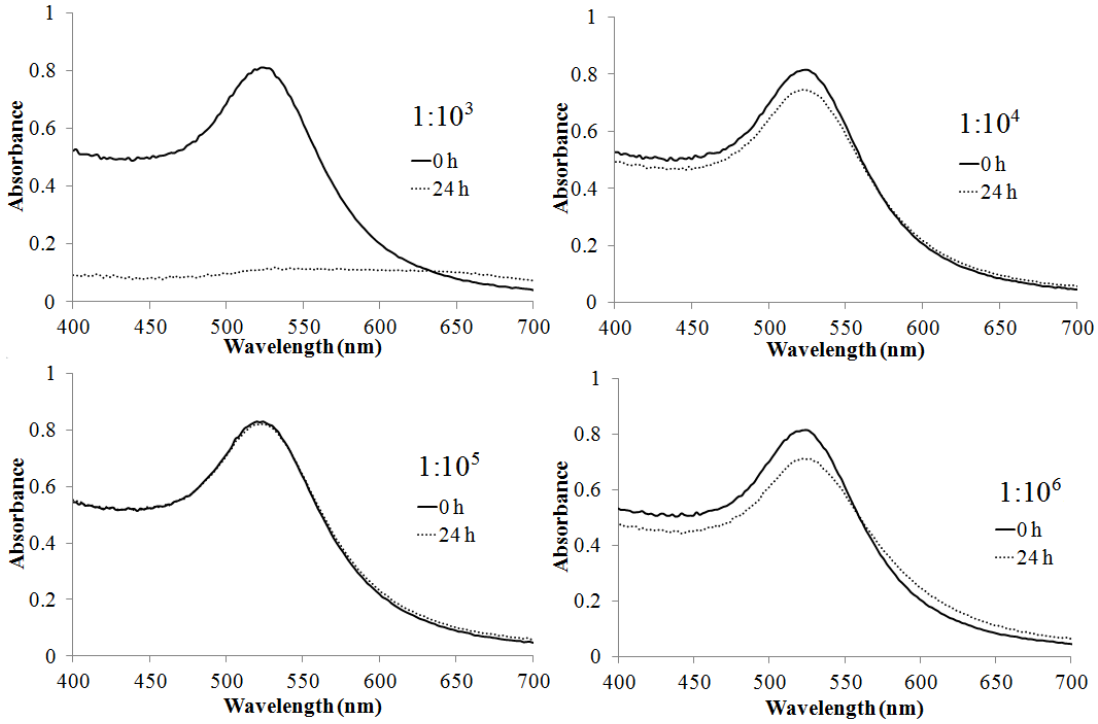

Figure 2.14. UV–vis spectra of the silica-modified oligo–AuNP conjugates prepared with different AuNP:MPTMS ratios incubated in 10 mM DTT.

To quantitatively characterize the displacement reaction, real-time fluorescence measurement was carried out during the DTT incubation period for the $1{:}10^5$ conjugate, of which the oligonucleotide was labeled with a fluorescent dye (6-FAM). Fluorescence signal was low if the oligonucleotide was in the bound state as the emission of 6-FAM was efficiently quenched by AuNP, and the signal increased upon desorption of the oligonucleotide from AuNP surface. It was found that more than 50% of the immobilized oligonucleotides desorbed after 10-min incubation for the

oligo–AuNP conjugate and nearly 0% for the silica-modified oligo–AuNP conjugate (Figure 2.15). After 2-h incubation, the amounts increased to 87% and 8%, respectively. Results of the UV–vis and fluorescence measurements indicate that the stability of the monothiol-modified oligo–AuNP conjugate is greatly enhanced by the silica reinforcement technique.

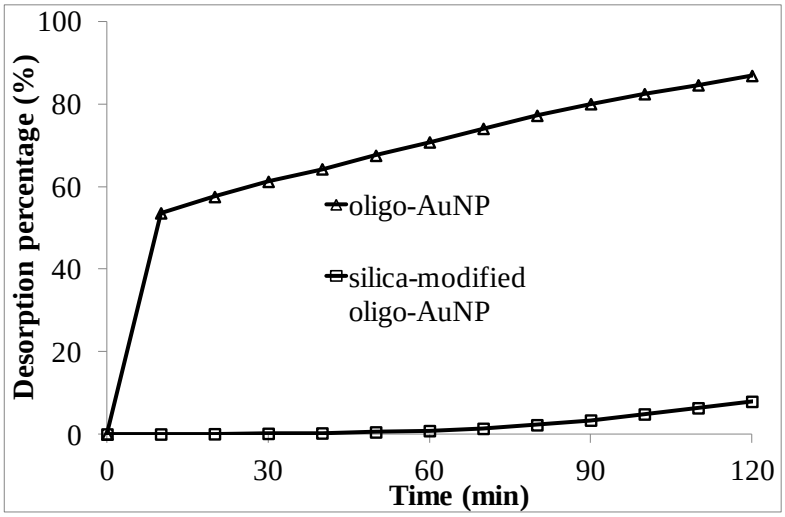

Figure 2.15. Desorption curves of the oligo–AuNP and silica-modified oligo–AuNP conjugates incubated in 10 mM DTT.

The formation of silica layer on AuNP is depended on the hydrolysis rate of MPTMS. A higher hydrolysis rate induces a higher condensation rate, which may favor the solution-phase polycondensation and affect the formation of silica layer on

AuNP surface. It should be noted that the hydrolysis rate of trimethoxysilyl groups is pH-dependent. In view of this, 1 mM of phosphate buffers at different pHs (ranging from 5–7) were added to the oligo–AuNP conjugate solutions prior to the addition of MPTMS. This range of pHs was chosen because of the slow hydrolysis process in slightly acidic condition [105]. After 24-h incubation in 10 mM DTT, UV–vis spectra of the silica-modified oligo–AuNP conjugates synthesized at different pHs all showed a decrease in the SPR absorption peak, but to different extents (Figure 2.16). A minimum decrease of 5.4% was observed for the silica-modified oligo–AuNP conjugate synthesized at pH 6 (Figure 2.17). In fact, the most stable silica-modified oligo–AuNP conjugate was synthesized without pH adjustment (pH 5.5–6.5).

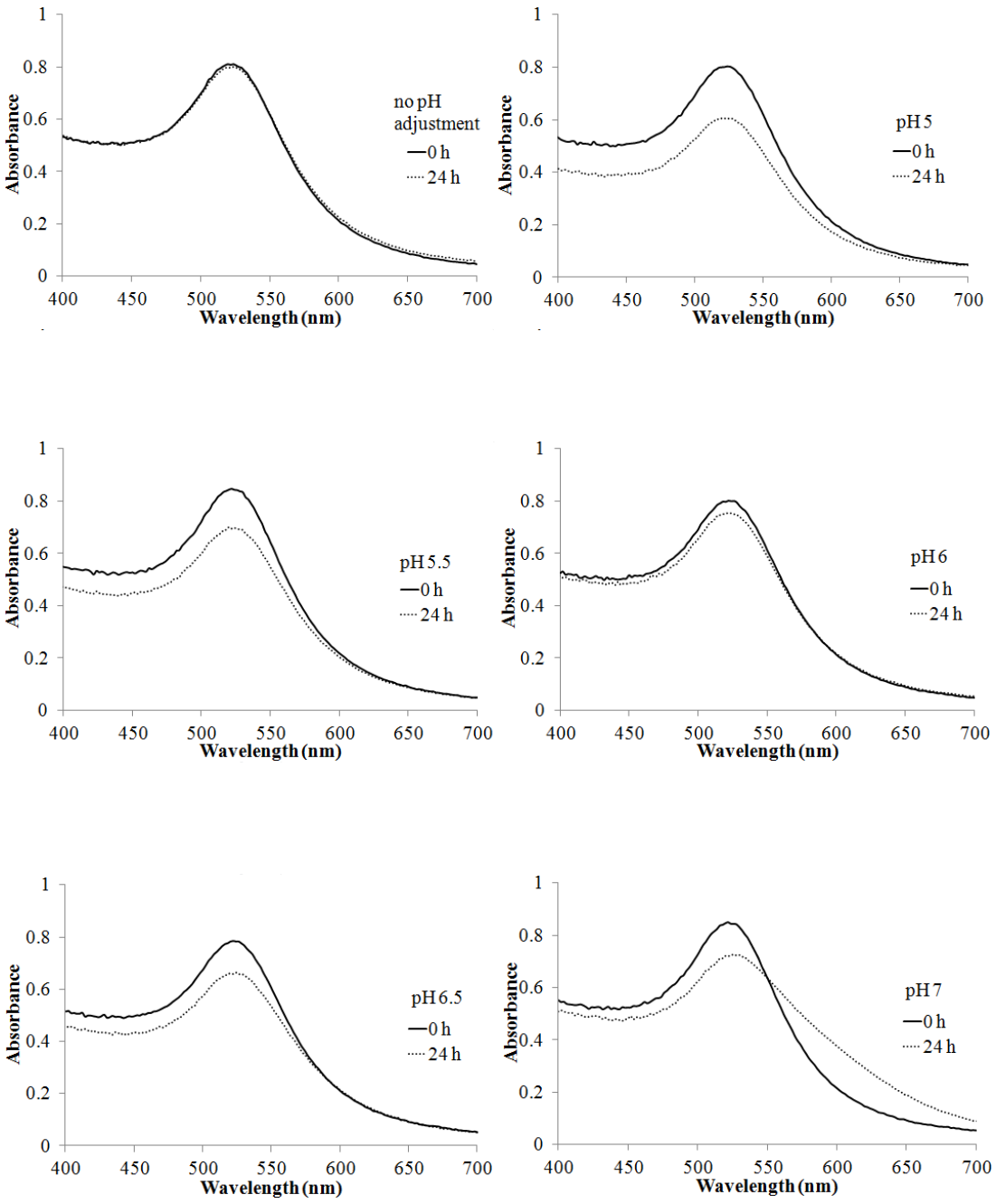

Figure 2.16. UV–vis spectra of the silica-modified oligo–AuNP conjugates synthesized at different pHs when incubated in 10 mM DTT.

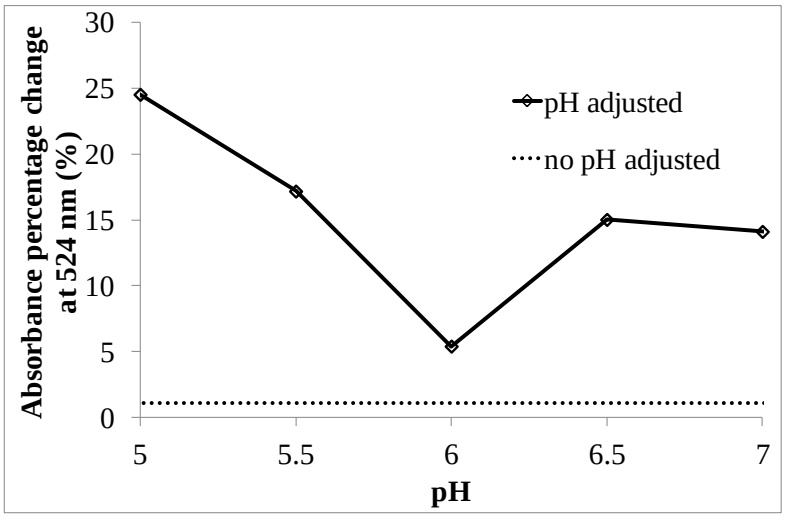

Figure 2.17. Percentage decrease of the SPR absorption peak for the silica-modified oligo–AuNP conjugates synthesized at different pHs when incubated in 10 mM DTT.

To confirm the hypothesis that the silica layer prevents the interaction between the Au–S linkage and DTT by acting as a physical barrier, the silica-modified conjugate was incubated with 2 mM NaCN. It was reported that cyanide ions (CN^-) could dissolve AuNPs by forming dicyanoaurate(I) complexes ($Au(CN)_2^-$) [112]. For the oligo–AuNP conjugate, the characteristic SPR absorption band diminished greatly and the solution turned colorless within a minute (Figure 2.18). As expected, the silica-modified oligo–AuNP conjugate was highly resistant to oxidative dissolution by NaCN. After 24-h incubation, the SPR absorption peak (i.e., 522 nm) dropped by 23% only and the solution remained red (Figure 2.19).

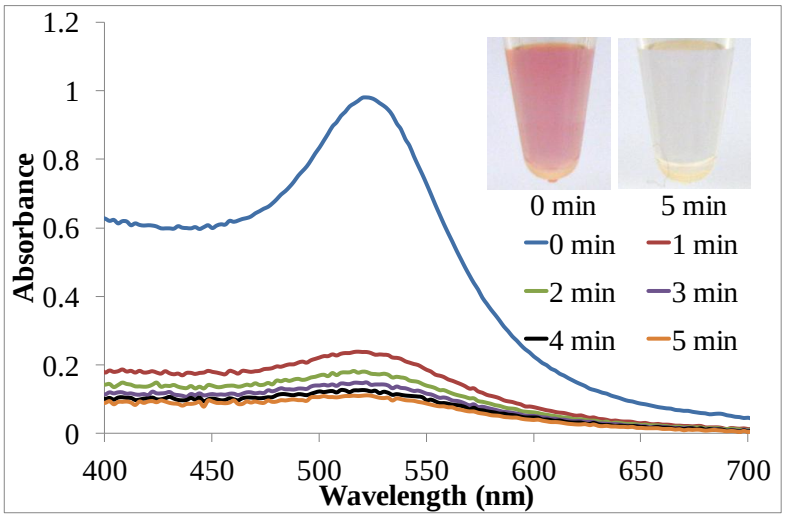

Figure 2.18. UV–vis spectra of the oligo–AuNP conjugate incubated in 2 mM NaCN. Insets are photographs showing the colors of the samples at different times.

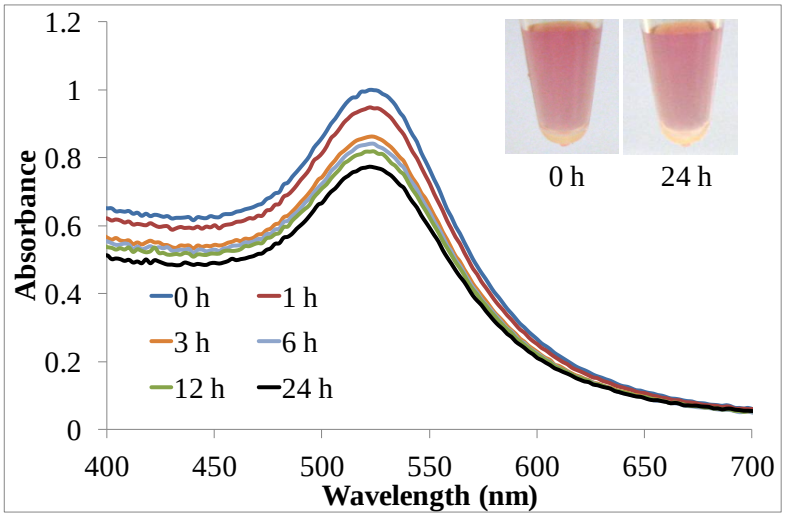

Figure 2.19. UV–vis spectra of the silica-modified oligo–AuNP conjugates incubated in 2 mM NaCN. Insets are photographs showing the colors of the samples at different times.

Plots of the absorbance at 522 nm versus incubation time manifest the significant improvement in chemical stability against oxidative dissolution of the AuNPs for the silica-modified oligo–AuNP conjugate (Figure 2.20). This indicates that the silica layer serves as a diffusion barrier for the cyanide reactant and/or $Au(CN)_2^-$ product. This finding supports the hypothesis that the silica layer physically entraps the Au–S linkage, thereby offering the oligo–AuNP conjugate extremely high resistance to ligand exchange reaction.

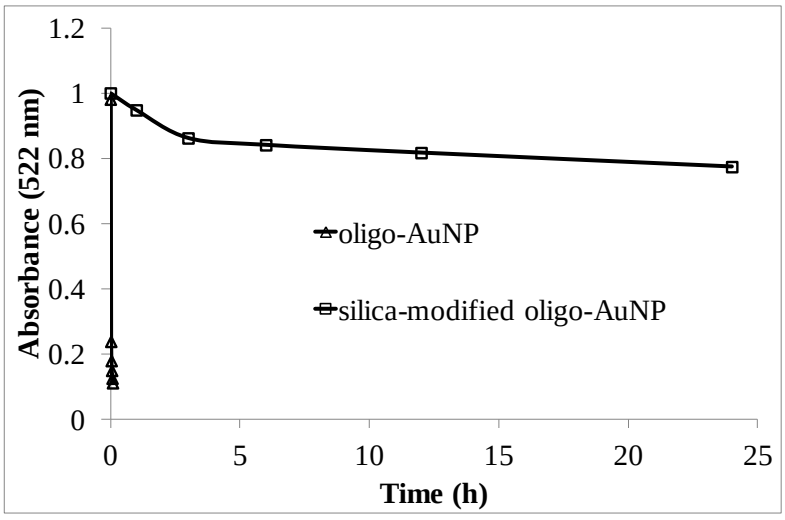

Figure 2.20. Plots of absorbance at 522 nm versus time of the oligo–AuNP and silica-modified oligo–AuNP conjugates incubated in 2 mM NaCN.

2.3.3. Hybridization Properties

In a previous study, a thick silica shell was first grown on AuNP, followed by surface functionalization with aldehyde groups and covalently conjugated with amino-modified oligonucleotides [107]. Despite the potentially higher chemical stability, there was no color change in response to target hybridization due to the thick silica shell. The hybridization-induced color change property of the silica-modified oligo–AuNP conjugate synthesized by the silica reinforcement technique was examined by Maeda's non-crosslink approach [39]. Before hybridization, the silica-modified oligo–AuNP conjugate was incubated in PBS with 10 mM DTT for 3 h. The conjugate remained stable with SPR absorption peak at 522 nm. Upon the addition of the complementary target and NaCl, the SPR absorption peak shifted to 549 nm and the solution color changed from red to purple within 10 min (Figure 2.21). This could be explained by the lower stability of the hybridized conjugate against salt-induced aggregation than the non-hybridized counterpart. To further confirm such hybridization-induced color change, the hybridized conjugate solution was heated at 94 ℃ for 1 min to effect dehybridization. As expected, the SPR absorption peak shifted back (525 nm) and the solution color returned to red.

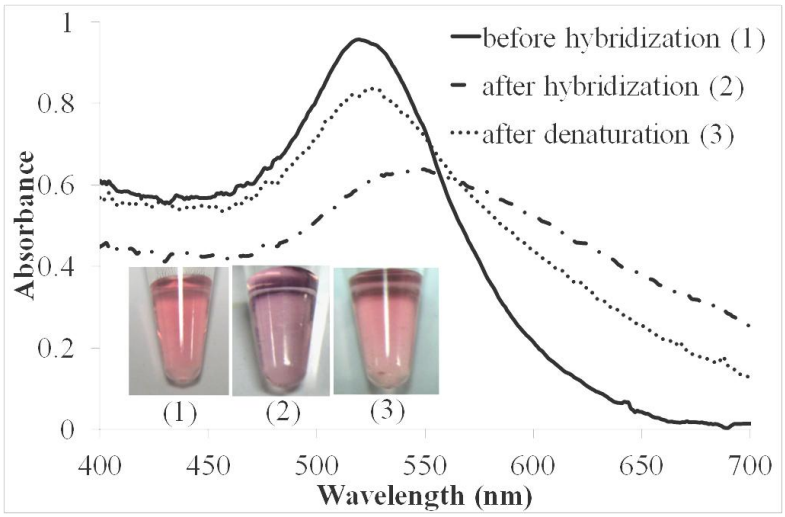

Figure 2.21. UV−vis spectra of the silica-modified oligo−AuNP conjugate (1) before hybridization; (2) after hybridization; and (3) after denaturation. Insets are photographs of the samples (1), (2), and (3).

Melting curve of the capture probe–target hybrid (0.4 μM each) featured a typical sigmoidal shape with a melting temperature of 65 ℃. Interestingly, the melting curves of both the unmodified and silica-modified oligo−AuNP conjugates consisted of two melting phases. The first phase occurred between 25 and 45 ℃, while the second phase occurred above 50 ℃ (Figure 2.22). The first phase is likely due to the aggregation status of the conjugates and the second phase is due to the dehybridization process.

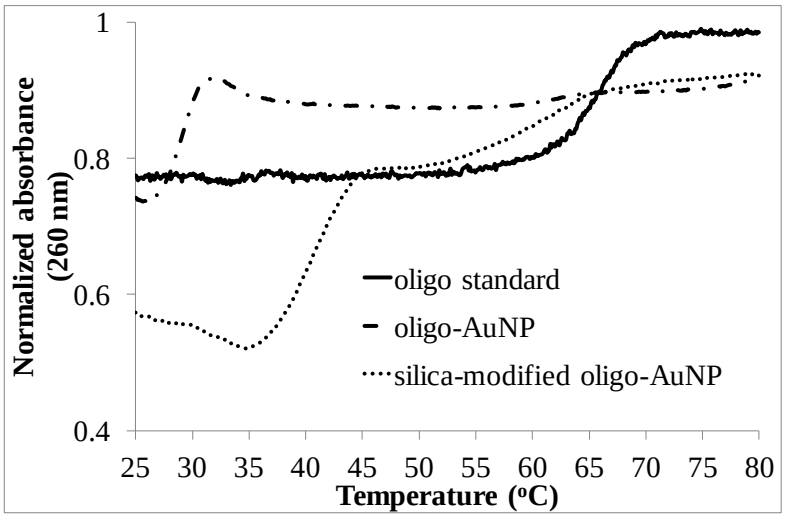

Figure 2.22. Melting curves of the oligonucleotides, oligo–AuNP conjugate and silica-modified oligo–AuNP conjugate.

UV–vis spectra and solution colors provided further evidence for this phenomenon (Figure 2.23). At 25 ℃, the oligo–AuNP and silica-modified oligo–AuNP conjugates were aggregated, hence red shift and broadening of the SPR absorption band were observed, giving rise to a purple-colored solution. At 50 ℃ (indeed below the melting temperature of the capture probe–target hybrid), the SPR absorption band returned to that of the monodispersed state and the solution color appeared red.

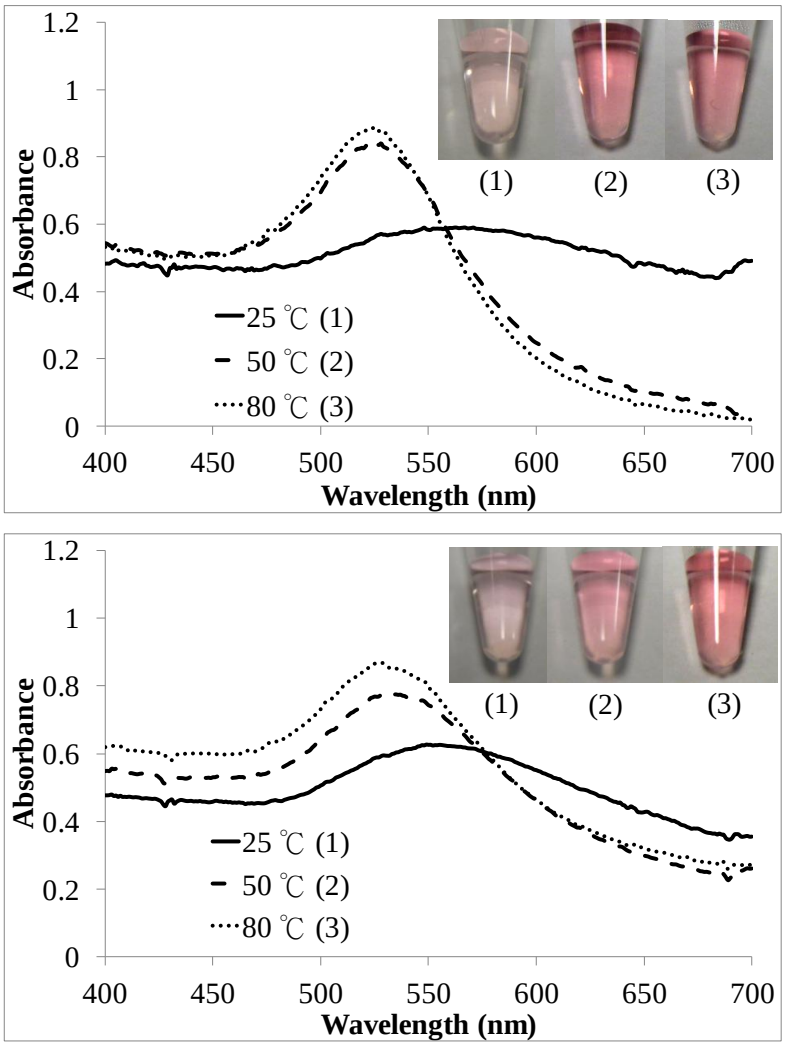

Figure 2.23. UV−vis spectra of the hybridized oligo−AuNP conjugate (top) and silica-modified oligo−AuNP conjugate (bottom) at 25, 50 and 80 ℃. Insets are photographs of the samples (1), (2), and (3).

2.3.4. Thermal Stability

The silica-modified oligo−AuNP conjugate displayed superior chemical stability thanks to the entrapment of the Au−S linkage with a thin silica layer. In fact,

it is very likely that the silica layer would enhance the thermal stability of the oligo–AuNP conjugates. After 2-h incubation at 94 ℃, 65% of the immobilized oligonucleotide desorbed from the unmodified conjugate (Figure 2.24). For the silica-modified oligo–AuNP conjugate prepared with AuNP:MPTMS ratio of $1:10^5$, the amount of desorption decreased to 15%. It should be pointed out that the $1:10^6$ conjugate is slightly thermally more stable than the $1:10^5$ conjugate (11% versus 15% of desorption), although the former one is less stable in DTT than the latter one (Figure 2.14).

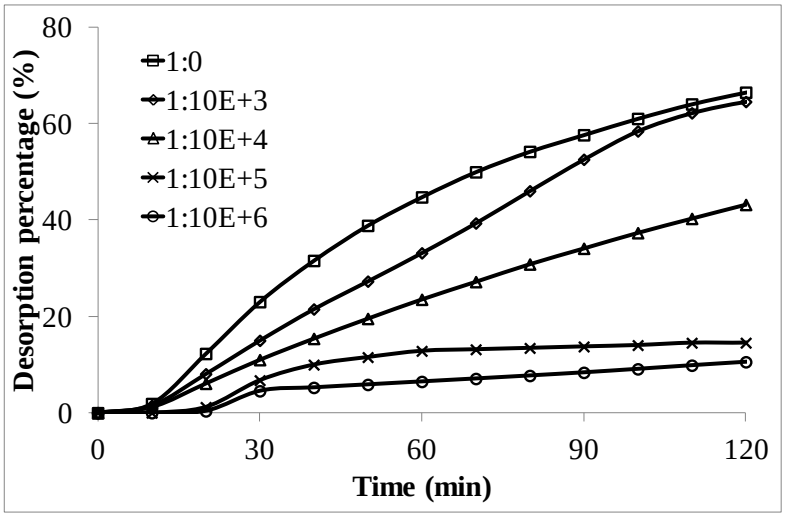

Figure 2.24. Desorption curves of the silica-modified oligo–AuNP conjugates synthesized with different AuNP:MPTMS ratios when incubated at 94 ℃.

Thermal stability at other temperatures (55 and 72 ℃) was also examined (Figure 2.25). The results reveal that the amount of desorption is highly dependent on the incubation temperature. At 55 ℃, no noticeable desorption occurred for both the unmodified and silica-modified oligo–AuNP conjugates. At 72 ℃, the amounts of desorption for the unmodified and silica-modified oligo–AuNP conjugates were 9% and 6%, respectively. Clearly, the thermally stable silica-modified oligo–AuNP conjugate is potentially applicable to high-temperature amplification system such as PCR.

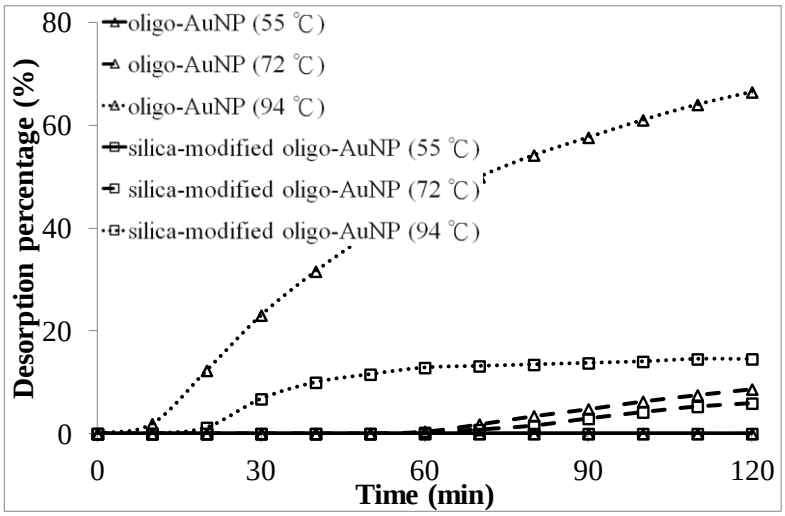

Figure 2.25. Desorption curves of the oligo–AuNP and silica-modified oligo–AuNP conjugates (AuNP:MPTMS = $1:10^5$) at 55, 72 and 94 ℃.

The unmodified and silica-modified oligo–AuNP conjugates were applied to a solution containing 6 mM $MgCl_2$ and 5 μM DTT to perform PCR thermal cycling (Figure 2.26). For the unmodified oligo–AuNP conjugate, 16% of the oligonucleotides were desorbed in the first PCR cycle, which included an initial denaturation step (94 ℃, 1 min). After 25 cycles, 34% of the oligonucleotides were desorbed. For the silica-modified oligo–AuNP conjugate, there were no appreciable desorption up to the first three cycles, and at the end of the PCR thermal cycling, 15% of the oligonucleotides were desorbed.

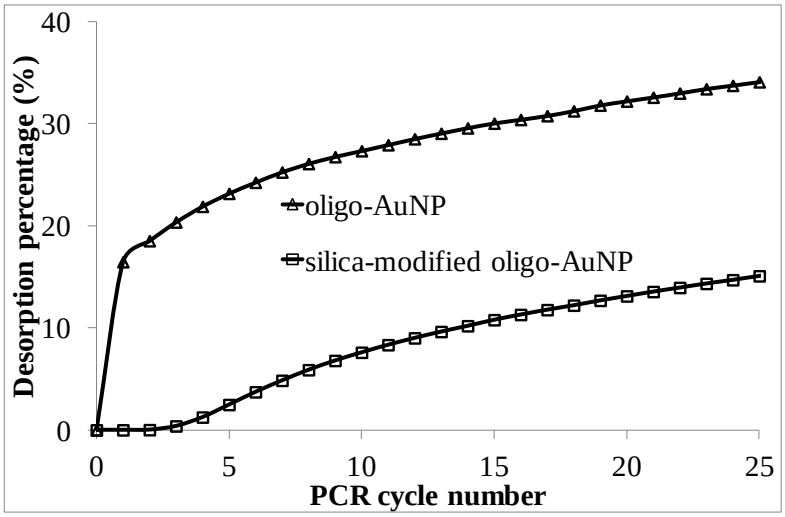

Figure 2.26. Desorption curves of the oligo–AuNP and silica-modified oligo–AuNP conjugates under PCR thermal cycling condition.

2.4. Summary

A facile silica reinforcement method was developed to significantly enhance the chemical and thermal stabilities of the monothiol-modified oligo–AuNP conjugate. The silica-modified conjugate was extremely stable against DTT-induced aggregation. There was no aggregation in 10 mM DTT after 24-h incubation, which compared favorably with the start-of-the-art disulfide- and trithiol-linkage approaches (stable for 1–3 and 8 h, respectively). Key synthesis parameters were optimized including the presence of a PEG_6 spacer for the immobilized oligonucleotide, AuNP:MPTMS ratio ($1:10^5$), and pH (~6 without added phosphate). Quantitative analysis revealed that, in 10 mM DTT for 2 h, the amount of oligonucleotide desorption greatly reduced from 87% for the unmodified oligo–AuNP conjugate to 8% for the silica-modified oligo–AuNP conjugate. Besides, the silica-modified oligo–AuNP conjugate extremely high resistance against oxidative dissolution by sodium cyanide as compared to the unmodified oligo–AuNP conjugate. In addition, the unique hybridization-induced color change property of the oligo–AuNP conjugate was preserved with the silica coating, even after prolonged incubation in high concentration of DTT. Apart from enhanced chemical stability, the silica layer offered higher thermal stability to the oligo–AuNP conjugate. At 94 °C

for 2 h, the amounts of oligonucleotide desorption for the unmodified and modified conjugates were 65% and 15%, respectively. Under PCR conditions, the amounts became 34% and 15%.

Chapter 3

Closed-Tube Gold Nanoparticle-Based Colorimetric Nicking Endonuclease Assisted Amplification

The work described in this chapter was done with the aim of developing a closed-tube colorimetric detection platform with isothermal amplification by nicking endonuclease based on the highly stable silica-modified oligo–AuNP conjugate, produced as described in Chapter 2. Although previous schemes for colorimetric detection of enzymatic amplification products using oligo–AuNP conjugates were simple and sensitive, post-amplification open-tube addition of the conjugates to the reaction mixtures was unavoidable [89-95]. This poses a high risk of carryover contamination. The main reason is the instability of the oligo–AuNP conjugates in the reaction buffers, which contain enzyme stabilizer of DTT or 2-ME. This chapter starts with a brief introduction of various isothermal amplification schemes as well as the developed closed-tube nicking endonuclease-assisted colorimetric detection scheme (Section 3.1). Experimental procedures are detailed in Section 3.2, results and discussion is presented in Section 3.3, and a brief summary is given in Section 3.4.

3.1. Introduction

In colorimetric detection schemes using oligo–AuNP conjugates, the distance between AuNPs should be altered by the presence or absence of target sequence only. Unfortunately, typical enzymatic reactions usually include buffer solutions with high concentrations of thiol-containing small molecule and salt that cause irreversible aggregation of oligo–AuNP conjugates. The salt issue can be addressed by using oligo–AuNP conjugate prepared under high salt concentration. The amount of immobilized oligonucleotides is directly related to the salt concentration during conjugation [113]. The overall negative charge of conjugate is increased by high oligonucleotide density that maintains the stability of the conjugate in the reaction buffer. Another strategy to increase oligonucleotide density is by utilizing oligonucleotide with a PEG_6 spacer, the amount of oligonucleotides that can be chemisorbed onto AuNP surface is 4 times more than that without the spacer.

The presence of thiol-containing small molecule in reaction mixture does not permit a closed-tube colorimetric detection of enzymatic amplification product with oligo–AuNP conjugate. In the amplification techniques described in Section 1.3, the reaction mixtures contained different concentrations of DTT (5 μM to 4 mM) [89-95]. DTT readily displaces oligonucleotides from monothiol-modified

oligo–AuNP conjugates, thereby reducing the overall charge on the conjugates and resulting in salt-induced aggregation. A possible solution is to dilute the reaction buffer in order to minimize the effect of DTT. A report illustrated the reduction of DTT from 4 mM to 50 μM in an isothermal amplification reaction would minimize the aggregate of oligo–AuNP conjugate [114].

Another noteworthy point is that when AuNP surface is exposed due to desorption of oligonucleotides, enzyme would absorb/chemisorb onto the AuNP surface via Au–N/Au–S linkage, which may affect the enzymatic amplification reaction. Additionally, the target/hybridization-induced color change property of the AuNPs would be affected due to the steric and electrostatic stabilization effects offered by the adsorbed enzyme. Therefore, multiple-step approach was adopted to separate enzymatic amplification from AuNP-based colorimetric detection.

As illustrated in Chapter 2, the silica-modified oligo–AuNP conjugate could perform hybridization-induced colorimetric detection even after 3-h incubation in 10 mM DTT. It is very likely that the silica-modified oligo–AuNP conjugate can be coupled to amplification reaction to accomplish a closed-tube colorimetric detection platform. In this chapter, a proof-of-concept experiment with isothermal enzymatic amplification reaction is performed to validate the compatibility of the

silica-modified oligo−AuNP conjugate in enzymatic reaction platform at high DTT concentration and low operating temperature.

3.1.1. Isothermal DNA Amplification

For isothermal DNA amplification, several strategies are available. Strand displacement amplification (SDA) employs two pairs of primers (S1, S2, B1 and B2), where the S1 and S2 primers contain a restriction site for HincII restriction endonuclease (Figure 3.1) [115]. The 3’ ends of the S1 and S2 primers hybridize to a target sequence and are extended in the presence of deoxyguanosine triphosphate (dGTP), deoxycytidine triphosphate (dCTP), 5-methyluridine triphosphate (TTP), and 2'-deoxyadenosine 5'-O-(l-thiotriphosphate) (dATP(αS)). Meanwhile, the B1 and B2 primers hybridize to the target (upstream of the S1 and S2 primers) and are extended, displacing the extended S1 and S2. The displaced strands then act as new templates for producing dsDNAs with the S1 and/or S2 sequences at their ends. Then, HincII nicks the S1 and S2 sequences. It should be noted that HincII would not cleave the complementary strands of the S1 and S2 attributed to the hemiphosphorothioate modification on the synthesized sequence. Subsequently, the nicked S1 and S2 sequences are extended, thereby generating more dsDNAs and

ssDNAs for further amplification. The amplification products are mostly double-stranded, which are not directly applicable to AuNP-based colorimetric detection schemes.

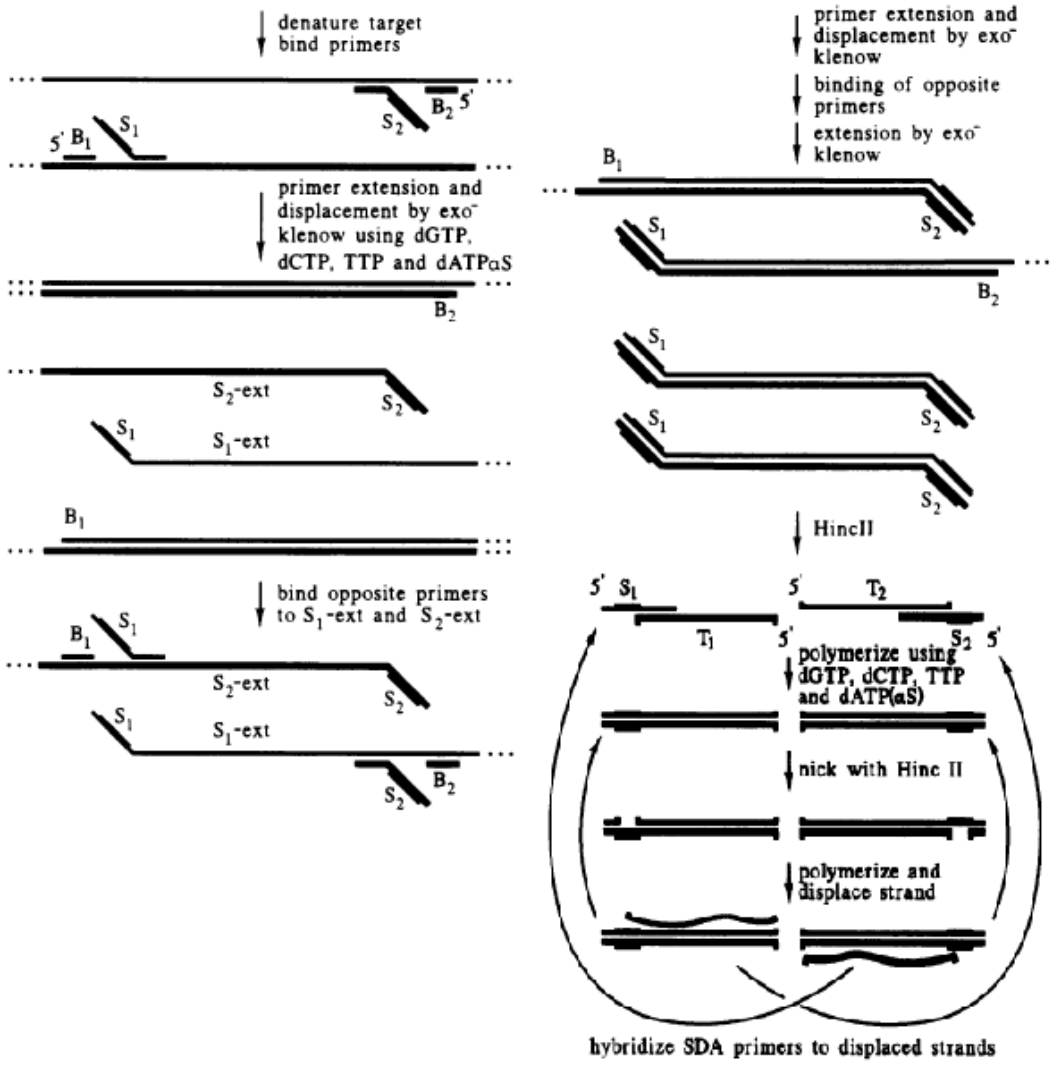

Figure 3.1. Strand displacement amplification (Adapted from [115]).

Rolling circle amplification (RCA) utilizes a polymerase with strand displacement property to extend a primer hybridized to a circular ssDNA template, generating a long ssDNA (Figure 3.2) [116]. For the detection of a linear DNA target, RCA can be coupled to ligation reaction. An initially open circular ssDNA template is used, and upon hybridization with the target and subsequent ligation, a closed circular template is formed for RCA. In this case, a two-step reaction is required.

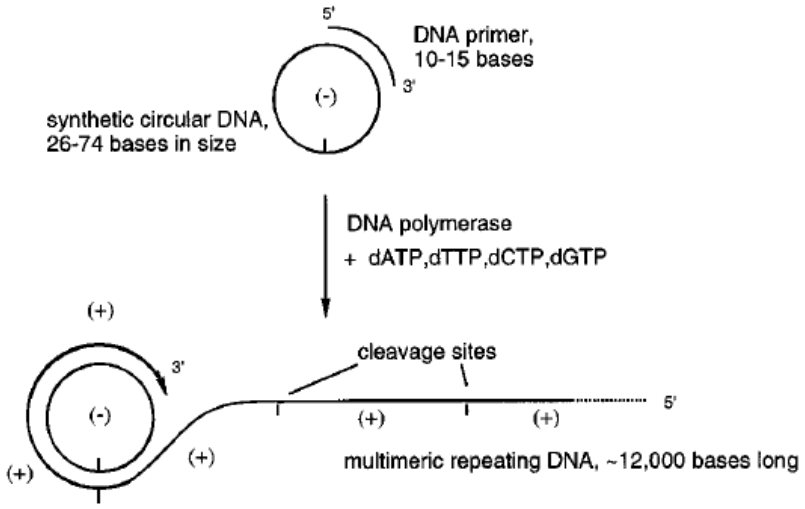

Figure 3.2. Rolling circle amplification (Adapted from [116]).

Loop-mediated isothermal amplification (LAMP) utilizes a set of four primers that recognize six sequences within a specific target and a polymerase having strand displacement ability (Figure 3.3) [117]. The multiple primers impart very high

specificity, but make the sequence design more complicated. The amplified products are very long and double-stranded, which are not directly applicable to AuNP-based colorimetric detection schemes.

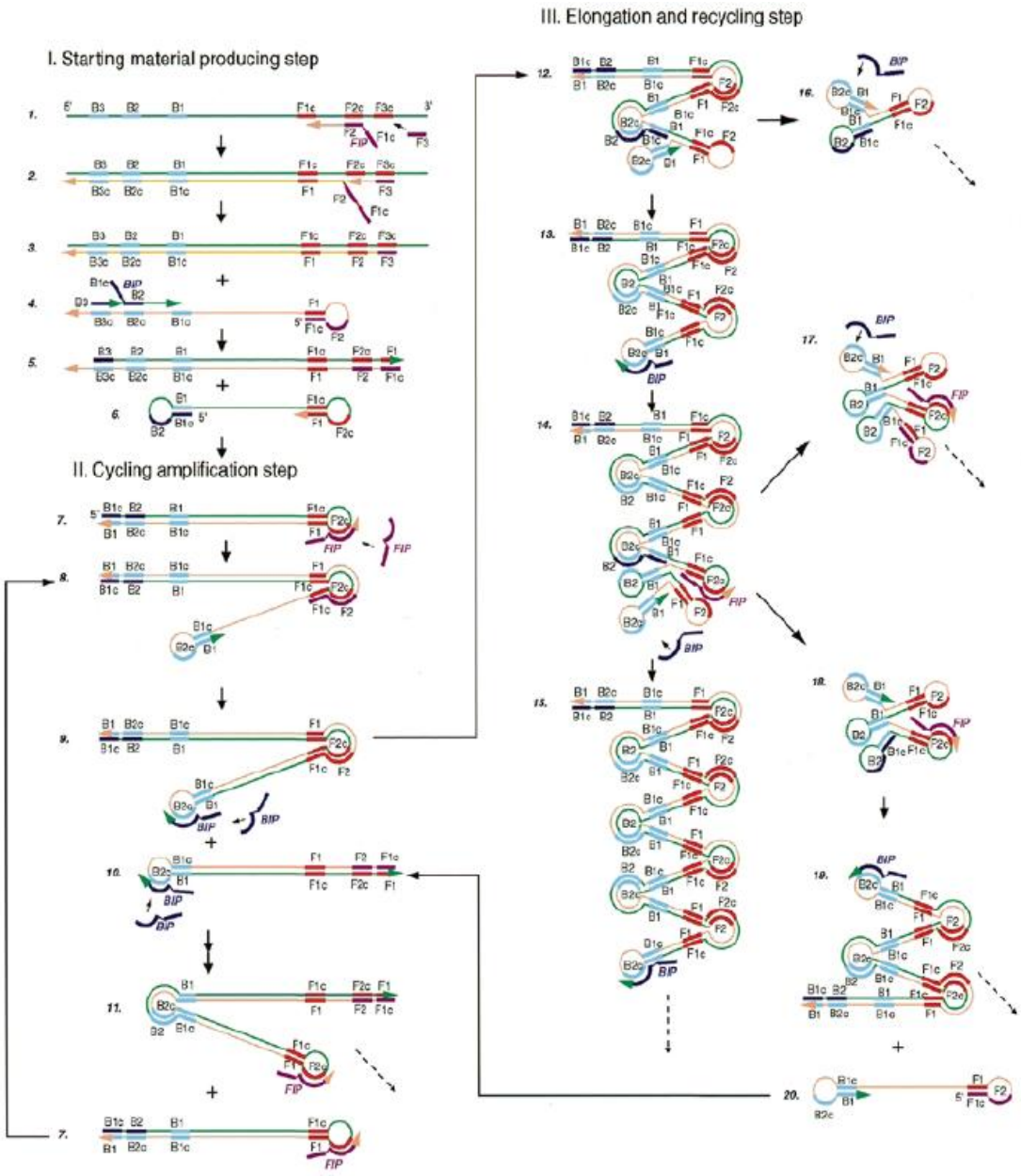

Figure 3.3. Loop-mediated isothermal amplification (Adapted from [117]).

Helicase-dependent amplification (HDA) uses helicase to separate a dsDNA target. After that, primers are hybridized to the target and extended by a DNA polymerase (Figure 3.4) [118]. The process allows target amplification at a single temperature without initial denaturation that is required in the above-mentioned isothermal amplification strategies for the dehybridization of dsDNA target.

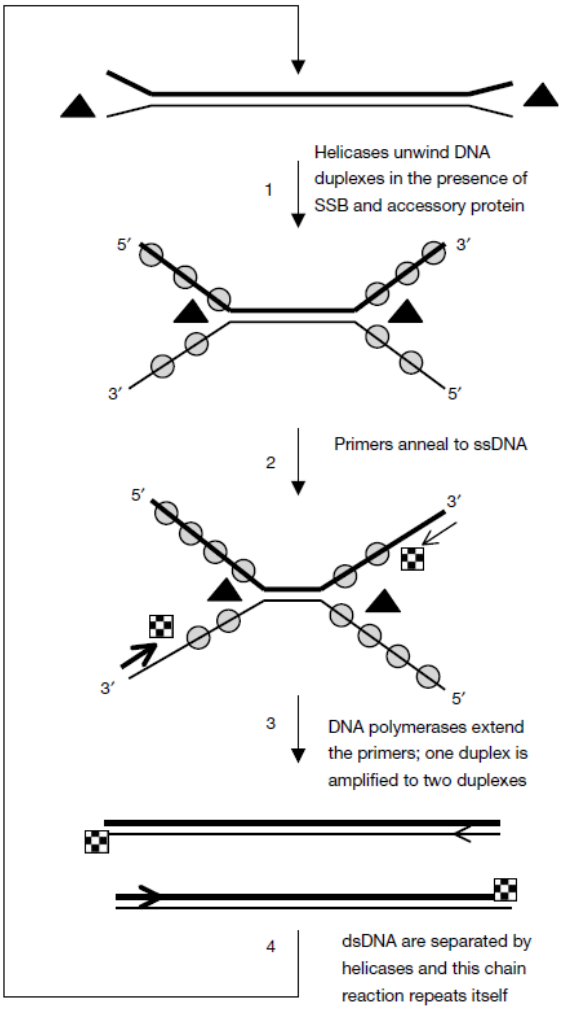

Figure 3.4. Helicase-dependent amplification (Adapted from [118]).

Nicking enzyme signal amplification (NESA) utilizes a beacon consisting of a fluorescent reporter and a quencher at both ends of the sequence, as well as a nicking endonuclease (Figure 3.5) [119]. The fluorescence signal of the beacon is quenched by FRET in its stem–loop configuration. The hybridization between the beacon and a complementary target sequence opens the stem–loop structure, setting the fluorescent reporter and quencher apart and thus the fluorescence signal increases. The nicking endonuclease cleaves the hybridized beacon, the two fragments of which then dehybridize from the target. This allows the target to hybridize with additional beacon for signal amplification.

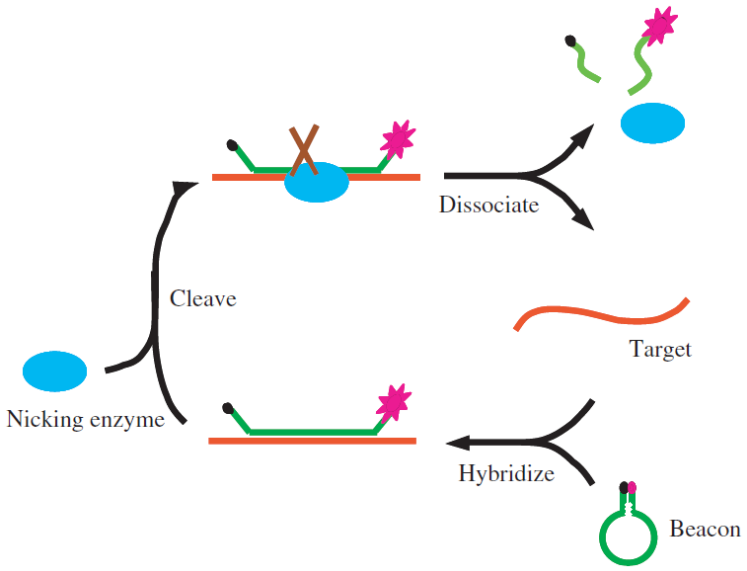

Figure 3.5. Nicking enzyme signal amplification (Adapted from [119]).

Cyclic enzymatic amplification method (CEAM) uses a displacing probe and exonuclease III (Figure 3.6) [120]. The displacing probe is constructed from two ssDNAs of different lengths (the shorter strand binds to the 5’ end of the longer strand), with the shorter strand labeled with a quencher at its 3’ end and the longer strand labeled with a fluorescent reporter at its 5’ end. In the hybridized state, the close proximity of the quencher and reporter results in FRET and the fluorescence signal is low. The presence of a target sequence competes with, and thus displaces, the shorter strand to hybridize with the longer strand, resulting in an increase in the fluorescence signal. The longer strand (in double-stranded state) is then digested by exonuclease III while the target remains intact due to the overhanging 3’ end. Therefore, the target is recycled for signal amplification.

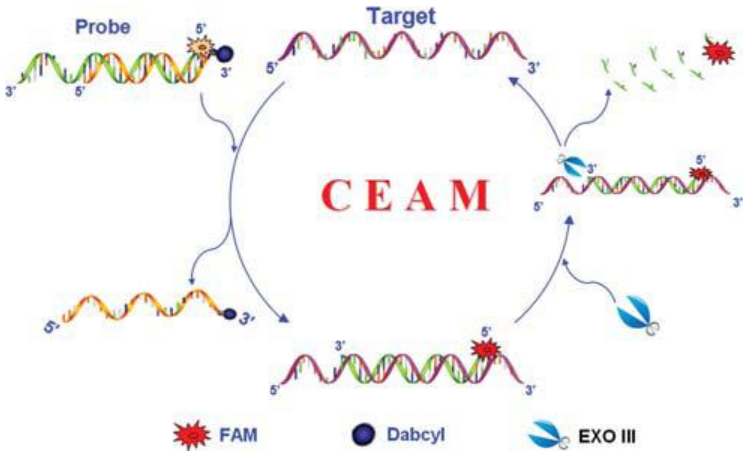

Figure 3.6. Cyclic enzymatic amplification method (Adapted from [120]).

3.1.2. Design of Detection Method

Among the isothermal amplification reaction schemes described above, NESA is an attractive strategy for closed-tube colorimetric isothermal amplification-assisted detection (Figure 3.7) [119]. A beacon of 80 bases long is used, with the first and last seven bases hybridized to form the stem. The hybridization a complementary target to the loop sequence results in the cleavage of the beacon by a nicking endonuclease. The two fragments are 22 and 58 bases long. After the nicking, the melting temperatures of all the complementary sequences become lower than the operating temperature (37 ℃), so dehybridization occurs to release the target and the two fragments from the beacon. For closed-tube colorimetric detection, silica-modified oligo–AuNP conjugate is incorporated into the amplification reaction mixture. The sensing mechanism is based on Meade's non-crosslink approach (detailed mechanism was described in Section 1.2.2.1) [39]. The AuNP-bound sequence is complementary to the 22-base fragment, with a melting temperature higher than 37 ℃. Therefore, at a constant operating temperature of 37 °C, the 22-base fragment hybridizes with the silica-modified oligo–AuNP conjugate, resulting in salt-induced aggregation and the solution change changed from red to purple.

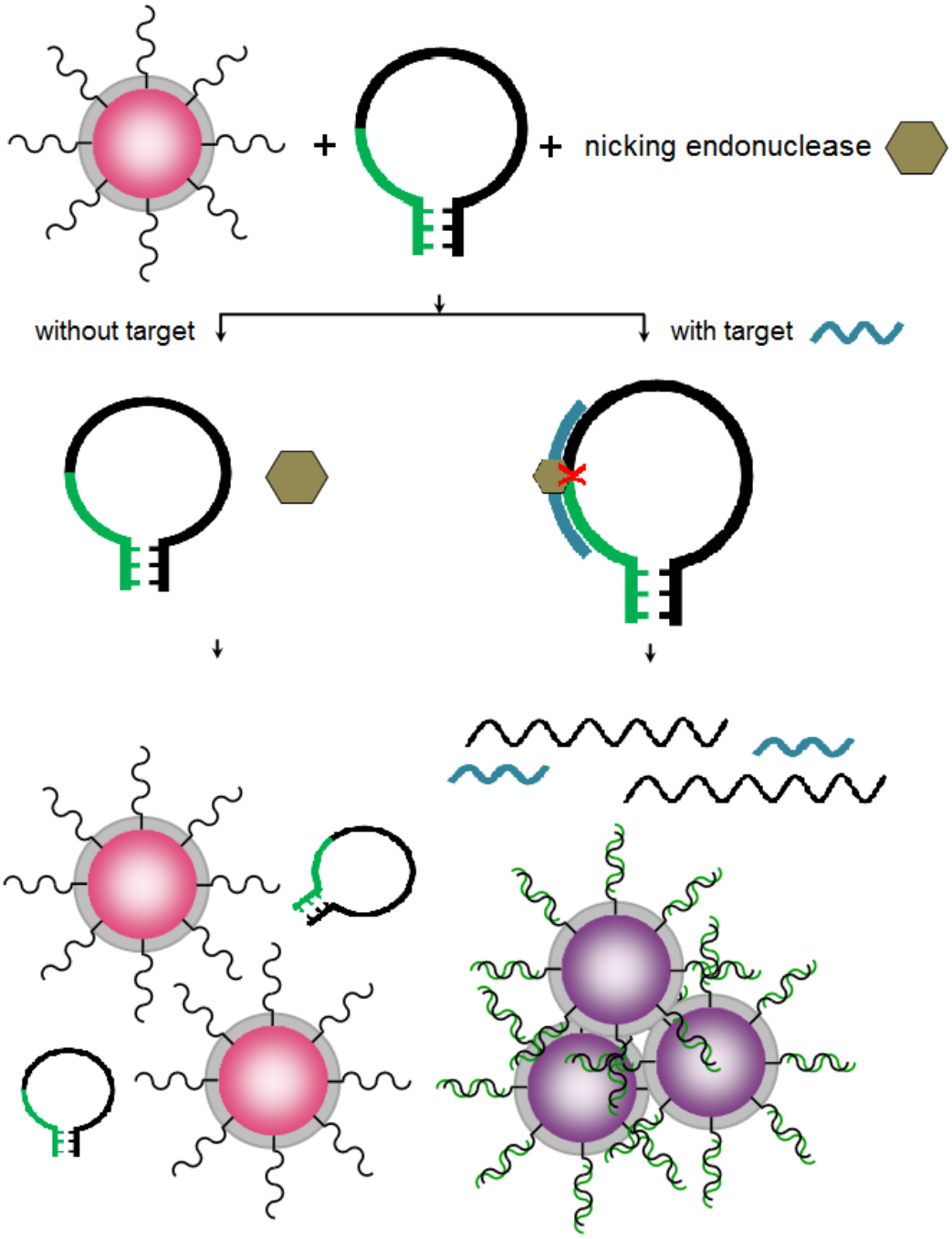

Figure 3.7. Detection scheme of the closed-tube AuNP-based colorimetric nicking endonuclease-assisted amplification.

3.2. Materials and Methods

3.2.1. Materials and Instrumentation

The materials, equipment, and procedures for the synthesis of AuNPs, oligo–AuNP conjugate, and silica-modified oligo–AuNP conjugate were as described in Section 2.2, except that both the unmodified and silica-modified conjugates were aged with 1 M NaCl, and prepared with UltraPure™ DNase/RNase-free distilled water (Invitrogen). Additionally, tris(hydroxymethyl)aminomethane (Tris), boric acid, ethylenediaminetetraacetic acid disodium salt dihydrate (EDTA), and ethidium bromide were purchased from Sigma-Aldrich. Nicking endonuclease (Nb.BbvCI, 10^4 units/mL) was purchased from New England BioLabs (Ipswich, MA, USA). Gel electrophoresis reagents were purchased from Invitrogen. Thermal incubation was done in a GeneAmp® PCR System 9700 (Applied Biosystems). ChemiGenius^2 gel imaging system from Syngene (Frederick, MD, USA) was used for gel visualization and image recording.

3.2.2. Nicking Endonuclease Reaction

The 80-base beacon (5’-CTGCTCCTGTTGAGTTTATTGCTGAGGTTTTTTT TTTTTTTTTTTTTTTTTTTTTTTTTTTTTTTTTTTTTTTGGAGCAG-3’) was

prepared in 1× NEBuffer (50 mM NaCl, 10 mM Tris-HCl, 10 mM $MgCl_2$ and 1 mM DTT, pH 7.9), heated at 94 °C for 5 min and then cooled to 25 °C at a rate of 1 °C/min. Reaction mixture comprised 1× NEBuffer, 4 mM DTT, beacon (0.5 μM) or 30-base linear probe (5'-CTGCTCCTGTTGAGTTTATTGCTGAGGTTT-3', 0.5 μM), target (5'-AAACCTCAGCAATAAAC-3', 0.5 μM) or no-target control, NbBbvCI nicking endonuclease (0.1 units/μL), and nanoparticles (oligo–AuNP or silica-modified oligo–AuNP conjugate, 2.5 nM). The reaction was carried out at 37 °C for 1 h and cooled to room temperature before taken out from the thermal cycler. Colorimetric results and UV–vis spectra were recorded immediately. The mixture was heated at 80 °C for 20 min to terminate the enzymatic reaction.

3.2.3. Gel Electrophoresis

Reaction products (10 μL) were loaded into in a 3% (w/w) agarose gel in 0.5× TBE buffer (45 mM Tris, 45 mM boric acid, 1 mM EDTA, pH 8.0) and electrophoresed at 120 V for 1.5 h. Then, the gel was stained with 1× SYBR® Gold nucleic acid gel stain for 30 min, followed by visualization under UV transillumination and recording with the gel imaging system.

3.2.4. Selectivity and Sensitivity Tests

The specificity of the detection scheme was evaluated by a non-target sequence (5′-GCGAACAATTCAGCGGCTTTA-3′, 0.5 μM). Colorimetric results were recorded after the 1-h reaction. For sensitivity determination, various amounts of the target (1, 10, 100 and 500 nM) were used. Colorimetric results and UV−vis spectra were recorded after the 1-h reaction.

3.3. Results and Discussion

3.3.1. Pre-Amplification Test

Before performing the isothermal reaction, it was necessary to determine whether the reaction conditions would affect the stability of the oligo−AuNP and silica-modified oligo−AuNP conjugates. It was found that the nicking endonuclease reaction buffer caused aggregation of the unmodified oligo−AuNP conjugate at an operating temperature of 37 ℃. At the end of the 1-h incubation, the solution color appeared purple (Figure 3.8). On the other hand, under the same conditions, the silica-modified oligo−AuNP conjugate had no sign of aggregation and appeared red. This was because the silica layer rendered the oligo−AuNP conjugate very high chemical and thermal stabilities by physically blocking DTT from displacing the

immobilized oligonucleotides and entrapping the Au–S linkage, as discussed in Chapter 2.

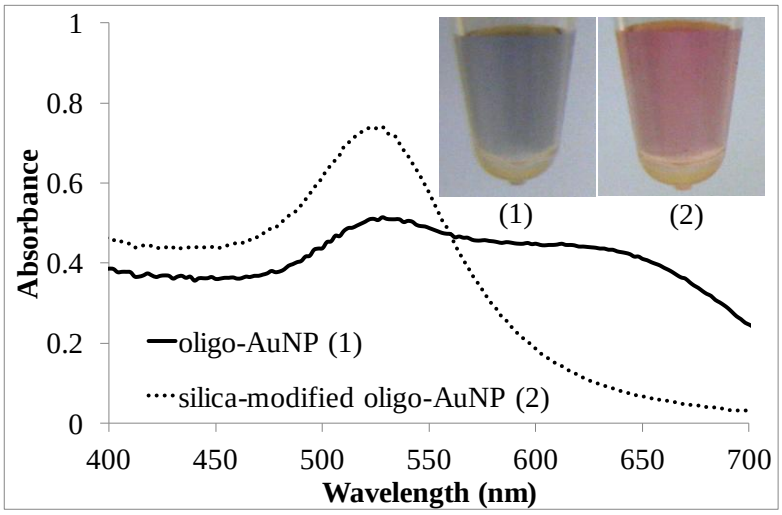

Figure 3.8. UV–vis spectra of the unmodified and silica-modified oligo–AuNP conjugates incubated in the isothermal reaction buffer at 37 ℃. Insets are photographs showing the colors of the samples after 1-h incubation.

Another essential aspect is that the color change should only take place upon the hybridization of the 22-base fragment of the nicked beacon with the silica-modified oligo–AuNP conjugate. In fact, a 30-base linear probe was originally used. Similar to the 80-base beacon, a 22-base fragment was generated after hybridization with the target and nicking reaction. However, when the 30-base linear

probe (0.5 μM) was added to the silica-modified oligo–AuNP conjugate in the nicking amplification reaction buffer, the solution color turned purple within 10 min. Precipitation was observed after 1-h incubation (Figure 3.9). This result indicates hybridization occurs between the linear probe and the modified conjugate that facilitates the salt-induced aggregation. Therefore, the 30-base linear probe is not suitable for closed-tube detection.

In view of this, the 80-base beacon was used to retard hybridization with the silica-modified oligo–AuNP conjugate. Additional energy was needed to dehybridize the stem–loop structure prior to hybridization with the modified conjugate. Besides, approximately 40 bases length is maintained after the formation of beacon. In order for the beacon to hybridize with the AuNP-bound sequence (22-base), the bulky non-hybridizing loop portion has to be brought close to the AuNP surface, which presents huge steric hindrance for hybridization to occur. When the beacon was incubated with the silica-modified oligo–AuNP conjugate for 1 h, the solution color remained red (Figure 3.9).

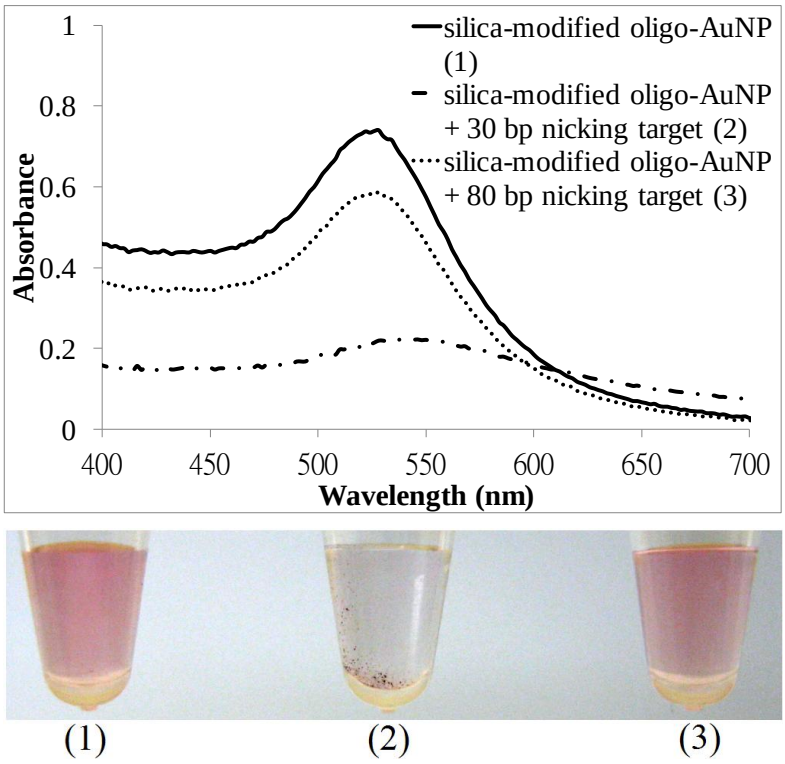

Figure 3.9. Top: UV–vis spectra of the silica-modified oligo–AuNP conjugate incubated with the 30-base linear probe or 80-base beacon in the isothermal nicking amplification reaction buffer at 37 ℃ for 1 h. Bottom: Photographs showing the colors of the samples after 1-h incubation.

3.3.2. Selectivity Test

Nicking endonuclease-assisted amplification was first performed without the silica-modified oligo–AuNP conjugate. Gel electrophoresis result of the no-target control showed a single band (Figure 3.10, lane 1), while the target-containing sample had two additional bands of shorter lengths (lane 2). This indicates that the

nicking endonuclease reaction is working properly. Moreover, the results indicate that the 80-base beacon can successfully recognize the specific target sequence. The selectivity of the platform was evaluated with a non-complementary sequence (non-target). As expected, the gel electrophoresis result showed a single band (lane 3), suggesting that the non-target did not hybridize with the beacon and thus no nicking reaction took place. When the sample contained both the target and non-target, three bands were observed (lane 4). With these, the detection platform was confirmed to be target-specific.

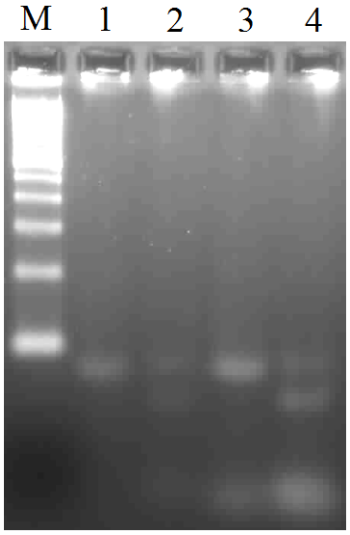

Figure 3.10. Gel electrophoresis results showing the nicking endonuclease-assisted amplification. Lane M: 100 bp ladder; lane 1: no target; lane 2: target; lane 3: non-target; and lane 4: both target and non-target.

Similar experiments were performed with the addition of the silica-modified oligo–AuNP conjugate (Figure 3.11). Gel electrophoresis results were consistent with that without the silica-modified oligo–AuNP conjugate. This confirms that the presence of the silica-modified oligo–AuNP conjugate has negligible influence on the isothermal nicking endonuclease-assisted amplification reaction.

It should be noted that 2.5 nM of the silica-modified oligo–AuNP conjugate was applied in this detection platform. Therefore, colorimetric results could be observed easily. For the samples containing the target (sample 2: target only; sample 4: target and non-target), the silica-modified oligo–AuNP conjugate aggregated and precipitated, while for the samples without the target (sample 1: no target; sample3: non-target), the silica-modified oligo–AuNP conjugate remained monodispersed and the solution color appeared red. As mentioned earlier, the detection scheme was based on the non-crosslink mechanism that the hybridization between the silica-modified oligo–AuNP conjugate and the 22-base complementary sequence from the nicked beacon lowered the conjugate's stability against salt-induced aggregation. It is interesting to note that the precipitate was red in color instead of grayish purple as in non-enzymatic system (i.e., hybridization with pure target).

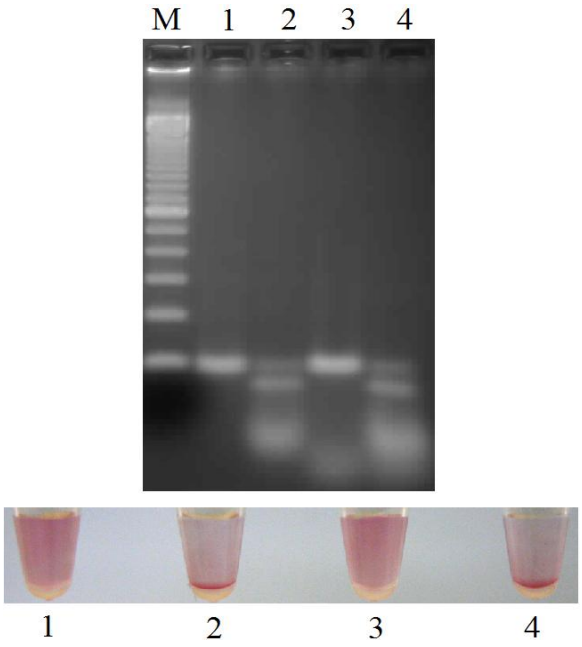

Figure 3.11. Top: Gel electrophoresis results showing the nicking endonuclease-assisted amplification with the silica-modified oligo–AuNP conjugate. Lane M: 100 bp ladder; lane 1: no target; lane 2: target; lane 3: non-target; and lane 4: both target and non-target. Bottom: Colorimetric results of the samples.

3.3.3. Sensitivity Test

The sensitivity of the detection platform was examined by applying various target concentrations. It was found that the intensity of the cleavage products was greatly diminished in gel electrophoresis when the target concentration was equal to or less than 10 nM for samples without and with the silica-modified oligo–AuNP conjugate (Figure 3.12, lanes 1–3 and 6–8). Aggregation of the silica-modified

oligo–AuNP conjugate occurred when the target concentration was equal to or higher than 100 nM, which was consistent with the gel results (lanes 9 and 10). UV–vis spectra of the samples with high target concentration (i.e., 100 and 500 nM) exhibited red shift of the SPR absorption peak (542 nm) as compared with that of the low target concentration samples (520 nm, Figure 3.13).

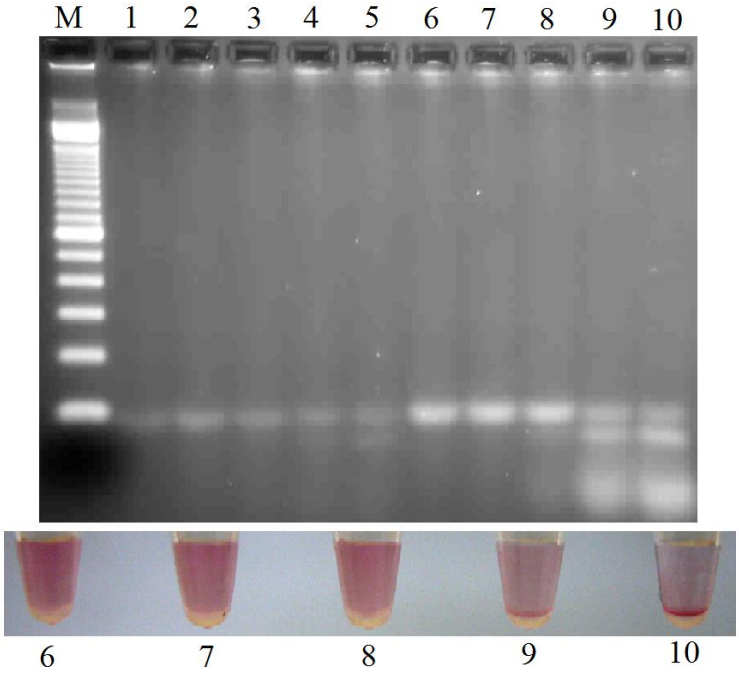

Figure 3.12. Top: Gel electrophoresis results showing the nicking endonuclease-assisted amplification with the silica-modified oligo–AuNP conjugate. Lane M: ladder; lane 1–5: control without conjugate; lanes 6–10: with conjugate; 0, 1, 10, 100, and 500 nM target were added in lanes 1–5 and 6–10, respectively. Bottom: Colorimetric results of the samples.

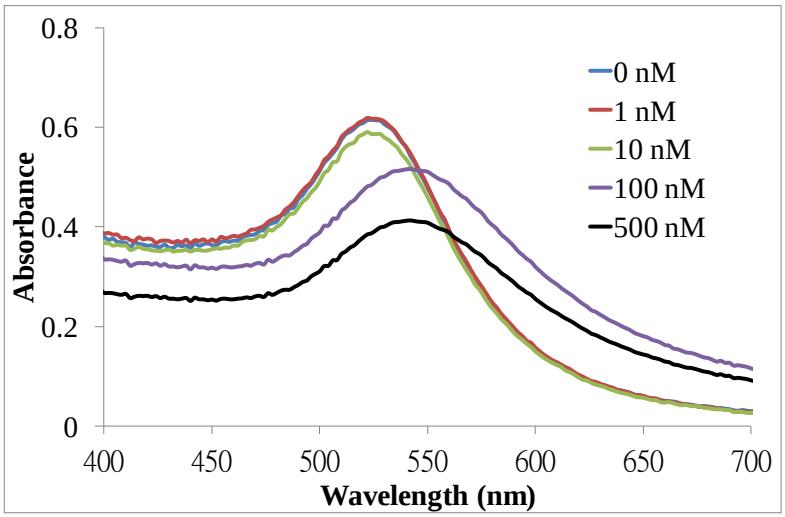

Figure 3.13. UV–vis spectra of the nicking endonuclease-assisted amplification reaction mixture containing the silica-modified oligo–AuNP conjugate with different target concentrations (0, 1, 10, 100 and 500 nM).

The absorbance ratio between 520 and 650 nm could be used as a semi-quantitative indicator to tell whether the concentration of the target in a sample has reached a certain threshold (Figure 3.14). For the monodispersed samples (i.e., 10 nM or below) the absorbance ratio (520 nm/650 nm) was about 10, while for the aggregated samples (i.e., 100 nM or above), the absorbance ratio was about 2. This enables semi-quantitative DNA analysis in point-of-care and on-site setting using a simple and portable colorimeter.

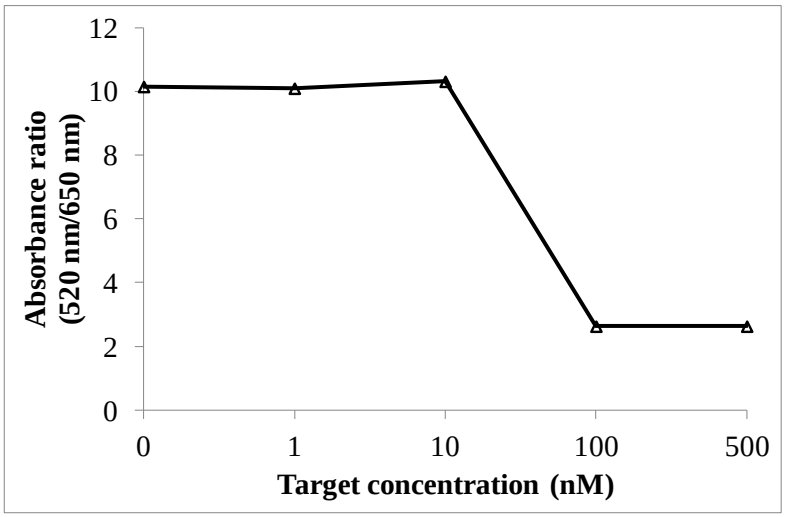

Figure 3.14. Plots of absorbance ratio (520 nm/650 nm) versus target concentration for the nicking endonuclease-assisted amplification reaction mixture containing the silica-modified oligo–AuNP conjugate.

It was believed that the low sensitivity of the current platform was probably due to the inefficient nicking amplification reaction. Therefore, 10 times higher concentration of nicking endonuclease (1 unit/μL) was applied into the same reaction mixture to examine the sensitivity of the platform. The detection limit was 100 nM (Figure 3.15), which did not show significant improvement as compared to the lower concentration one (0.1 unit/μL, Figure 3.12). It was known that the non-crosslink approach required higher target concentration [39] than the crosslink approach [37] to effect aggregation. Indeed, 100-fold improvement in sensitivity could be attained

by using the crosslink approach. Besides, the sequence design of the beacon can be further optimized to achieve more efficient hybridization with the target along with target-induced dehybridization of the stem.

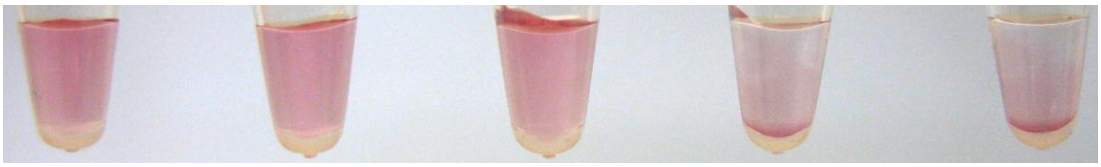

Figure 3.15. Colorimetric results of the nicking endonuclease-assisted amplification reaction mixture with the silica-modified oligo–AuNP conjugate containing 0, 1, 10, 100 and 500 nM of the target (from left to right). The concentration of the nicking endonuclease was 1 unit/μL.

3.4. Summary

Closed-tube colorimetric detection of nicking endonuclease-assisted amplification reaction was accomplished successfully with the silica-modified oligo–AuNP conjugate. The unmodified oligo–AuNP conjugate aggregated in the nicking endonuclease reaction buffer containing 10 mM $MgCl_2$ and 5 mM DTT, while the silica-modified oligo–AuNP conjugate was very stable.

The 80-base beacon hybridized with the specific target and cleaved by the

nicking endonuclease, generating the 22-base fragment which hybridized with the silica-modified oligo–AuNP conjugate for visual readout. The sensitivity of the unoptimized platform was determined to be 100 nM, consistent with the gel electrophoresis results. Besides, for samples with target concentration equal to or higher than 100 nM, the absorbance ratio of 520 nm/650 nm after 1-h reaction was ~2, whereas for samples with target concentration equal to or lower than 10 nM, the ratio was ~10.

Chapter 4

Closed-Tube Gold Nanoparticle-Based Colorimetric Polymerase Chain Reaction

The work described in this chapter was done with the aim of achieving colorimetric detection with high sensitivity by incorporating the silica-modified oligo–AuNP conjugate into PCR. Section 4.1 describes PCR principle and the conventional detection methods, key issues associated with the incorporation of AuNPs into PCR mixture, as well as the design of the new closed-tube colorimetric PCR detection platform. Section 4.2 details the experimental methods, Section 4.3 presents the results and discussion, and Section 4.4 gives a brief summary.

4.1. Introduction

PCR is a molecular biology technique for exponential enzymatic amplification of DNA. The technique is used in medical and biological research laboratories for a variety of tasks [121]. It is an in vitro method involving a repeated temperature cycling process. Key reaction components include DNA polymerase, four deoxyribonucleoside triphosphates (dNTPs), DNA template, and two oligonucleotide primers that hybridize to the region of interest. The amplification involves three

temperature steps, namely denaturation, annealing, and extension (Figure 4.1).

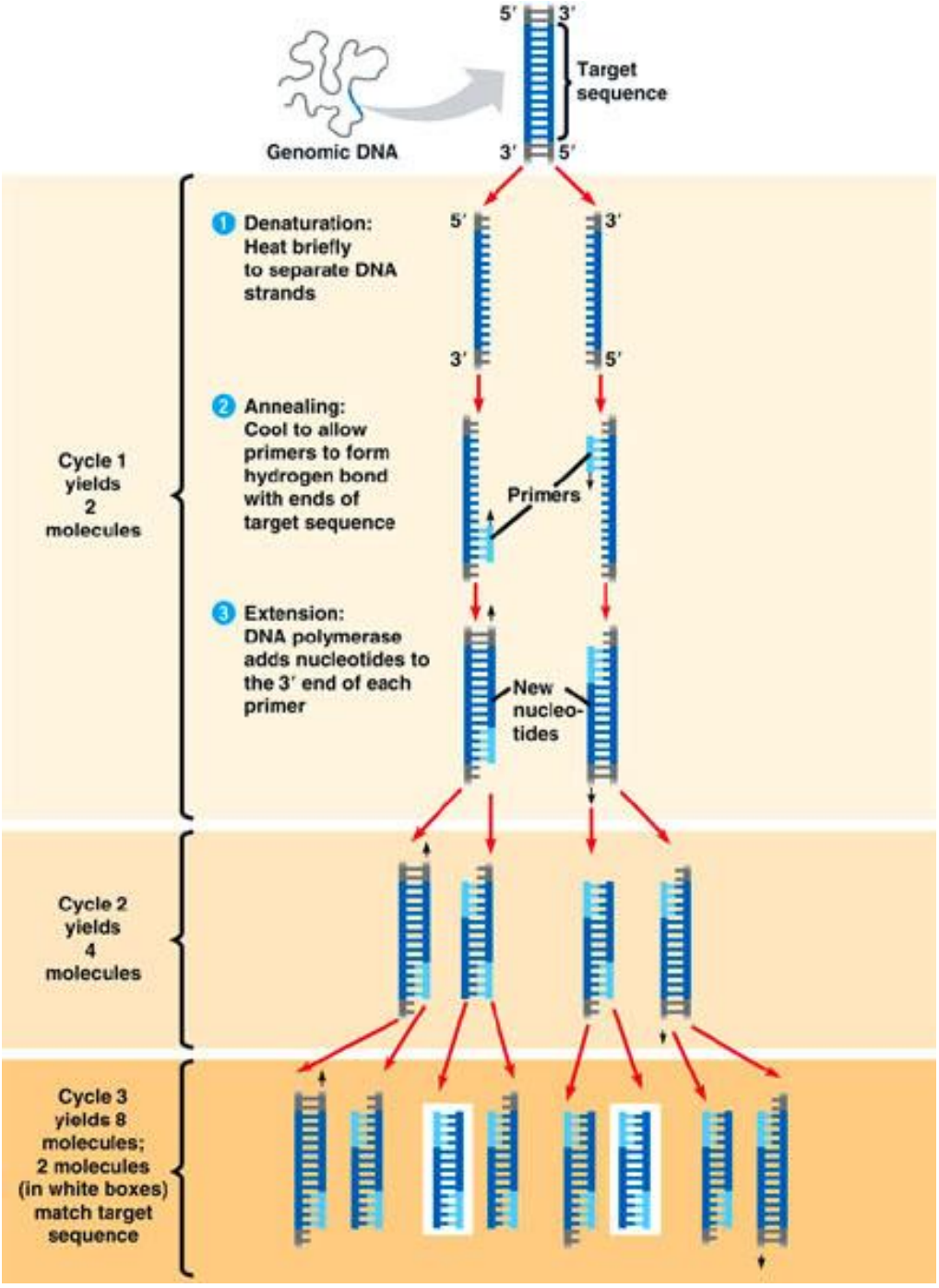

Figure 4.1. PCR method (Adapted from [122]).

In the denaturation step, double-stranded DNA template/amplicon is separated into single-stranded counterparts at 94 °C for about 30 s. Then, in the annealing step, the primers hybridize to the denatured template/amplicon at 55–65 °C (depending on the primers' melting temperatures) for about 30 s. And in the extension step, the primers are extended by Taq DNA polymerase at 72 °C (about 1 min per 1,000 bases). Large quantity of the target sequence can be obtained by repeating the amplification process for 25 to 40 cycles as the double-stranded amplicon from each cycle becomes new template for amplification in the remaining cycles.

Conventionally, agarose gel electrophoresis with ethidium bromide stain is conducted to determine the presence of amplified target in the reaction mixture after PCR. Gel electrophoresis is only a qualitative method for the analysis of target sequence. Quantitative analysis can be achieved by real-time PCR using fluorescent DNA binding agent, hydrolysis probe, and hybridization probe (Figure 4.2) [123]. For fluorescent DNA binding agent, fluorescence intensity greatly increases after binding to dsDNA. As the amount of dsDNA increases tremendously in a positive sample that contains a specific target sequence, therefore high fluorescence intensity is observed.

Hydrolysis probe consists of a ssDNA probe with a reporter dye and a quencher

dye labeled at its two ends. The fluorescence signal emitted from the reporter dye is absorbed by the quencher dye due to FRET if the ssDNA probe is intact. The probe hybridizes with the template/amplicon adjacent to the 3’ end of the primer binding site during the annealing step. Extension of the primer causes the hydrolysis cleavage of the probe by the 5’ to 3’ exonuclease action of DNA polymerase. The reporter dye is no longer quenched after the cleavage and thus the fluorescence signal increases.

Hybridization probe utilizes two ssDNA probes, one is labeled with a donor dye and the other one is labeled with an acceptor dye. When the two probes hybridize to the template/amplicon during the annealing step, which brings the donor and acceptor very close to each other, the emission from the donor can then excite the acceptor by FRET. Therefore, the fluorescence signal from the acceptor increases and can be used to monitor the generation of specific amplicon during PCR.

These real-time PCR methods allow simultaneous amplification and detection without opening the reaction tubes, while gel electrophoresis requires off-tube analysis of the amplification product. However, one major drawback of real-time PCR is its high cost when compared with the conventional PCR as a result of the fluorescent dyes as well as sophisticated fluorescence imaging equipment. In view of

this, it is highly desirable to develop a PCR method that is cost effective and adopts a closed-tube analysis format. One attractive platform would be closed-tube colorimetric PCR using oligo–AuNP conjugate.

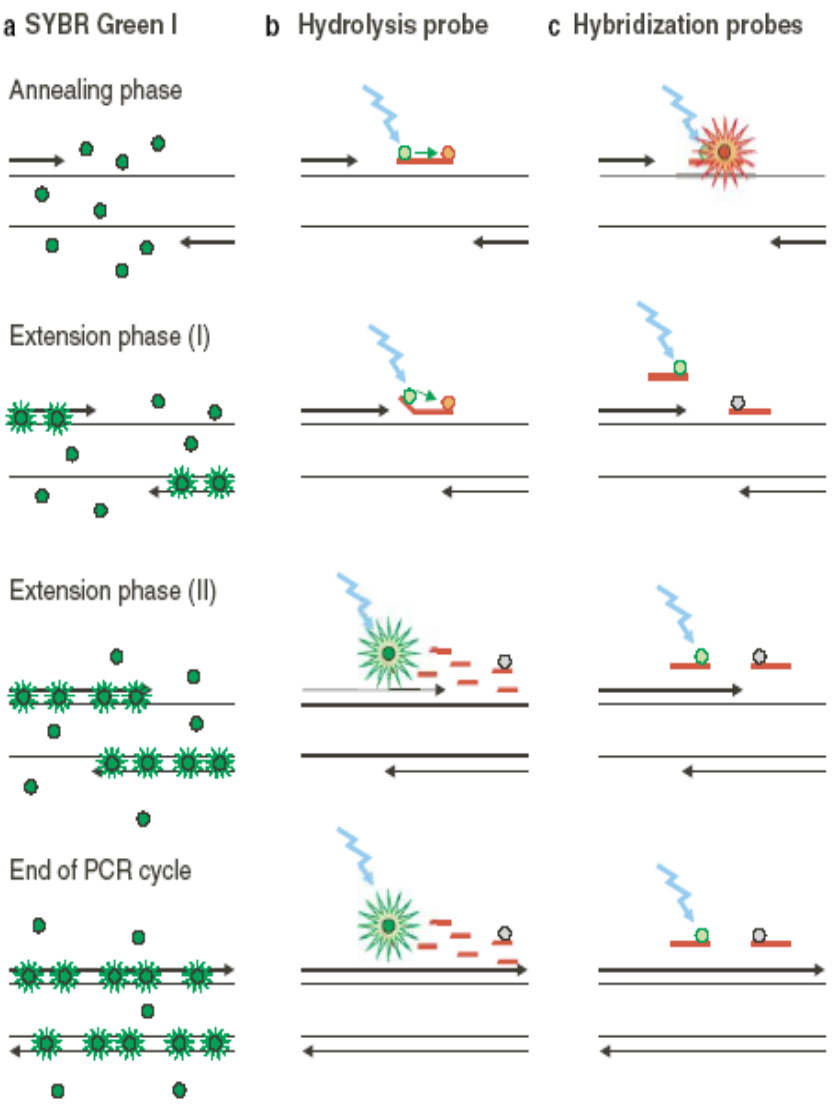

Figure 4.2. Real-time PCR methods (Adapted from [123]).

4.1.1. Polymerase Chain Reaction with Gold Nanoparticles

The first demonstration of the incorporation of AuNPs into PCR mixture was not for colorimetric detection but for specificity enhancement [124]. It was reported that AuNPs could enhance the specificity of PCR by acting as single-strand binding protein to minimize mismatched binding of primers. Non-specific amplification in a two-round PCR process was effectively minimized by adding an appropriate concentration of AuNPs into the reaction mixture (Figure 4.3). Nevertheless, the PCR efficiency diminished as the concentration was above 0.8 nM. Another issue is that the concentration is too low for colorimetric detection, if possible at all. It should be note that the concentration of AuNPs should be above 1 nM (for 15 nm AuNPs) for visually noticeable color.

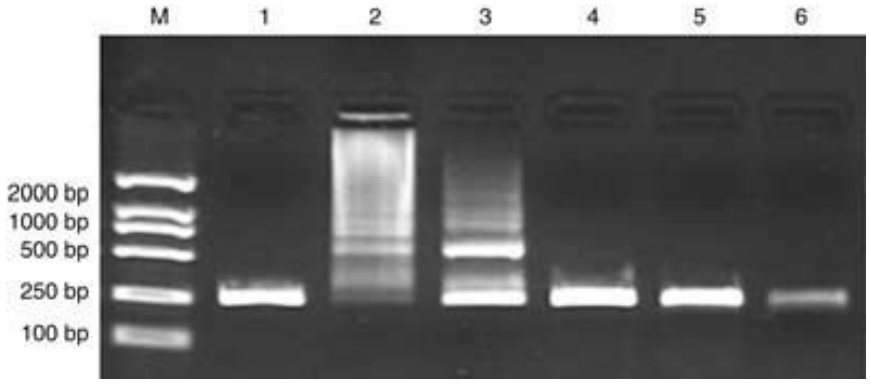

Figure 4.3. PCR specificity analysis with 0.6, 0, 0.2, 0.4, 0.8, and 1 nM of AuNPs (lanes 1–6) (Adapted from [124]).

PCR efficiency could be improved by adding 0.7 nM of AuNPs, particularly for fast thermal cycling [125]. With one-sixth of the ordinary PCR cycling time, control sample (without AuNPs) with 10^9 copies gave positive result, while sample with AuNPs required 100-fold less (10^7 copies) to give positive result (Figure 4.4). This phenomenon was contributed to the excellent heat transfer property of AuNPs.

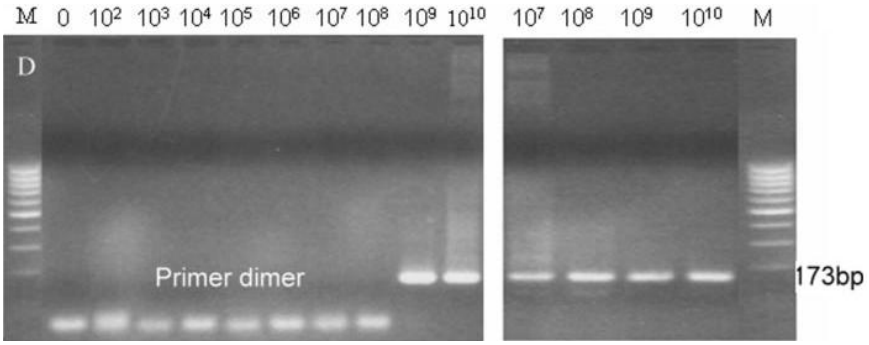

Figure 4.4. PCR efficiency analysis with various target concentrations under reduced fast PCR cycling (left: control without AuNPs; right: with AuNPs) (Adapted from [125]).

In a later study, it was discovered that the presence of AuNPs in PCR mixture favored the formation of smaller amplicons, no matter the primers were specific or not [126]. The experiments utilized one forward primer and three reverse primers, which had zero, one, and two mismatches with corresponding binding sites on the

template (Figure 4.5). This combination would generate three amplicons with three different lengths. The shortest amplicon had two mismatches while the longest amplicon was perfectly matched. It was found that the shortest amplicon was preferentially produced when more and more AuNPs were added. Similar results were observed with reducing amounts of DNA polymerase. Hence, it is likely that this phenomenon is due to the non-specific adsorption of enzyme onto AuNP surface.

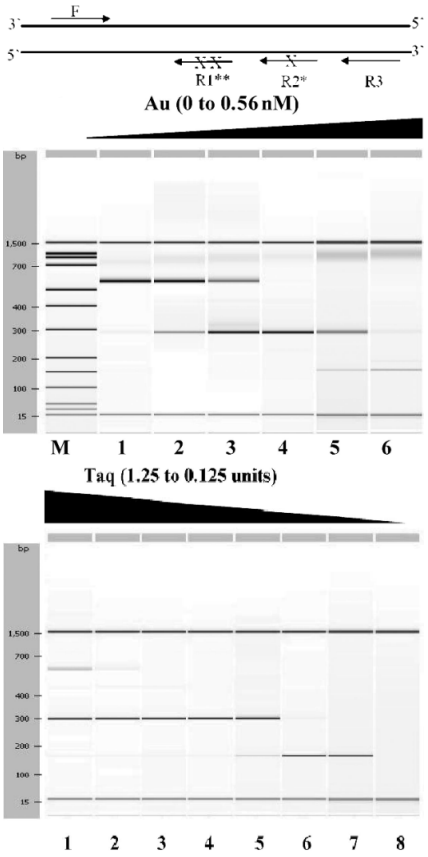

Figure 4.5. PCR specificity analysis with different concentrations of AuNPs and Taq DNA polymerase (Adapted from [126]).

Although high concentration of AuNPs allows easier determination of color change, PCR inhibition becomes another important issue [127]. It was discovered that total PCR inhibition happened for various sizes of AuNPs having similar total surface area (~1.3×10^{13} nm^2). This indicated that the adsorption of polymerase onto AuNP surface was responsible for the inhibition.

The high temperature steps in the PCR thermal cycling process, especially the denaturation step at 94 ℃, would trigger the dissociation of chemisorbed oligonucleotides from oligo–AuNP conjugate and thus irreversible particle aggregation [96]. It was found that the higher the temperature, the higher the rate of oligonucleotide desorption from the AuNP surface (Figure 4.6). The dissociation resulted in the exposure of bare AuNP surface and non-specific adsorption of DNA polymerase, thereby inhibiting PCR. Moreover, the adsorbed enzyme would affect the hybridization-induced color change property of the oligo–AuNP conjugate. Therefore, all the AuNP-based colorimetric PCR detection platforms reported so far required post-amplification addition of AuNP probes [89-92]. This open-tube format poses a serious concern of carryover contamination.

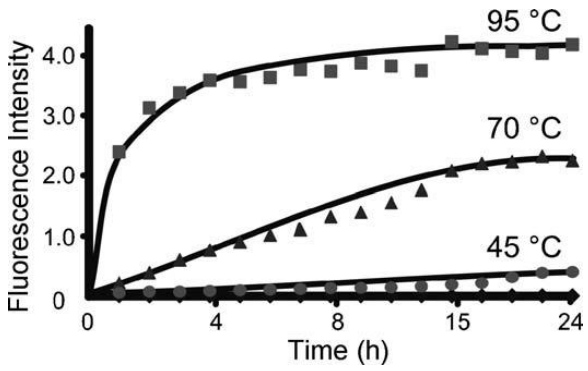

Figure 4.6. Plots of the amount of oligonucleotides desorbed from oligo–AuNP conjugates at different temperatures (Adapted from [96]).

4.1.2. Design of Detection Method

Taking advantage of the high thermal stability of the silica-modified oligo–AuNP conjugate in PCR buffer when subjected to thermal cycling (Section 2.3.4), a closed-tube colorimetric PCR detection platform is developed. The detection scheme (Figure 4.7) is based on Meade's non-crosslink approach (detailed mechanism was described in Section 1.2.2.1) [39]. The capture probe on the silica-modified oligo–AuNP conjugate is labeled with a phosphate group at its 3' end to prevent extension that might affect target amplification and colorimetric detection. The capture probe is complementary to one of the two primers (termed as Primer 1). In the absence of the target, Primer 1 remains intact after PCR and hybridizes with the silica-modified oligo–AuNP conjugate, thereby leading to particle aggregation

and the solution color turns purple. In the presence of the target, both primers are extended and give rise to double-stranded amplicon. Hence, Primer 1 is no longer available to trigger the aggregation and the solution remains red.

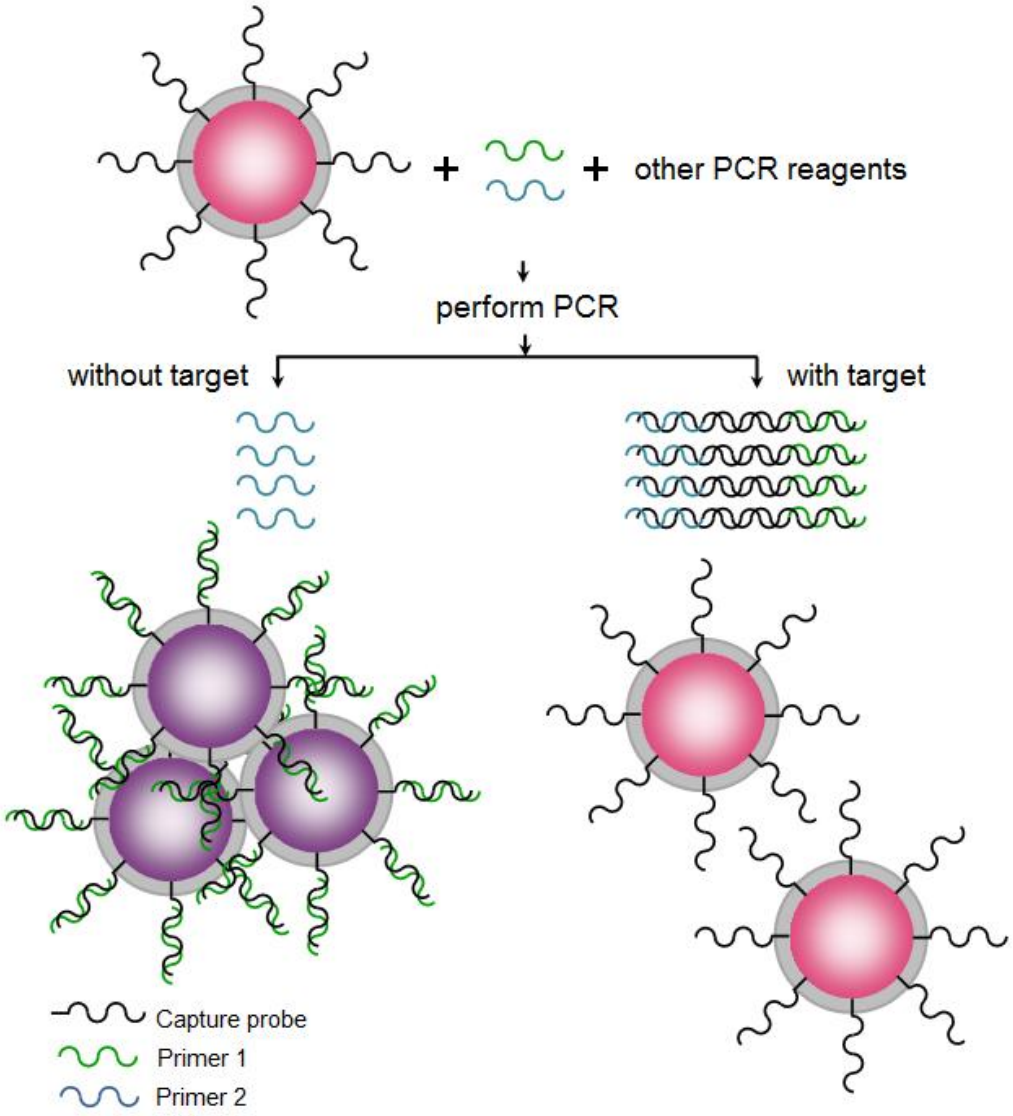

Figure 4.7. Detection scheme of closed-tube AuNP-based colorimetric PCR.

4.2. Materials and Methods

4.2.1. Materials and Instrumentation

The materials, equipment, and procedures for the synthesis of AuNPs, oligo–AuNP conjugate, and silica-modified oligo–AuNP conjugate were as described in Section 2.2, except that both the unmodified and silica-modified conjugates were prepared with UltraPure™ DNase/RNase-free distilled water (Invitrogen). Tris(hydroxymethyl)amino-methane (Tris), boric acid, ethylenediaminetetraacetic acid disodium salt dihydrate (EDTA), and ethidium bromide were purchased from Sigma-Aldrich. Bovine serum albumin (BSA) and amplification targets (ϕX174 and pBR322) were purchased from New England BioLabs. PCR and gel electrophoresis reagents were purchased from Invitrogen.

PCR was done in a GeneAmp® PCR System 9700 (Applied Biosystems). ChemiGenius^2 gel imaging system from Syngene was used for gel visualization and image recording.

4.2.2. Polymerase Chain Reaction

PCR mixture comprised 1× PCR buffer, $MgCl_2$ (1.5 or 6.5 mM), dNTPs (0.2 mM each), Primer 1 (complementary to the capture probe: 5′-CTGCTCCTGTTGAGTT

TATTGC-3′, 0.2 μM), Primer 2 (5′-GCGAACAATTCAGCGGCTTTA-3′, 0.2 μM), Taq DNA polymerase (0.025 units/μL), template (ϕX174, 10^7 copies) or no-template control, and nanoparticles (AuNPs, oligo–AuNP conjugate, or silica-modified oligo–AuNP conjugate, 2.5 nM) or no-particle control. Thermal cycling profile used was: 94 °C for 1 min (initial denaturation); 25 cycles of 94 °C for 5 s (denaturation), 55 °C for 5 s (annealing), and 72 °C for 30 s (extension); and 72 °C for 2 min (final extension). The samples were cooled to room temperature before being taken out from the thermal cycler. Colorimetric results and UV–vis spectra were recorded every 10 min for an hour and 40 min after PCR, respectively. To verify the PCR inhibition effect by the non-specific adsorption of Taq DNA polymerase, the bare AuNPs or oligo–AuNP conjugate (0.25 nM) was added to the PCR mixture in the absence or presence of BSA (3 mg/mL).

4.2.3. Gel Electrophoresis

PCR products (8 μL product with 2 μL BlueJuice™ gel loading buffer) were loaded into in an agarose gel (3%, w/w) in 0.5× TBE buffer and performed electrophoresis at 120 V for 1.5 h. Then, the gel was stained with ethidium bromide

(0.5 μg/mL) for 10 min, followed by visualizing and recording with UV transillumination in gel imaging system.

4.2.4. Hybridization Test

PCR mixtures containing the silica-modified oligo–AuNP conjugate (2.5 nM) were prepared with different $MgCl_2$ concentrations (1.5, 3.5, 5.5 and 7.5 mM) and incubated with Primer 1 (complementary sequence, 0.2 μM), or no-sequence control, or Primer 2 (non-complementary sequence, 0.2 μM), or both primers (0.2 μM each). Colorimetric results were recorded every 10 min for an hour after mixing. The same experiment with Primer 1 and different $MgCl_2$ concentrations (1.5, 3.5, 5.5, 6, 6.5, 7 and 7.5 mM) was performed with PCR thermal cycling.

4.2.5. Sensitivity and Selectivity Tests

For sensitivity determination, various amounts of the ϕX174 template (10^4 to 10^7 copies) were used. Colorimetric results and UV–vis spectra were recorded every 10 min for an hour and 40 min after PCR, respectively. The specificity of the detection scheme was evaluated by a non-specific template (pBR322, 10^7 copies). Colorimetric results were recorded every 10 min for an hour after PCR.

4.3. Results and Discussion

4.3.1. Inhibition of Polymerase Chain Reaction in the Presence of Gold Nanoparticles

For colorimetric detection, the concentration of AuNPs needs to be higher than 1 nM for a clear visual readout (Figure 4.8). Unfortunately, total PCR inhibition occurred when 0.25 nM of bare AuNPs or oligo–AuNP conjugate was added into the PCR mixtures (Figure 4.9, lanes 4 and 6 versus lane 2). To confirm that the PCR inhibition was a result of the adsorption of Taq DNA polymerase onto AuNP surface during thermal cycling process, BSA, which acted as a sacrificial protein to compete with Taq DNA polymerase for adsorption, was introduced to the reaction mixture. As expected, PCR was recovered for both the bare AuNPs and oligo–AuNP conjugate (lanes 5 and 7 versus lane 3). Nevertheless, an abnormally high concentration (3 mg/mL), which was 30 times higher than the typical concentration used in PCR, was required for just 0.25 nM of AuNPs. The PCR product band intensity of the bare AuNPs-containing sample was slightly lower than that of the oligo–AuNP conjugate-containing sample. This can be explained by the fact that the exposed surface of the bare AuNPs is larger than that of the oligo–AuNP conjugate (certain amount of the chemisorbed oligonucleotide remains attached on the AuNP surface

during PCR), therefore, with the same amount of BSA, more enzyme is adsorbed onto the bare AuNPs surface.

The silica-modified oligo–AuNP conjugate (2.5 nM) prepared with different AuNP:MPTMS ratios (1:0, $1:10^3$, $1:10^4$, $1:10^5$, and $1:10^6$) were included in PCR mixture (Figure 4.10). No observable PCR inhibition was noticed for the conjugates with $1:10^4$ and $1:10^5$ AuNP:MPTMS ratios, slight inhibition for the conjugate with $1:10^6$ ratio, and complete inhibition for the conjugates with 1:0 and $1:10^3$ ratios. Considering the higher chemical and thermal stabilities of the conjugate prepared with AuNP:MPTMS ratio of $1:10^5$ (Section 2.3.2 and Section 2.3.4) than the conjugate prepared with AuNP:MPTMS ratio of $1:10^4$, the former one is the best candidate for achieving closed-tube colorimetric PCR.

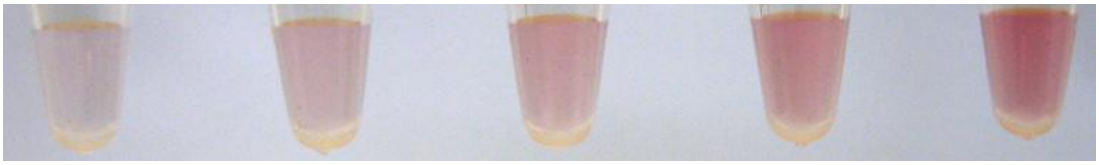

Figure 4.8. Colors of different concentrations of AuNPs (0.5, 1, 1.5, 2, and 2.5 nM, from left to right).

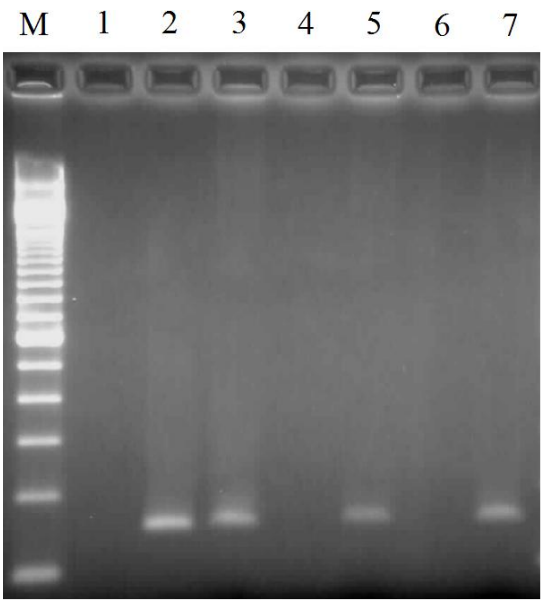

Figure 4.9. Gel electrophoresis results showing the effects of BSA in PCR with bare AuNPs (lanes 4 and 5) or oligo–AuNP conjugate (lanes 6 and 7). Lane M: 100 bp ladder; lanes 1–3: control without AuNPs; lane 1: negative sample without BSA; lanes 2, 4 and 6: positive samples without BSA; lanes 3, 5 and 7: positive samples with 3 mg/mL BSA.

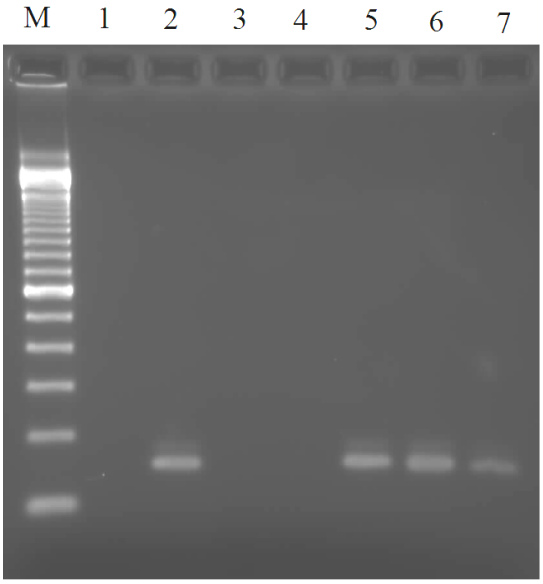

Figure 4.10. Gel electrophoresis results showing the effects of different silica-modified oligo–AuNP conjugates prepared with different AuNP:MPTMS ratios on PCR amplification efficiency. Lane M: ladder; lanes 1 and 2: negative and positive controls without silica-modified oligo–AuNP conjugate, respectively; lanes 3–7: positive samples with the silica-modified oligo–AuNP conjugate prepared with 1:0, $1:10^3$, $1:10^4$, $1:10^5$, and $1:10^6$ AuNP:MPTMS ratios.

4.3.2. Hybridization Test

Typical PCR mixture containing 1× PCR buffer and 1.5 mM $MgCl_2$ did not permit the hybridization-induced aggregation of the silica-modified oligo–AuNP conjugate even after 1-h incubation with 0.2 μM of Primer 1 (Figure 4.11g, first tube

from the left). In Maeda's approach, 0.5 M NaCl was employed to facilitate the aggregation of hybridized conjugates [39]. It is not possible to perform PCR under such a high NaCl concentration. An alternative way is to increase the concentration of $MgCl_2$ which has a stronger ability to trigger salt-induced aggregation of oligo–AuNP conjugate than NaCl [64].

Hybridization-induced color change of the silica-modified oligo–AuNP conjugate occurred readily when the concentration of $MgCl_2$ was equal to or higher than 5.5 mM (Figure 4.11, columns 3 and 4). Red to purple color change was observed after 20-min incubation and red precipitate was clearly observed at the bottom of the tube after 1-h incubation. It should be noted that the hybridized conjugates with 1.5 and 3.5 mM $MgCl_2$ remained monodispersed and red after 1-h incubation. To confirm that the aggregation was indeed caused by the hybridization of the complementary sequence (Primer 1), three additional experiments were carried out with Primer 1 substituted by water, Primer 2 (non-complementary), as well as Primer 1 and Primer 2 (Figure 4.12). As expected, the first two samples remained red whereas the last sample turned purple after 20-min incubation.

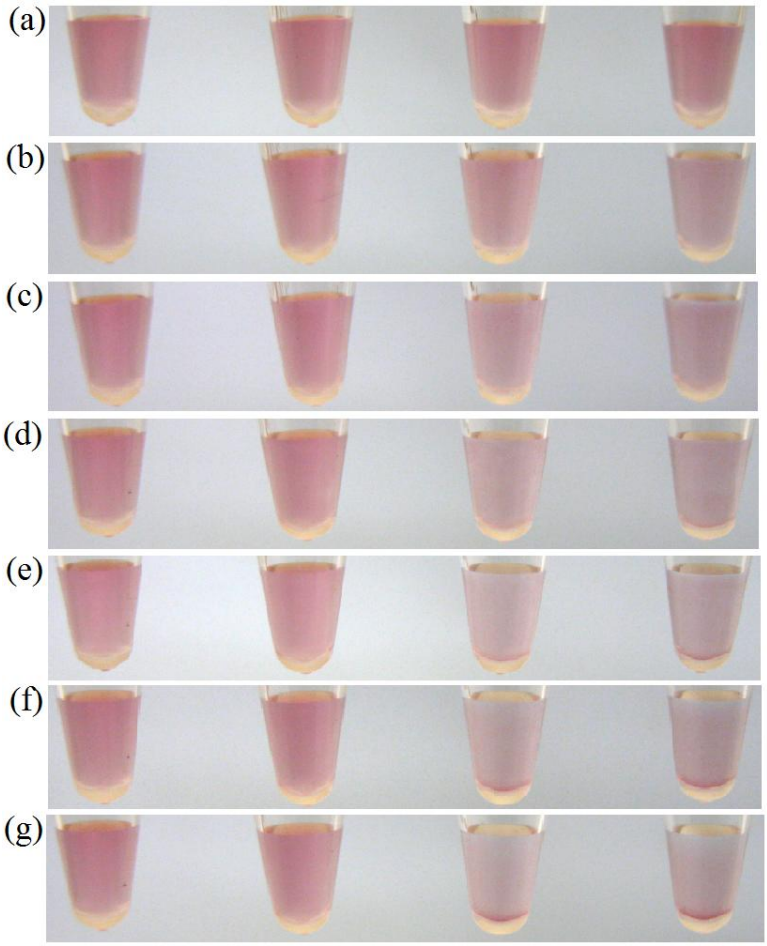

Figure 4.11. Colorimetric results of the silica-modified oligo–AuNP conjugate incubated with 0.2 μM of Primer 1 (complementary) and various $MgCl_2$ concentrations (1.5, 3.5, 5.5, and 7.5 mM) for 1 h (recorded at 10-min intervals for a–g).

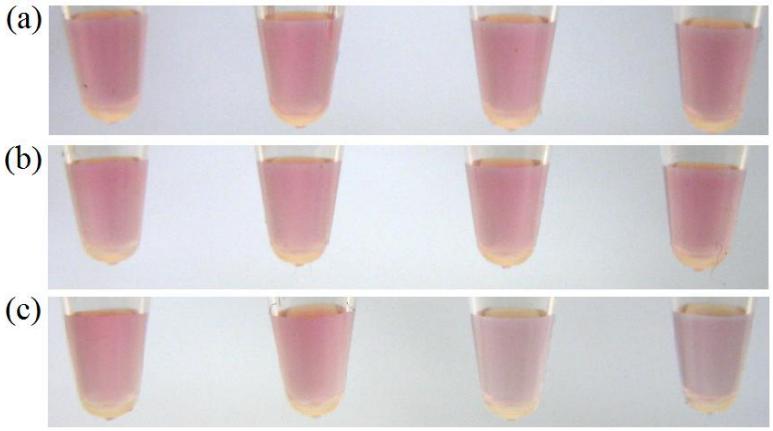

Figure 4.12. Colorimetric results of the silica-modified oligo–AuNP conjugate incubated with (a) water; (b) 0.2 μM of Primer 2 (non-complementary); (c) 0.2 μM each of Primer 1 and Primer 2 (both complementary and non-complementary) under various $MgCl_2$ concentrations (1.5, 3.5, 5.5, and 7.5 mM) after 20-min incubation.

The next step was to evaluate the effect of PCR thermal cycling on the hybridization-induced aggregation property (Figure 4.13). Without PCR thermal cycling, the hybridized silica-modified oligo–AuNP conjugate aggregated with 5.5 and 7.5 mM $MgCl_2$, while with PCR thermal cycling, aggregation occurred with 7.5 mM $MgCl_2$ but not 5.5 mM. It was found that 15% of the oligonucleotides were desorbed from the silica-modified oligo–AuNP conjugate under PCR thermal cycling (Figure 2.26). As a result, the silica-modified oligo–AuNP conjugate may interact with Taq DNA polymerase, thereby stabilizing against hybridization-induced

aggregation. In other words, higher concentration of $MgCl_2$ is needed to effect aggregation. Another possible reason is the undesirable primer extension due to primer dimer formation that reduces the amount of intact Primer 1 for hybridization with the silica-modified oligo–AuNP conjugate. As unhybridized conjugate is more stable toward $MgCl_2$ than hybridized conjugate (Figure 4.12), the less hybridized conjugate would require higher concentration of $MgCl_2$ to effect aggregation.

Figure 4.13. Colorimetric results of the silica-modified oligo–AuNP conjugate subjected to PCR thermal cycling with 0.2 μM of Primer 1 (complementary) and various $MgCl_2$ concentrations (1.5, 3.5, 5.5, and 7.5 mM). Photograph was taken 20 min after PCR.

To locate the aggregation point more precisely, an increment 0.5 mM was used between 5.5 and 7.5 mM of $MgCl_2$. The results showed that the minimum $MgCl_2$ concentration required to trigger the aggregation was 6.5 mM $MgCl_2$ (Figure 4.14). Regarding the incubation time to obtain an observable color change, the lower the

$MgCl_2$ concentration, the longer the time needed. The time for the 6.5 mM $MgCl_2$ sample to accomplish color change was 40 min, while for the 7.5 mM $MgCl_2$ sample was 20 min.

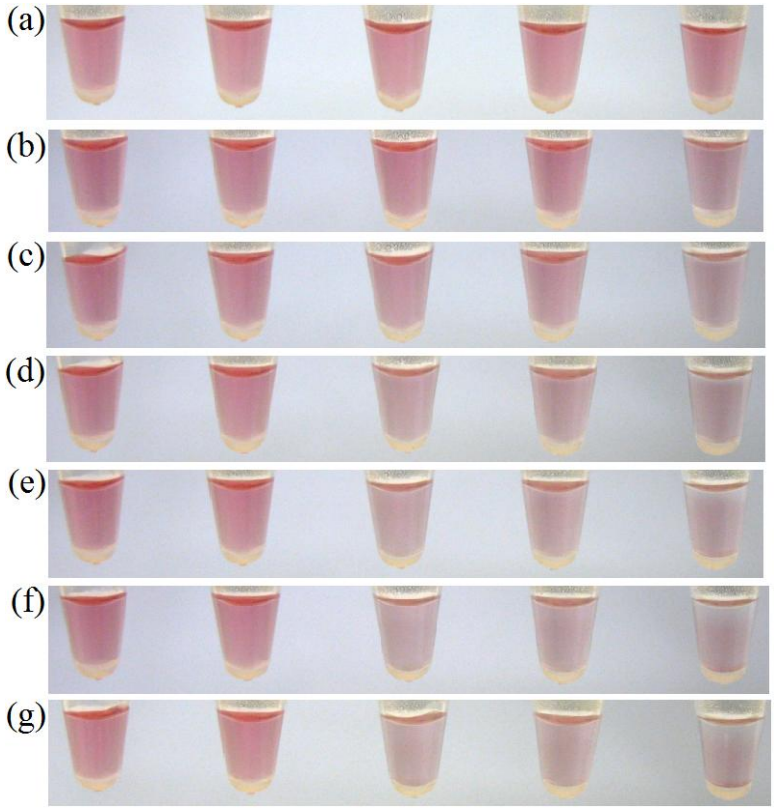

Figure 4.14. Colorimetric results of the silica-modified oligo–AuNP conjugate subjected to PCR thermal cycling with 0.2 μM of Primer 1 (complementary) and various $MgCl_2$ concentrations (5.5, 6, 6.5, 7, and 7.5 mM). Photographs were taken at 10-min intervals (0–60 min) for a–g.

4.3.3. Closed-Tube Reaction

After optimizing the detection parameters, a closed-tube reaction was performed. The negative sample (no target) appeared purple and the positive sample (10^7 copies of the target) appeared red at 40 min post-PCR incubation (Figure 4.15). The results indicate that the detection scheme is functioning well (Section 4.1.2). In essence, the primers in the positive sample are extended, hence the amount of intact Primer 1 remained in the mixture at the end of PCR is no longer sufficient to cause aggregation of the silica-modified oligo–AuNP conjugate and the solution color appears red.

It should be noted that the colors of the solutions, both negative and positive samples, were red right after PCR (Figure 4.15a). This is because the hybridization of Primer 1 with the silica-modified oligo–AuNP conjugate is not favorable during PCR. In the denaturation and extension steps, the temperatures are much higher than the melting temperature of the AuNP-bound capture probe–Primer 1 hybrid. In the annealing step, the time is too short (5 s) for the hybridization between the AuNP-bound capture probe and Primer 1 to take place.

Consistent with the result presented earlier (Figure 4.10), the PCR product intensity for the positive sample with the silica-modified oligo–AuNP conjugate was

similar to that without the conjugate, demonstrating the excellent PCR compatibility offered by the silica coating.

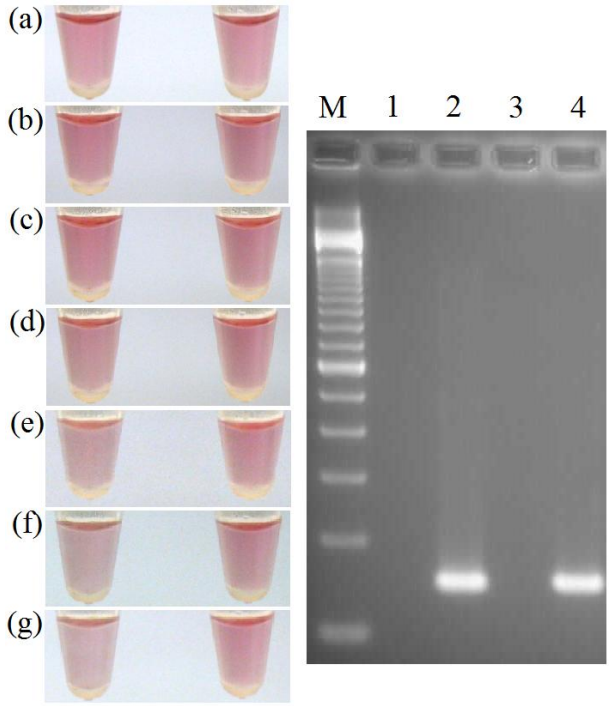

Figure 4.15. Left: Colorimetric PCR results of the silica-modified oligo–AuNP conjugate (left column) without and (right column) with target. Photographs were taken 0–60 min post-PCR at 10-min intervals for a–g. Right: Gel electrophoresis results showing the PCR amplification efficiency. Lane M: ladder; lanes 1 and 2: controls without silica-modified oligo–AuNP conjugate; lanes 3 and 4: silica-modified oligo–AuNP conjugate; odd lanes: no target; even lanes: 10^7 copies of the target.

4.3.4. Sensitivity Test

A 10-fold dilution series of 10^4 to 10^7 copies of the target were used to evaluate the sensitivity of the detection system. Gel electrophoresis result showed an observable product band for the silica-modified oligo–AuNP conjugate-containing sample with 10^7 copies and for the control (without the conjugate) with 10^6 copies (lane 10 and lane 4 in Figure 4.16, respectively).

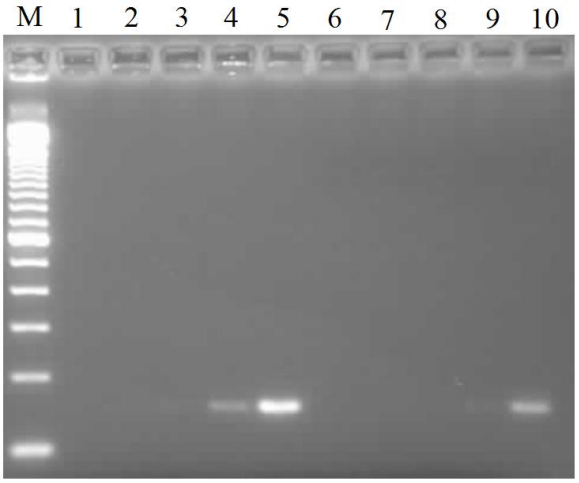

Figure 4.16. Gel electrophoresis results showing the PCR amplification efficiency in the presence of the silica-modified oligo–AuNP conjugate. Lane M: ladder; lanes 1–5: control without silica-modified oligo–AuNP conjugate; lanes 6–10: silica-modified oligo–AuNP conjugate, lanes 1–5 and 6–10: 0, 10^4, 10^5, 10^6 and 10^7 copies of the target.

In terms of the colorimetric results, the sample with 10^6 copies was clearly distinguishable from the negative sample (Figure 4.17). The sensitivity of the colorimetric approach is comparable to that of the gel electrophoresis technique. For the samples containing 10^5 or less copies of the target, the aggregated solutions exhibited red shift (from 520 nm to 526 nm) and broadening of the SPR absorption band (Figure 4.17).

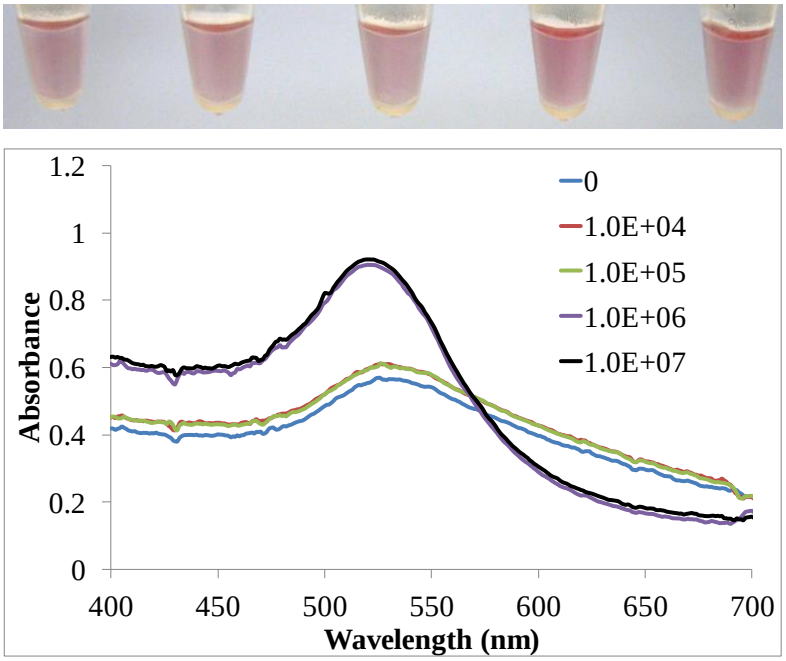

Figure 4.17. Top: Colorimetric results of the silica-modified oligo–AuNP conjugate in samples containing (from left to right) 0, 10^4, 10^5, 10^6 and 10^7 copies of the target. Photograph was taken 40 min post-PCR. Bottom: UV–vis spectra of the samples.

The absorbance ratio between 520 nm and 650 nm could be used to provide a semi-quantitative analysis of the colorimetric PCR results. For the samples containing 10^5 or less copies of the target, the absorbance ratio of 520 nm/650 nm was ~2, while for the samples containing 10^6 or more copies of the target, the absorbance ratio was ~5 (Figure 4.18). The platform's sensitivity could be further enhanced by increasing the number of thermal cycle (e.g. from 25 to 35 cycles).

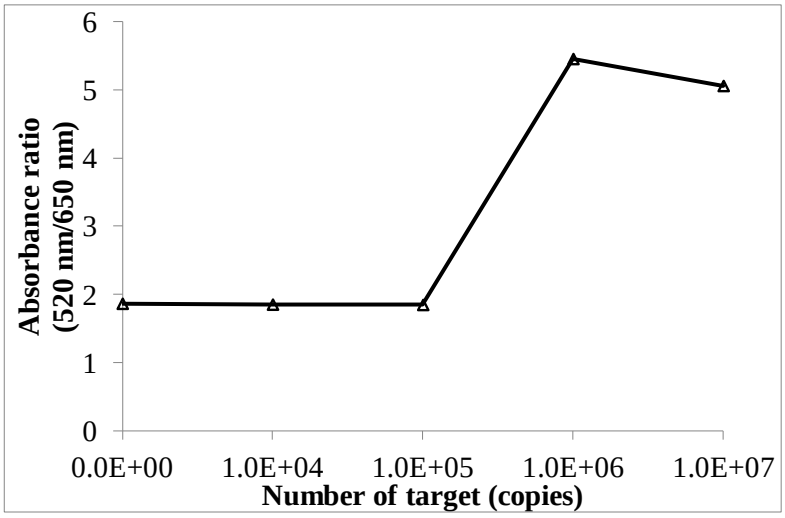

Figure 4.18. Plots of absorbance ratio (520 nm/650 nm) versus target copy number for the silica-modified oligo–AuNP conjugate. Measurements were taken 40 min after PCR.

4.3.5. Selectivity Test

The selectivity of the detection system was evaluated by 10^7 copies of the target (ϕX174) or non-target (pBR322). As expected, the solution color remained red only for samples containing the target (Figure 4.19, lane 6: target only; and lane 8: mixture of target and non-target). Gel electrophoresis result revealed that the silica-modified oligo–AuNP conjugate would not lead to non-specific amplification.

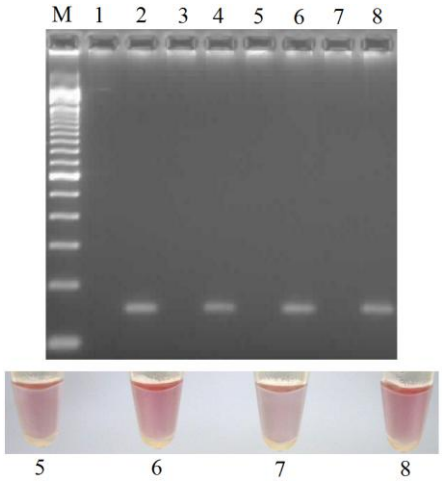

Figure 4.19. Top: Gel electrophoresis results showing the PCR amplification of different targets in the presence of the silica-modified oligo–AuNP conjugate. Lane M: ladder; lanes 1–4: controls with silica-modified oligo–AuNP conjugate; lanes 5–8: silica-modified oligo–AuNP conjugate; lanes 1 and 5: no target; lanes 2 and 6: target, lanes 3 and 7: non-target; lanes 4 and 8: both target and non-target. Bottom: Colorimetric results of the samples. Photograph was taken 40 min post-PCR.

4.4. Summary

Closed-tube colorimetric PCR using silica-modified oligo–AuNP conjugate was successfully demonstrated in this chapter. Silica-modified oligo–AuNP conjugate prepared with AuNP:MPTMS ratio of $1:10^4$ and $1:10^5$ showed negligible PCR inhibition effect even at particle concentration as high as 2.5 nM. Taking into account of the thermal stability, silica-modified oligo–AuNP conjugate prepared with AuNP:MPTMS ratio of $1:10^5$ was chosen for the closed-tube colorimetric PCR detection platform. Hybridization-induced aggregation/color change of the silica-modified oligo–AuNP conjugate was achieved with 1× PCR buffer, 6.5 mM $MgCl_2$, and 0.2 μM complementary target (also served as primer), which was compatible with the standard PCR protocol. The sensitivity of the current unoptimized system was 10^6 copies, comparable to the gel electrophoresis technique under the same PCR thermal cycling profile. Besides visual readout, a simple analysis with absorbance ratio of 520 nm/650 nm was demonstrated. For samples with 10^6 copies or more, the ratio was ~5 at 40 min post-PCR, while for samples with 10^5 copies or less, the ratio was ~2.

Chapter 5

Extension of the Reinforcement Concept

The work described in this chapter was done with the aim of investigating the applicability of the developed silica reinforcement method to other oligonucleotide–nanoparticle conjugates. The main requirement is a strong affinity between the nanoparticle and silica precursor molecule. In this chapter, results on two variants are presented, which include AgNP and (3-aminopropyl)triethoxysilane (APTES). Background information of oligo–AgNP conjugate is given in Section 5.1. Experimental details are presented in Section 5.2. Results and discussion of the silica-modified oligo–AgNP conjugate and APTES-reinforced oligo–AuNP conjugate are delivered in Section 5.3 and Section 5.4, respectively. A brief summary is given in Section 5.5.

5.1. Introduction

AgNPs exhibit a characteristic SPR absorption peak within 390 and 420 nm and the solution appears yellow in color. It was reported that the sensitivity of DNA detection with oligo–AgNP conjugate could be 50 times higher than that with oligo–AuNP conjugate [128]. This is because AgNP has higher extinction coefficient

than AuNP. Nevertheless, a vast majority of the reported colorimetric detection schemes utilized oligo–AuNP conjugates, with a few examples of using oligo–AgNP conjugates [128-131]. Analogous to Au–S linkage, monothiol-modified oligonucleotide can be conjugated to AgNP by Ag–S linkage, but with lower binding affinity. This means the immobilized oligonucleotides on AgNP are easier to be displaced by thiol-containing small molecules than on AuNP, which limits their practical application. Therefore, different approaches were developed to enhance the stability of oligo–AgNP conjugates.

Mirkin et al. utilized AgNP for DNA detection by the crosslink approach [129]. A gold shell was first deposited onto the AgNP, followed by the chemisorption of monothiol-modified oligonucleotide through Au–S linkage. Although the hybridization-induced color change was preserved for the oligonucleotide-conjugated Ag/Au core–shell nanoparticles, the synthesis of the core–shell nanoparticles required complicated protocol, which made the approach less favorable.

Graham et al. synthesized thioctic acid-modified oligonucleotide and the resulting oligo–AgNP conjugate possessed higher stability against DTT-induced aggregation [99]. The thioctic acid-modified oligo–AgNP conjugate was stable in 10

mM DTT for 15 min (defined as the mid-point of the completely aggregated state based on absorbance at 675 nm), while monothiol-modified oligo–AgNP conjugate was stable for less than 1 min (Figure 5.1).

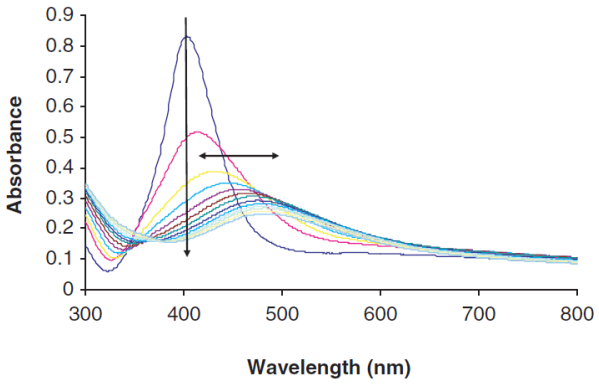

Figure 5.1. UV–vis spectra of thioctic acid-modified oligo–AgNP conjugate incubated with 10 mM DTT and recorded at 10-min intervals (Adapted from [99]).

Triple cyclic disulfide-modified oligonucleotide was successfully employed to enhance the stability of oligo–AgNP conjugate [130]. This conjugate was stable in 1 M NaCl (as opposed to monothiol-modified oligo–AgNP conjugate that was stable up to 0.3 M NaCl) and preserved the hybridization-induced color change property (Figure 5.2). Nonetheless, the low coupling yield for three consecutive cyclic disulfide molecules resulted in high synthesis cost and thus limited the widespread use of this method.

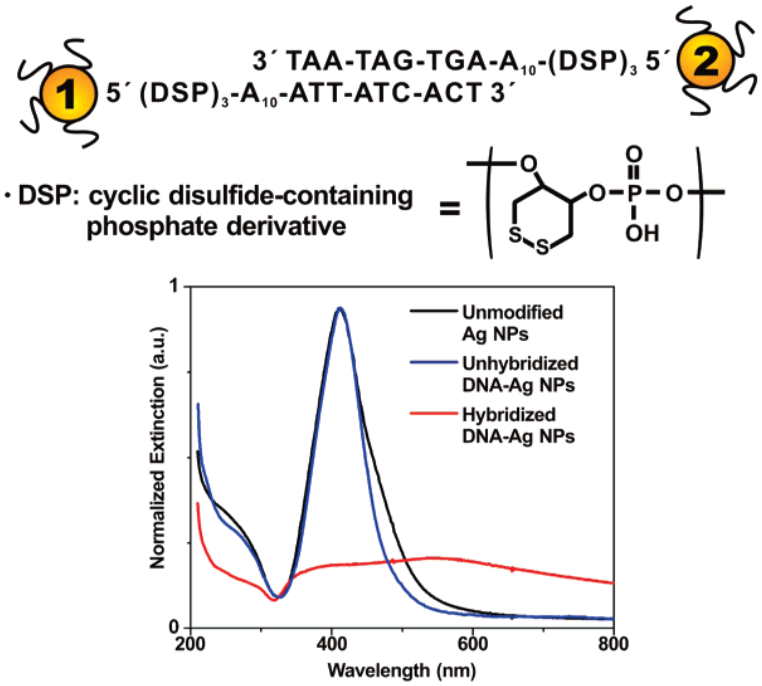

Figure 5.2. Oligo–AgNP conjugate with triple cyclic disulfide linkage and UV–vis spectra of hybridization test (Adapted from [130]).

Liu et al. demonstrated a technique of synthesizing oligo–AgNP conjugate by covalently conjugating oligonucleotide onto silica-coated AgNP [132]. A silica layer was formed on AgNP surface through the hydrolysis and polycondensation of TEOS. After that, the silica-coated AgNP was functionalized with aldehyde group by 11-triethoxysilylundecanaldehyde, which could covalently conjugate with amino-modified oligonucleotide. The synthesized oligo–AgNP conjugate had a Ag core of ~50 nm in diameter and a silica shell of ~40 nm in thickness. The

hybridization behavior of the conjugate was illustrated by the absorbance change at fixed wavelength (436 nm). A sharp increase of extinction value was observed when the incubation temperature was above the melting temperature of the hybridized conjugate. UV−vis spectra revealed that the SPR absorption peaks of the hybridized and heat-denatured conjugates were nearly the same (Figure 5.3). This means that the oligo−AgNP conjugate prepared by this method does not have color change property upon target hybridization and the readout is based on precipitation, which takes a longer time.

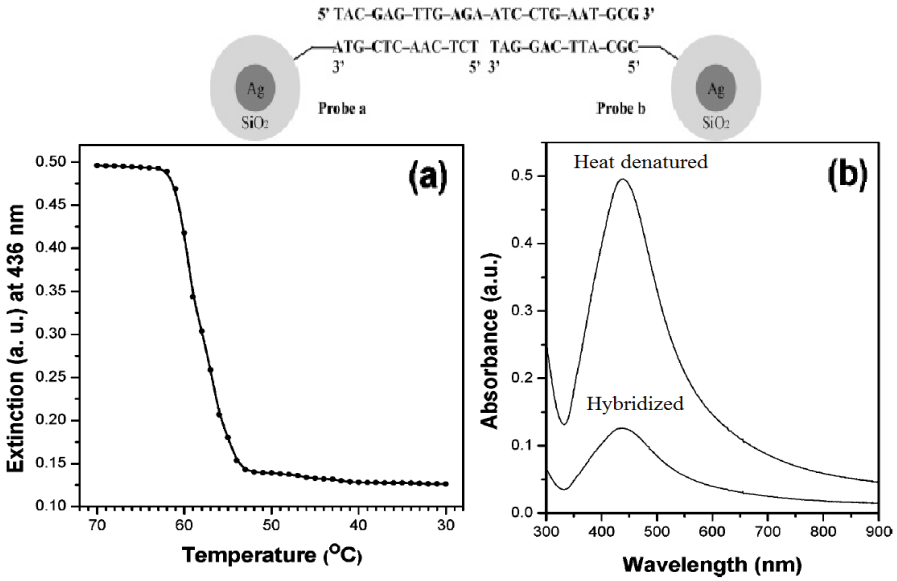

Figure 5.3. (a) Melting curve of the hybridized silica-coated oligo−AgNP conjugate at 436 nm. (b) UV−vis spectra of the hybridized and heat-denatured conjugates (Adapted from [132]).

According to the findings on the stabilities and colorimetric detection property of the silica-modified oligo–AuNP conjugate, the silica reinforcement method should improve the stability of the monothiol-modified oligo–AgNP conjugate toward DTT and preserve the characteristic hybridization-induced aggregation/color change property.

Other than changing the core material, the silica precursor molecule can be replaced by other molecules having affinity toward the core material. Therefore, the replacement of MPTMS by APTES was investigated. APTES has similar structure with APTMS, which was utilized for creating a silica monolayer on AuNP surface through the Au–N linkage [101].

5.2. Materials and Methods

5.2.1. Materials and Instrumentation

The materials, instruments, and procedures for the synthesis of AuNPs, oligo–AuNP conjugate, and silica-modified oligo–AuNP conjugate were as described in Section 2.2. APTES and H_2O_2 were purchased from Sigma-Aldrich. AgNPs of diameter 30 nm (PELCO® BioPure™ citrate-capped silver colloids) were purchased from Ted Pella (Redding, CA, USA).

Equipment for the chemical stability and reversible hybridization analyses were mentioned in Section 2.2. UV lamp (EN-280L/FE) with emission wavelength of 365 nm was purchased from Spectronics (Westbury, NY, USA).

5.2.2. Preparation of Oligonucleotide–Silver Nanoparticle Conjugates

The preparation of oligo–AgNP conjugate was based on the protocol described by Graham and co-workers with minor modifications [128]. Oligonucleotide (5′-HS-$(CH_2)_6$-$(OCH_2CH_2)_6$-GCAATAAACTCAACAGGAGCAG-3′) was activated and purified using the same procedures described in Section 2.2.3. Then, the purified oligonucleotide (12.5 μM) was mixed with AgNPs (6.25 nM) and incubated for 16 h. After that, the mixture was progressively brought to 2, 4, 8, 16, 32, 64, 100, 150 and 300 mM of NaCl by adding NaCl/sodium phosphate (0.33 M/11.11 mM, pH 7.4) at 1-h interval. The final mixture was incubated for 24 h. Next, the solution was centrifuged at 13,200 rpm for 30 min to remove excess capture probe. The supernatant was discarded and the yellow oily precipitate (i.e., oligo–AgNP conjugate) was redispersed in sodium phosphate (10 mM, pH 7.4). The solution was centrifuged again and redispersed in water. UV–vis spectrum of the as-prepared oligonucleotide–AgNP

conjugate was measured and the particle concentration was determined by the following equation:

$$c_{\text{oligo–AgNP}} = c_{\text{AgNP}} \times (A_{\text{SPR,oligo–AgNP}}/A_{\text{SPR,AgNP}}) \quad \text{[Eq. (5.1)]}$$

where c_{AgNP} and the corresponding $A_{\text{SPR,AgNP}}$ were available from the manufacturer.

5.2.3. Preparation of Silica-Modified Oligonucleotide–Nanoparticle Conjugates

The oligo–AgNP conjugate (0.25 nM) was mixed with MPTMS (0.1 mM) and the oligo–AuNP conjugate (1 nM) was mixed with APTES (0.1 mM). The mixtures were shaken at 1,400 rpm for 24 h, and then supplied with sodium phosphate (10 mM, pH 7.4). After that, they were centrifuged and redispersed again as above. UV–vis spectra of the as-prepared silica-modified oligo–AgNP and oligo–AuNP conjugates were measured and their particle concentrations were determined by the following equations:

$$c_{\text{modified oligo–AgNP}} = c_{\text{AgNP}} \times (A_{\text{SPR,modified oligo–AgNP}}/A_{\text{SPR,AgNP}}) \quad \text{[Eq. (5.2)]}$$

$$c_{\text{modified oligo–AuNP}} = c_{\text{AuNP}} \times (A_{\text{SPR,modified oligo–AuNP}}/A_{\text{SPR,AuNP}}) \quad \text{[Eq. (5.3)]}$$

5.2.4. Chemical Stability Test

Stability tests using DTT and NaCN were investigated using the protocols described in Section 2.2.6. The concentrations of the oligo–AgNP and silica-modified oligo–AgNP conjugates used in DTT and NaCN tests were 0.1 nM. The concentration of the APTES-modified oligo–AuNP conjugate used in DTT test was 2.5 nM.

5.2.5. Reversible Hybridization Test

Silica-modified oligo–AgNP conjugate (0.1 nM) and complementary target (5′-CTGCTCC TGTTGAGTTTATTGC-3′, 0.5 μM) were added together with DTT (10 μM), 1×PBS, and NaCl (0.5 M). Hybridization was allowed to proceed for 10 min. Finally, the solution was heated at 94 °C for 1 min. UV–vis spectra and colorimetric results were recorded before and after hybridization, as well as after heat denaturation.

5.2.6. Photostability Test

Silica-modified oligo–AgNP conjugate (0.1 nM) and H_2O_2 (1 mM) was illuminated under UV light (365 nm, 1.533 mW/cm^2) in a glass vial. UV–vis spectra

and colorimetric results were recorded at different time intervals.

5.3. Change of Core Material

This section starts with examining the chemical stabilities of oligo–AgNP and silica-modified oligo–AgNP, follows by investigating the reversible hybridization property of the silica-modified conjugate. Finally, the photo-oxidation effects of these AuNP derivatives are evaluated.

5.3.1. Chemical Stability

The oligo–AgNP conjugate (diameter of 30 nm) displayed an SPR absorption peak at 410 nm and appears yellow (Figure 5.4). When 10 mM DTT was added, particle aggregation took place within minutes. The absorbance at 410 nm decreased dramatically while that at longer wavelengths (> 500 nm) increased and a new absorption peak at ~700 nm appeared. For the silica-modified oligo–AgNP conjugate, the displacement reaction was much slower. The SPR absorption peak intensity was decreased by 20% after 30-min incubation whereas by 77% for the unmodified conjugate (Figure 5.5). Plots of the SPR absorption peak intensity versus incubation time illustrate the significant improvement in stability toward DTT displacement

offered by the silica coating (Figure 5.6). In fact, the stability of the silica-modified oligo–AgNP conjugate is better than that of the conjugate prepared with bidentate linkage [99]. Nonetheless, the stability of the silica-modified oligo–AgNP conjugate is considerably lower than the silica-modified oligo–AuNP conjugate as the lower binding affinity of the Ag–S linkage would possibly result in a less compact silica layer.

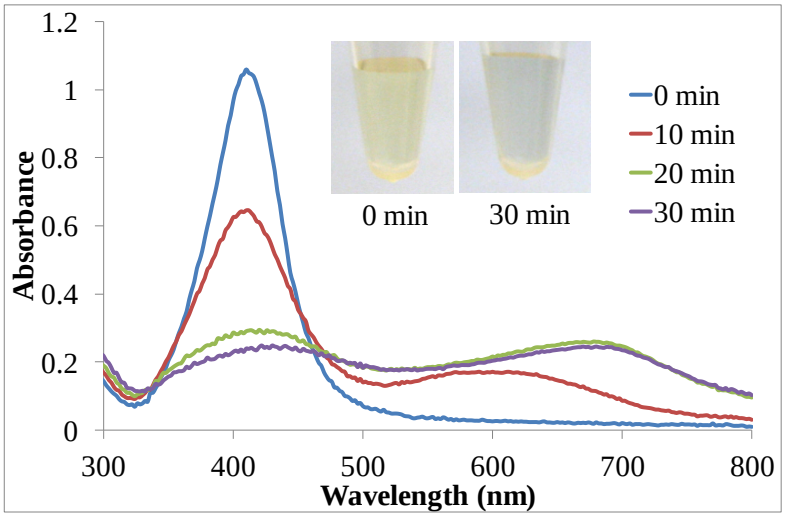

Figure 5.4. UV–vis spectra of the oligo–AgNP conjugate incubated in 10 mM DTT. Insets are photographs showing the colors of the samples at different times.

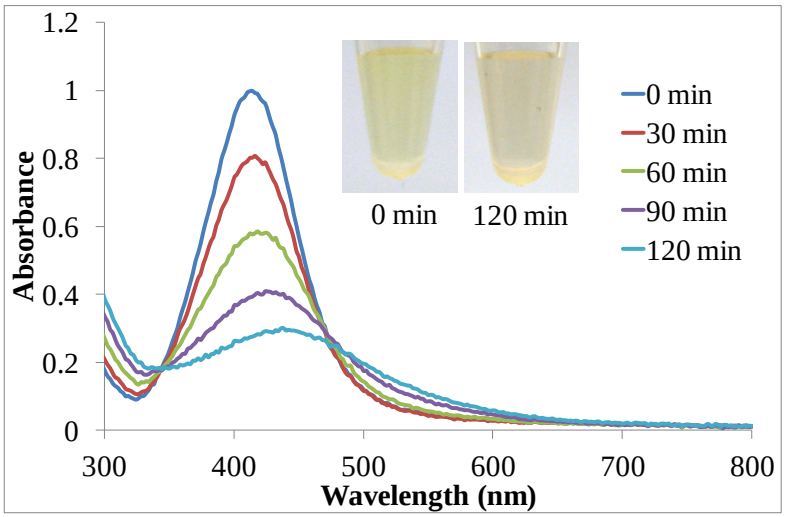

Figure 5.5. UV–vis spectra of the silica-modified oligo–AgNP conjugate incubated in 10 mM DTT. Insets are photographs showing the colors of the samples at different times.

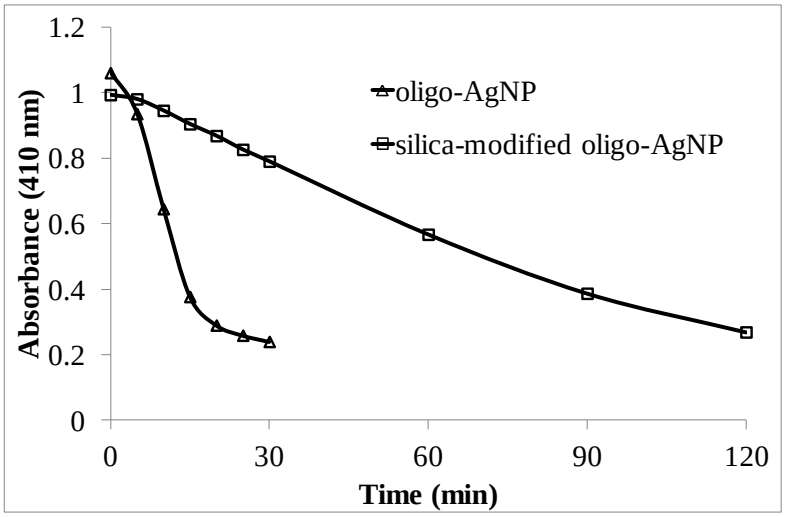

Figure 5.6. Plots of absorbance at 410 nm versus time of oligo–AuNP and silica-modified oligo–AuNP in 10 mM DTT.

Stability test for AgNP dissolution by NaCN was carried out for the silica-modified oligo–AgNP conjugate. The unmodified oligo–AgNP conjugate underwent rapid oxidative dissolution in the cyanide solution (2 mM). The amplitude of the SPR absorption peak diminished quickly, and the solution color changed from yellow to colorless within 2 min (Figure 5.7). For the silica-modified oligo–AgNP conjugate, the amplitude of the SPR absorption peak reduced to 50% after 3-h incubation in 2 mM NaCN (Figure 5.8).

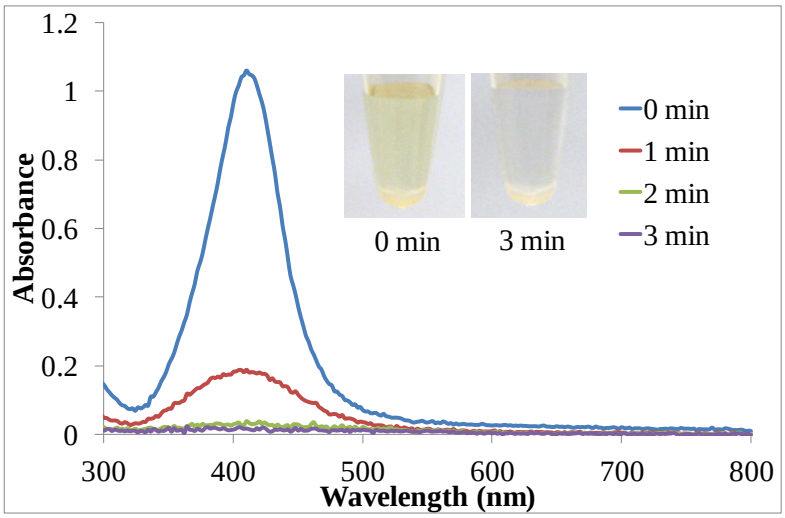

Figure 5.7. UV–vis spectra of the oligo–AgNP conjugate incubated in 2 mM NaCN. Insets are photographs showing the colors of the samples at different times.

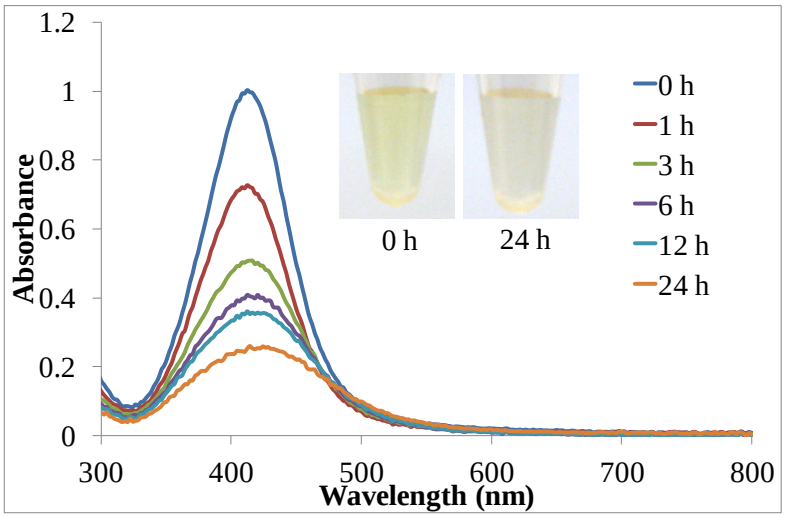

Figure 5.8. UV–vis spectra of the silica-modified oligo–AgNP conjugate incubated in 2 mM NaCN. Insets are photographs showing the colors of the samples at different times.

Plots of absorbance at the SPR absorption peak (410 nm) versus incubation time illustrate the significant enhancement in the stability of the oligo–AgNP conjugate against oxidative dissolution by NaCN offered by the silica reinforcement coating (Figure 5.9). This is again attributed to the fact that the silica layer acts as a physical barrier for the diffusion of CN^- reactant and $Ag(CN)_2^-$ product. However, it should be noted that the stability of the silica-modified oligo–AgNP conjugate was lower than that of the silica-modified oligo–AuNP conjugate due to the formation of a less compact silica layer on AgNP surface.

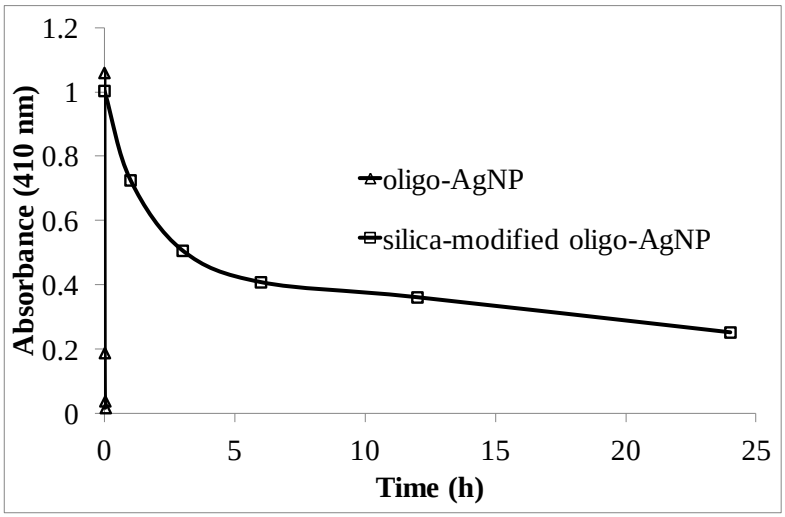

Figure 5.9. Plots of absorbance at 410 nm versus time of the oligo–AuNP and silica-modified oligo–AuNP conjugates in 2 mM NaCN.

5.3.2. Reversible Hybridization Property

The hybridization-induced color change property of the silica-modified oligo–AgNP conjugate was examined by using Maeda's non-crosslink approach (detailed mechanism was described in Section 1.2.2.1) [39]. For the unmodified oligo–AgNP conjugate, the SPR absorption peak was at 410 nm and the solution appeared yellow. Upon the hybridization of the complementary target in the presence of DTT (10 μM), 1×PBS, and NaCl (0.5 M), the SPR absorption peak shifted to ~500 nm and the color changed to pale yellowish orange. However, the solution color did not change back to yellow after heat denaturation (Figure 5.10), implying

that the earlier color change might not be contributed by hybridization-induced aggregation, but DTT-induced irreversible aggregation.

For the silica-modified oligo–AgNP conjugate, heat denaturation caused a blue shift of the SPR absorption peak and the solution color returned to yellow (Figure 5.11). One noteworthy point is that a low DTT concentration (10 μM) was used because the silica-modified oligo–AgNP conjugate would otherwise undergo irreversible aggregation under heating at 94 ℃ in the denaturation step.

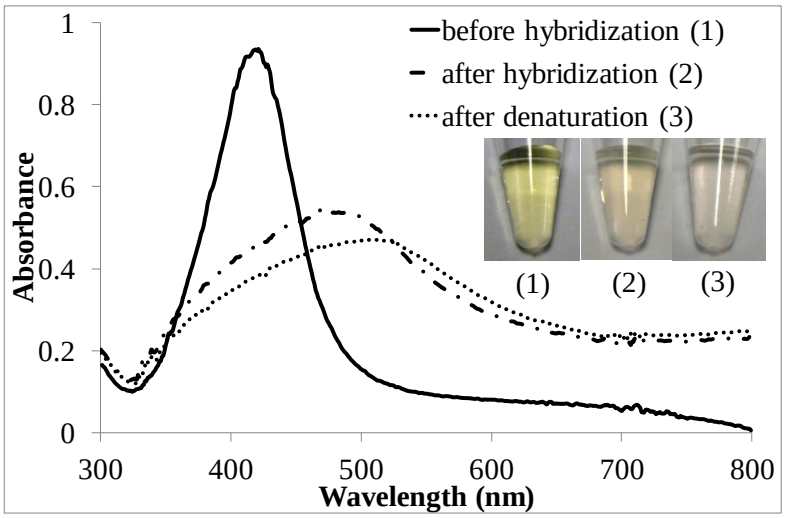

Figure 5.10. UV–vis spectra of the oligo–AgNP conjugate (1) before hybridization, (2) after hybridization, and (3) after denaturation. The hybridization buffer contained DTT (10 μM), 1×PBS, and NaCl (0.5 M). Insets are photographs of the samples (1), (2), and (3).

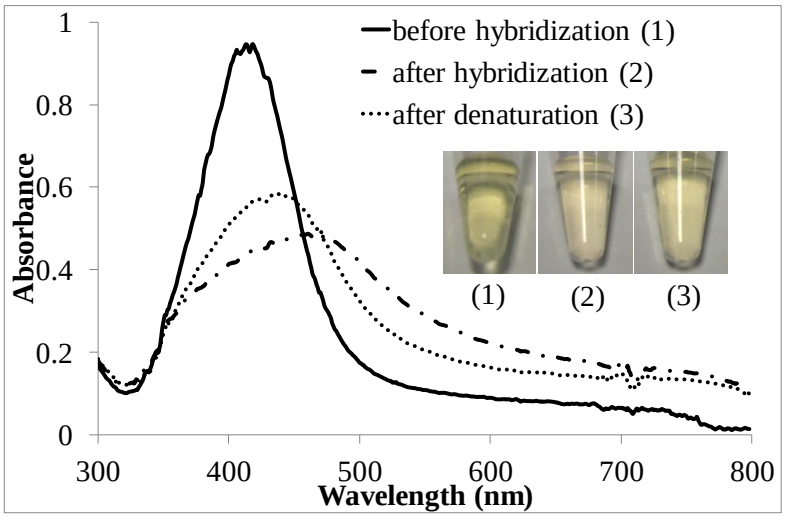

Figure 5.11. UV−vis spectra of the silica-modified oligo−AgNP conjugate (1) before hybridization, (2) after hybridization, and (3) after denaturation. The hybridization buffer contained DTT (10 μM), 1×PBS, and NaCl (0.5 M). Insets are photographs of the samples (1), (2), and (3).

5.3.3. Photostability

AgNPs is susceptible to oxidation in the presence of oxidative substances. When silver oxide (Ag_2O) is formed on the AgNP surface, the SPR absorption band is red-shifted, broadened, and diminished [133]. Hydroxyl radical from UV photolysis of H_2O_2 was chosen to assess whether the silica reinforcement method could enhance the photostability of AgNPs.

The SPR absorption band of the unmodified oligo−AgNP conjugate greatly

diminished under UV in the presence of H_2O_2, with SPR absorption peak dropped to 10% of the original value after 20 min (Figure 5.12). The silica-modified oligo–AgNP conjugate was much more resistant to free radical oxidation (Figure 5.13). It took more than 3 h for the SPR absorption peak to reach 50% of the original value. This suggests that the silica layer could retard the diffusion of hydroxyl radical to the AgNP surface, resulting in enhanced oxidation resistance.

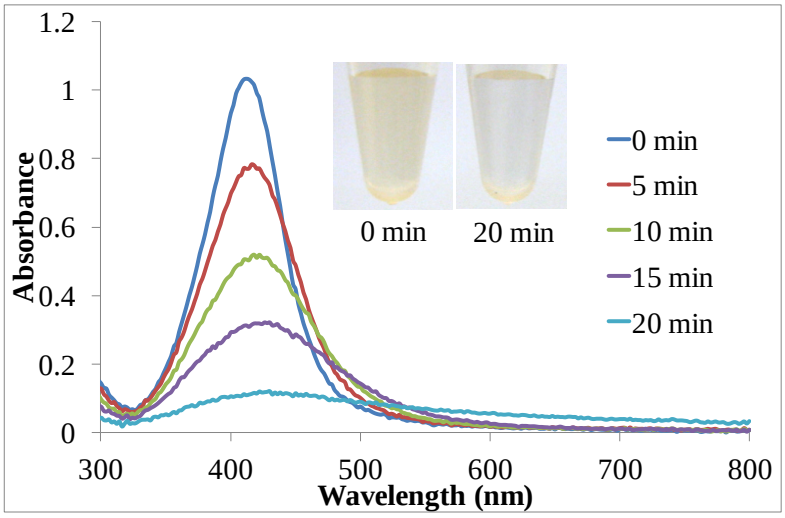

Figure 5.12. UV–vis spectra of the oligo–AgNP conjugate incubated with H_2O_2 under UV. Insets are photographs showing the colors of the samples at different times.

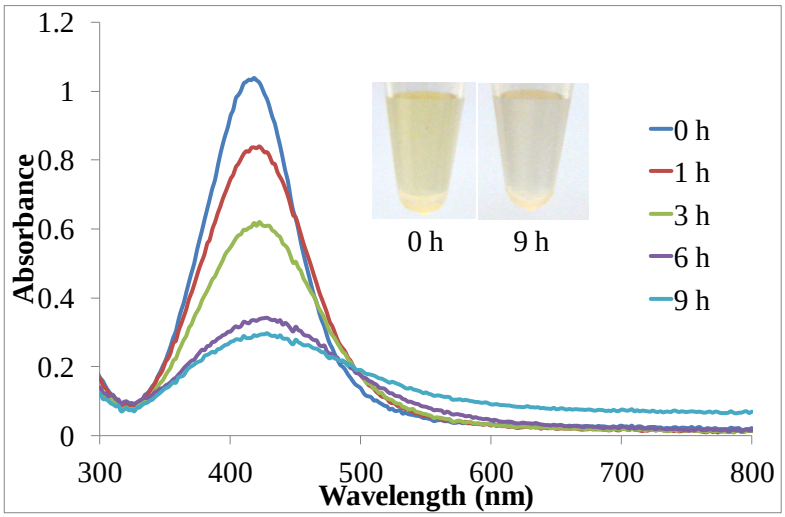

Figure 5.13. UV–vis spectra of the silica-modified oligo–AgNP conjugate incubated with H_2O_2 under UV. Insets are photographs showing the colors of the samples at different times.

5.4. Change of Reinforcement Material

The silica precursor molecule for the synthesis of the silica-modified oligo–AuNP conjugate was changed from MPTMS to APTES in order to investigate whether other silica precursor molecules could be used. APTES is a silane agent containing an amino group which binds to AuNP surface by Au–N linkage.

In 10 mM DTT, the unmodified oligo–AuNP conjugate aggregated and the solution color changed from red to purple in several minutes (Figure 5.14). The SPR absorption peak decreased slightly and a new peak appeared at ~650 nm. After

modifying the conjugate with APTES, aggregation process was slightly retarded (Figure 5.15). Shifting of absorption peak, appearance of new absorption peak at ~650 nm, as well as red-to-purple color change were similar to the unmodified conjugate. Plots of absorbance ratio between 520 and 650 nm illustrate the minor improvement in stability against DTT-induced aggregation for a very short period of time (less than 10 min, Figure 5.16).

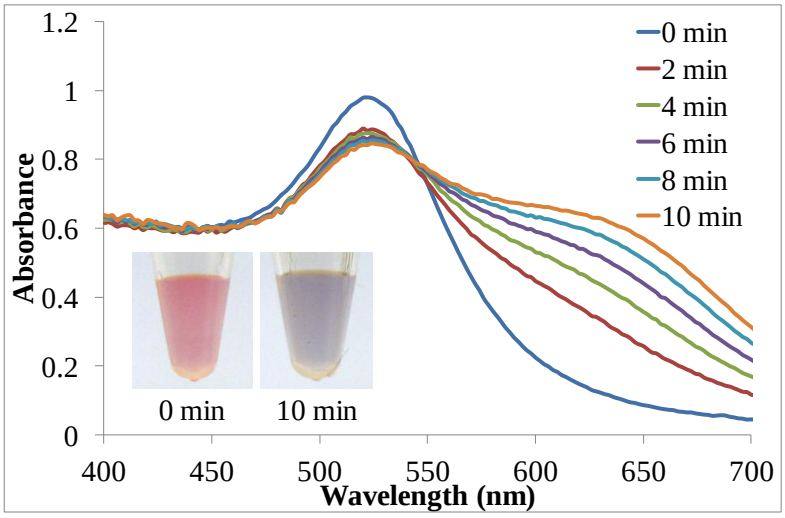

Figure 5.14. UV–vis spectra of the oligo–AuNP conjugate incubated in 10 mM DTT. Insets are photographs showing the colors of the samples at different times.

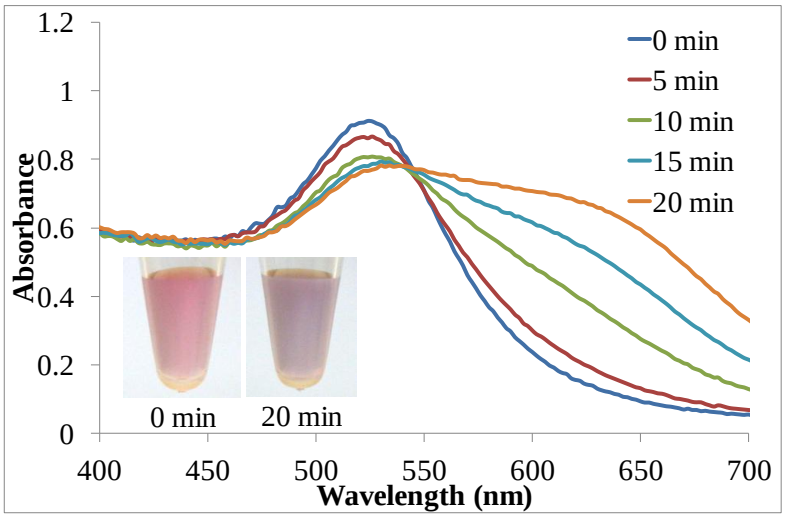

Figure 5.15. UV–vis spectra of the APTES-modified oligo–AuNP conjugate incubated in 10 mM DTT. Insets are photographs showing the colors of the samples at different times.

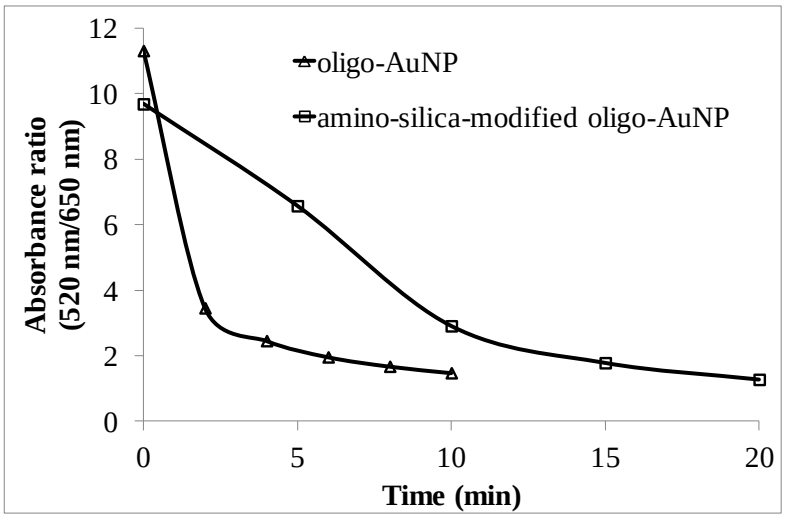

Figure 5.16. Plots of absorbance ratio (520 nm/650 nm) versus time of the oligo–AuNP and APTES-modified oligo–AuNP conjugates incubated in 10 mM DTT.

The results could be explained by two reasons. First, the affinity of amino group toward gold is lower than that of thiol group, so the number of APTES molecules being conjugated to the AuNP surface during the reinforcement process is smaller. This in turns makes the formed silica layer too loose to properly entrap the AuNP-bound oligonucleotides. Another reason is the slower hydrolysis rate of ethoxysilane than methoxysilane [134], which affects their polycondensation to form a crosslinked compact silica network. Therefore, the chemical nature of the silica precursor molecule would have a very significant influence on the conjugate's stability.

5.5. Summary

The silica reinforcement method was successfully applied to enhance the chemical stability of the oligo–AgNP conjugate. The unmodified oligo–AgNP conjugate was not stable in DTT, NaCN, and H_2O_2/UV. When coated with a silica layer using MPTMS, the conjugate's stability was significantly enhanced. In terms of the time for a certain degree of change in the SPR absorption peak, the silica-modified oligo–AgNP conjugate was 6, 1440, and 18 times more stable than the unmodified oligo–AgNP conjugate in DTT, NaCN, and H_2O_2/UV, respectively.

Moreover, the silica-modified oligo–AgNP conjugate exhibited reversible hybridization-induced aggregation and color change property even in the presence of DTT. Apart from changing the core material, the original MPTMS silica precursor molecule was changed to APTES. DTT-induced aggregation results showed that the APTES-modified oligo–AuNP conjugate had only slightly higher stability than the unmodified oligo–AuNP conjugate, but had much lower stability than the MPTMS-modified oligo–AuNP conjugate.

Chapter 6

Conclusions and Recommendations for Future Work

This chapter summarizes the key findings in this study and suggests potential directions for further investigation.

6.1. Key Findings and Conclusions

Sensitive AuNP-based colorimetric detection of nucleic acid has received considerable attention for point-of-care and on-site testing applications. Previous efforts required the enzymatic amplification step separated from the colorimetric detection step due to the instability of the AuNP probes under the amplification reaction conditions as well as the inhibition of the enzymatic amplification reaction resulting from the non-specific adsorption of enzyme onto the AuNP surface. The carryover contamination associated with the open-tube format has become a major concern for the practical application of these methods. This also reflected by limited choice of AuNP-based detection platforms in the market. Those available systems are fully automated and integrated in order to minimize contamination. Nevertheless, the difficulty in customizing recognition target reduces attractiveness toward users. Therefore, this thesis endeavors to develop a new AuNP probe that allows enzymatic

amplification reaction and colorimetric detection to be performed in a closed-tube format, thereby achieving a sensitive and carryover contamination-free nucleic acid detection with visual readout.

A silica reinforcement method was successfully developed for enhancing the chemical and thermal stabilities, as well as enzymatic amplification reaction compatibility of oligo–AuNP conjugate. The method was simple-to-perform by treating the conventional monothiol-modified oligo–AuNP conjugate with MPTMS. A thin silica layer was formed on the AuNP surface, thereby entrapping and reinforcing the Au–S linkage of the chemisorbed oligonucleotides. With an optimum AuNP:MPTMS ratio of $1:10^5$, the silica-modified oligo–AuNP conjugate excellent stability against irreversible aggregation by DTT (stable in 10 mM DTT for at least 24 h; the most stable conjugate reported so far was based on triple Au–S linkages and was stable for 8 h) and oxidative dissolution by NaCN (remained red in 2 mM NaCN after 24-h incubation). In fact, the silica layer served as an effective physical barrier to retard the diffusion of DTT and NaCN to the AuNP surface. Moreover, the silica layer preserved the hybridization-induced color change property of the oligo–AuNP conjugate.

Taking advantage of the excellent stability of the silica-modified oligo–AuNP

conjugate in DTT, a closed-tube colorimetric DNA scheme with isothermal nicking endonuclease-assisted amplification was achieved. Importantly, the presence of the silica-modified oligo–AuNP conjugate in the amplification reaction mixture did not affect the enzymatic reaction. This isothermal platform had a detection limit of 100 nM.

Another highly sensitive closed-tube colorimetric DNA detection platform was developed by using PCR amplification. Two important issues were addressed including thermal stability and PCR inhibition. Compared with bare AuNPs and unmodified oligo–AuNPs that caused complete PCR inhibition at a concentration of 0.25 nM, the silica-modified oligo–AuNP conjugate had no inhibition at a concentration of 2.5 nM, which enabled clear visual readout. This colorimetric PCR scheme had a detection limit of 10^6 copies (i.e., ~100 fM).

Last but not least, this silica reinforcement method was applicable to other oligonucleotide–nanoparticle conjugates such as oligo–AgNP conjugate. The silica-modified oligo–AgNP conjugate also exhibited significantly enhanced chemical stability (DTT and NaCN) as compared to the unmodified oligo–AgNP conjugate. Analogous to the silica-modified oligo–AuNP conjugate, the silica-modified oligo–AgNP conjugate demonstrated hybridization-induced color

change property even in the presence of DTT.

To conclude, closed-tube colorimetric and sensitive nucleic acid detection was accomplished by performing enzymatic amplification reactions in the presence of the silica-modified oligo–AuNP conjugate. With the silica reinforcement method developed in this thesis, the conventional monothiol-modified oligo–AuNP conjugate was made much more chemically and thermally stable than the unmodified conjugate, yet preserving the hybridization-induced color change property. Moreover, the silica coating was successfully applied to the oligo–AgNP conjugate. Importantly, the reinforcement technique is potentially a general strategy for enhancing the stability of biomolecule/polymer–nanoparticle conjugates.

6.2. Recommendations for Future Work

Based on the new silica reinforcement method developed in this study, several immediate and long-term further investigations can be carried out. First, despite the significantly enhanced thermal stability of the silica-modified oligo–AuNP conjugate as compared to the unmodified one, zero oligonucleotide desorption at high temperature (e.g., denaturation step in PCR) is a challenging task. Toward this goal, new silica precursor molecules or crosslinked polymer networks have to be studied

systematically.

Second, the sensitivity of the current closed-tube colorimetric platform with isothermal amplification by nicking endonuclease is quite low. To achieve lower detection limit (picomolar concentrations as in other open-tube platforms with oligo–AuNP conjugates), three important aspects have to be considered including the use of crosslink approach (instead of the non-crosslink approach), optimization of the beacon design, as well as the use of exponential amplification strategy.

Third, the colorimetric PCR experiments performed in this study involved pure DNA template. Aiming at point-of-care and on-site testing, efforts have to be made in evaluating the performance of the platform for raw sample analysis. Besides, it is highly desirable to further improve the detection limit as PCR can ideally amplify a single copy of target. This can be achieved by optimizing the PCR protocol and silica-modified oligo–AuNP conjugate.

Fourth, the silica reinforcement method is potentially broadly applicable to other biomolecule/polymer–nanoparticle conjugates. In theory, all three key components (i.e., nanoparticle, immobilized molecule, and reinforcement layer) can be varied. Different nanoparticles (e.g., AuNP, AgNP, quantum dot, and magnetic nanoparticle), immobilized molecules (e.g., oligonucleotide, aptamer, peptide, and

polymer), and reinforcement layer (e.g., silica and crosslinked polymer) can be used, provided that strong linkages are established between the nanoparticle and immobilized molecule as well as between the nanoparticle and reinforcement layer, and a compact crosslinked reinforcement network is formed. The highly stable biomolecule/polymer–nanoparticle conjugates thus formed would enable novel diagnostic and therapeutic applications.

References

[1] M. C. Daniel and D. Astruc, "Gold Nanoparticles: Assembly, Supramolecular Chemistry, Quantum-Size-Related Properties, and Applications toward Biology, Catalysis, and Nanotechnology", *Chem. Rev.,* Vol. 104, 2004, pp. 293–346.

[2] R. Wilson, "The Use of Gold Nanoparticles in Diagnostics and Detection", *Chem. Soc. Rev.,* Vol. 37, 2008, pp. 2028–2045.

[3] D. A. Giljohann, D. S. Seferos, W. L. Daniel, M. D. Massich, P. C. Patel, and C. A. Mirkin, "Gold Nanoparticles for Biology and Medicine", *Angew. Chem. Int. Ed.,* Vol. 49, 2010, pp. 3280–3294.

[4] C. S. Thaxton, D. G. Georganopoulou, and C. A. Mirkin, "Gold Nanoparticle Probes for the Detection of Nucleic Acid Targets", *Clin. Chim. Acta*, Vol. 363, 2006, pp. 120–126.

[5] Y. Lu and J. Liu, "Smart Nanomaterials Inspired by Biology: Dynamic Assembly of Error-Free Nanomaterials in Response to Multiple Chemical and Biological Stimuli", *Acc. Chem. Res.,* Vol. 40, 2007, pp. 315–323.

[6] W. Zhao, M. A. Brook, and Y. Li, "Design of Gold Nanoparticle-Based Colorimetric Biosensing Assays", *ChemBioChem,* Vol. 9, 2008, pp. 2363–2371.

[7] Y.-W. Lin, C.-W. Liu, and H.-T. Chang, "DNA Functionalized Gold Nanoparticles for Bioanalysis", *Anal. Methods,* Vol. 1, 2009, pp. 14–24.

[8] M. Faraday, "The Bakerian Lecture: Experimental Relations of Gold (and Other Metals) to Light", *Philos. Trans.,* Vol. 147, 1857, pp. 145–181.

[9] J. Turkevich, P. C. Stevenson, and J. Hillier, "A Study of the Nucleation and Growth Processes in the Synthesis of Colloidal Gold", *Discuss. Faraday Soc.,* Vol. 11, 1951, pp. 55–75.

[10] G. Frens, "Controlled Nucleation for the Regulation of the Particle Size in Monodisperse Gold Suspensions", *Nature: Phys. Sci.,* Vol. 241, 1973, pp. 20–22.

[11] M. Brust, M. Walker, D. Bethell, D. J. Schiffrin, and R. Whyman, "Synthesis of Thiol-Derivatised Gold Nanoparticles in a Two-Phase Liquid-Liquid System", *J. Chem. Soc., Chem. Commun.,* 1994, pp. 801–802.

[12] K. R. Brown, D. G. Walter, and M. J. Natan, "Seeding of Colloidal Au Nanoparticle Solutions. 2. Improved Control of Particle Size and Shape",

Chem. Mater., Vol. 12, 2000, pp. 306–313.

[13] N. R. Jana, L. Gearheart, and C. J. Murphy, "Evidence for Seed-Mediated Nucleation in the Chemical Reduction of Gold Salts to Gold Nanoparticles", *Chem. Mater.*, Vol. 13, 2001, pp. 2313–2322.

[14] P. N. Njoki, J. Luo, M. M. Kamundi, S. Lim, and C.-J. Zhong, "Aggregative Growth in the Size-Controlled Growth of Monodispersed Gold Nanoparticles", *Langmuir,* Vol. 26, 2010, pp. 13622−13629.

[15] N. G. Bastús, J. Comenge, and V. Puntes, "Kinetically Controlled Seeded Growth Synthesis of Citrate-Stabilized Gold Nanoparticles of up to 200 nm: Size Focusing versus Ostwald Ripening", *Langmuir,* Vol. 27, 2011, pp. 11098−11105.

[16] I. Kandela. (2011). Making and Conjugating Colloidal Metals [Online]. Available: http://www.ansci.wisc.edu/facstaff/Faculty/pages/albrecht/albrecht_web/Programs/microscopy/colloid.html

[17] NanoComposix, Inc. (2012). Gold Nanoparticles: Optical Properties [Online]. Available: http://www.nanocomposix.com/kb/gold/optical-properties

[18] K. H. Su, Q. H. Wei, X. Zhang, J. J. Mock, D. R. Smith, and S. Schultz, "Interparticle Coupling Effects on Plasmon Resonances of Nanogold Particles", *Nano Lett.*, Vol. 3, 2003, pp. 1087−1090.

[19] B. Dubertret, M. Calame, and A. J. Libchaber, "Single-Mismatch Detection using Gold-Quenched Fluorescent Oligonucleotides", *Nat. Biotechnol.*, Vol. 19, 2001, pp. 365–370.

[20] S. K. Ghosh, A. Pal, S. Kundu, S. Nath, and T. Pal, "Fluorescence Quenching of 1-Methylaminopyrene near Gold Nanoparticles: Size Regime Dependence of the Small Metallic Particles", *Chem. Phys. Lett.*, Vol. 395, 2004, pp. 366–372.

[21] E. Oh, M.-Y. Hong, D. Lee, S.-H. Nam, H. C. Yoon, and H.-S. Kim, "Inhibition Assay of Biomolecules based on Fluorescence Resonance Energy Transfer (FRET) between Quantum Dots and Gold Nanoparticles", *J. Am. Chem. Soc.*, Vol. 127, 2005, pp. 3270–3271.

[22] C. Rahul, J. Sharma, H. Wang, S. Zou, S. Lin, H. Yan, S. Lindsay, and Y. Liu, "Distance-Dependent Interactions Between Gold Nanoparticles and Fluorescent Molecules with DNA as Tunable Spacers", *Nanotechnology,* Vol. 20, 2009, p. 485201.

[23] C. Pale-Grosdemange, E. S. Simon, K. L. Prime, and G. M. Whitesides, "Formation of Self-Assembled Monolayers by Chemisorption of Derivatives of Oligo(Ethylene Glycol) of Structure $HS(CH_2)_{11}(OCH_2CH_2)_mOH$ on Gold", *J. Am. Chem. Soc.,* Vol. 113, 1991, pp. 12–20.

[24] M. Ö stblom, B. Liedberg, L. M. Demers, and C. A. Mirkin, "On the Structure and Desorption Dynamics of DNA Bases Adsorbed on Gold: A Temperature-Programmed Study", *J. Phys. Chem. B,* Vol. 109, 2005, pp. 15150–15160.

[25] M. A. Hayat, *Colloidal Gold, Principles, Methods and Applications*, New York, Academic Press, 1989.

[26] S. Guo and E. Wang, "Synthesis and Electrochemical Applications of Gold Nanoparticles", *Anal. Chim. Acta,* Vol. 598, 2007, pp. 181–192.

[27] J. F. Hainfeld, D. N. Slatkin, T. M. Focella, and H. M. Smilowitz, "Gold Nanoparticles: A New X-ray Contrast Agent", *Br. J. Radiol.,* Vol. 79, 2006, pp. 248–253.

[28] C. Alric, J. Taleb, G. L. Duc, C. Mandon, C. Billotey, A. L. Meur-Herland, T. Brochard, F. Vocanson, M. Janier, P. Perriat, S. Roux, and O. Tillement, "Gadolinium Chelate Coated Gold Nanoparticles As Contrast Agents for Both X-ray Computed Tomography and Magnetic Resonance Imaging", *J. Am. Chem. Soc.*, Vol. 130, 2008, pp. 5908–5915.

[29] N. Chanda, V. Kattumuri, R. Shukla, A. Zambre, K. Katti, A. Upendran, R. R. Kulkarni, P. Kan, G. M. Fent, S. W. Casteel, C. J. Smith, E. Boote, J. D. Robertson, C. Cutler, J. R. Lever, K. V. Katti, and R. Kannan, "Bombesin Functionalized Gold Nanoparticles Show In Vitro and In Vivo Cancer Receptor Specificity", *Proc. Natl. Acad. Sci.,* Vol. 107, 2010, pp. 8760–8765.

[30] S. D. Perrault and W. C. W. Chan, "In Vivo Assembly of Nanoparticle Components to Improve Targeted Cancer Imaging", *Proc. Natl. Acad. Sci.,* Vol. 107, 2010, pp. 11194–11199.

[31] Y.-H. Kim, J. Jeon, S. H. Hong, W.-K. Rhim, Y.-S. Lee, H. Youn, J.-K. Chung, M. C. Lee, D. S. Lee, K. W. Kang, and J.-M. Nam, "Tumor Targeting and Imaging Using Cyclic RGD-PEGylated Gold Nanoparticle Probes with Directly Conjugated Iodine-125", *Small,* Vol. 7, 2011, pp. 2052–2060.

[32] A. Samanta, K. K. Maiti, K.-S. Soh, X. Liao, M. Vendrell, U. S. Dinish, S.-W. Yun, R. Bhuvaneswari, H. Kim, S. Rautela, J. Chung, M. Olivo, and Y.-T. Chang, "Ultrasensitive Near-Infrared Raman Reporters for SERS-Based In

Vivo Cancer Detection", *Angew. Chem. Int. Ed.*, Vol. 50, 2011, pp. 6089–6092.

[33] G. F. Paciotti, D. G. I. Kingston, and L. Tamarkin, "Colloidal Gold Nanoparticles: A Novel Nanoparticle Platform for Developing Multifunctional Tumor-Targeted Drug Delivery Vectors", *Drug Dev. Res.*, Vol. 67, 2006, pp. 47–54.

[34] C. K. Kim, P. Ghosh, and V. M. Rotello, "Multimodal Drug Delivery using Gold Nanoparticles", *Nanoscale*, Vol. 1, 2009, pp. 61–67.

[35] A. K. R. Lytton-Jean, R. Langer, and D. G. Anderson, "Five Years of siRNA Delivery: Spotlight on Gold Nanoparticles", *Small*, Vol. 7, 2011, pp. 1932–1937.

[36] F. Westerlund and T. Bjørnholm, "Directed Assembly of Gold Nanoparticles", *Curr. Opin. Colloid Interface Sci.*, Vol. 14, 2009, pp. 126–134.

[37] R. Elghanian, J. J. Storhoff, R. C. Mucic, R. L. Letsinger, and C. A. Mirkin, "Selective Colorimetric Detection of Polynucleotides Based on the Distance-Dependent Optical Properties of Gold Nanoparticles", *Science*, Vol. 277, 1997, pp. 1078–1081.

[38] J. Li, X. Chu, Y. Liu, J.-H. Jiang, Z. He, Z. Zhang, G. Shen, and R.-Q. Yu, "A Colorimetric Method for Point Mutation Detection Using High-Fidelity DNA Ligase", *Nucleic Acids Res.*, Vol. 33, 2005, p. e168.

[39] K. Sato, K. Hosokawa, and M. Maeda, "Rapid Aggregation of Gold Nanoparticles Induced by Non-Cross-Linking DNA Hybridization", *J. Am. Chem. Soc.*, Vol. 125, 2003, pp. 8102–8103.

[40] J. Conde, J. de la Fuente, and P. Baptista, "RNA Quantification Using Gold Nanoprobes - Application to Cancer Diagnostics", *J. Nanobiotechnology*, Vol. 8, 2010, p. 5.

[41] Y. Zu, A. L. Ting, and Z. Gao, "Visualizing Low-Level Point Mutations: Enzyme-like Selectivity Offered by Nanoparticle Probes", *Small*, Vol. 7, 2011, pp. 306–310.

[42] H. Li and L. Rothberg, "Colorimetric Detection of DNA Sequences Based on Electrostatic Interactions with Unmodified Gold Nanoparticles", *Proc. Natl. Acad. Sci.*, Vol. 101, 2004, pp. 14036–14039.

[43] H. Li and L. Rothberg, "Detection of Specific Sequences in RNA Using Differential Adsorption of Single-Stranded Oligonucleotides on Gold Nanoparticles", *Anal. Chem.*, Vol. 77, 2005, pp. 6229–6233.

[44] F. Xia, X. Zuo, R. Yang, Y. Xiao, D. Kang, A. Vallée-Bélisle, X. Gong, J. D. Yuen, B. B. Y. Hsu, A. J. Heeger, and K. W. Plaxco, "Colorimetric Detection of DNA, Small Molecules, Proteins, and Ions Using Unmodified Gold Nanoparticles and Conjugated Polyelectrolytes", *Proc. Natl. Acad. Sci.,* Vol. 107, 2010, pp. 10837–10841.

[45] R. Kanjanawarut and X. Su, "Colorimetric Detection of DNA Using Unmodified Metallic Nanoparticles and Peptide Nucleic Acid Probes", *Anal. Chem.,* Vol. 81, 2009, pp. 6122–6129.

[46] X. Xue, F. Wang, and X. Liu, "One-Step, Room Temperature, Colorimetric Detection of Mercury (Hg^{2+}) Using DNA/Nanoparticle Conjugates", *J. Am. Chem. Soc.*, Vol. 130, 2008, pp. 3244–3245.

[47] B. Li, Y. Du, and S. Dong, "DNA Based Gold Nanoparticles Colorimetric Sensors for Sensitive and Selective Detection of Ag(I) Ions", *Anal. Chim. Acta*, Vol. 644, 2009, pp. 78–82.

[48] X. Zhu, J. Zhao, Y. Wu, Z. Shen, and G. Li, "Fabrication of a Highly Sensitive Aptasensor for Potassium with a Nicking Endonuclease-Assisted Signal Amplification Strategy", *Anal. Chem.*, Vol. 83, 2011, pp. 4085–4089.

[49] J. Liu and Y. Lu, "A Colorimetric Lead Biosensor Using DNAzyme-Directed Assembly of Gold Nanoparticles", *J. Am. Chem. Soc.*, Vol. 125, 2003, pp. 6642–6643.

[50] J. S. Lee, M. S. Han, and C. A. Mirkin, "Colorimetric Detection of Mercuric Ion (Hg^{2+}) in Aqueous Media using DNA-Functionalized Gold Nanoparticles", *Angew. Chem. Int. Ed.*, Vol. 46, 2007, pp. 4093–4096.

[51] X. Xu, W. L. Daniel, W. Wei, and C. A. Mirkin, "Colorimetric Cu^{2+} Detection Using DNA-Modified Gold-Nanoparticle Aggregates as Probes and Click Chemistry", *Small,* Vol. 6, 2010, pp. 623–626.

[52] W. Zhao, J. C. F. Lam, W. Chiuman, M. A. Brook, and Y. Li, "Enzymatic Cleavage of Nucleic Acids on Gold Nanoparticles: A Generic Platform for Facile Colorimetric Biosensors", *Small,* Vol. 4, 2008, pp. 810–816.

[53] Y. Kim, R. C. Johnson, and J. T. Hupp, "Gold Nanoparticle-Based Sensing of "Spectroscopically Silent" Heavy Metal Ions", *Nano Lett.*, Vol. 1, 2001, pp. 165–167.

[54] S.-Y. Lin, S.-W. Liu, C.-M. Lin, and C.-h. Chen, "Recognition of Potassium Ion in Water by 15-Crown-5 Functionalized Gold Nanoparticles", *Anal. Chem.,* Vol. 74, 2002, pp. 330–335.

[55] C. Y. Lin, C. J. Yu, Y. H. Lin, and W. L. Tseng, "Colorimetric Sensing of Silver(I) and Mercury(II) Ions Based on an Assembly of Tween 20-Stabilized Gold Nanoparticles", *Anal. Chem.*, Vol. 82, 2010, pp. 6830–6837.

[56] M. H. Kim, S. Kim, H. H. Jang, S. Yi, S. H. Seo, and M. S. Han, "A Gold Nanoparticle-Based Colorimetric Sensing Ensemble for the Colorimetric Detection of Cyanide Ions in Aqueous Solution", *Tetrahedron Lett.*, Vol. 51, 2010, pp. 4712–4716.

[57] Z. Wang, J. H. Lee, and Y. Lu, "Label-Free Colorimetric Detection of Lead Ions with a Nanomolar Detection Limit and Tunable Dynamic Range by using Gold Nanoparticles and DNAzyme", *Adv. Mater.*, Vol. 20, 2008, pp. 3263–3267.

[58] L. Wang, X. Liu, X. Hu, S. Song, and C. Fan, "Unmodified Gold Nanoparticles as a Colorimetric Probe for Potassium DNA Aptamers", *Chem. Commun.*, 2006, pp. 3780–3782.

[59] Y. L. Hung, T. M. Hsiung, Y. Y. Chen, Y. F. Huang, and C. C. Huang, "Colorimetric Detection of Heavy Metal Ions Using Label-Free Gold Nanoparticles and Alkanethiols", *J. Phys. Chem. C*, Vol. 114, 2010, pp. 16329–16334.

[60] J. Du, Y. Sun, L. Jiang, X. Cao, D. Qi, S. Yin, J. Ma, F. Y. C. Boey, and X. Chen, "Flexible Colorimetric Detection of Mercuric Ion by Simply Mixing Nanoparticles and Oligopeptides", *Small*, Vol. 7, 2011, pp. 1407–1411.

[61] W. Li, Z. Nie, K. He, X. Xu, Y. Li, Y. Huang, and S. Yao, "Simple, Rapid and Label-Free Colorimetric Assay for Zn^{2+} Based on Unmodified Gold Nanoparticles and Specific Zn^{2+} Binding Peptide", *Chem. Commun.*, Vol. 47, 2011, pp. 4412–4414.

[62] F. Li, J. Zhang, X. Cao, L. Wang, D. Li, S. Song, B. Ye, and C. Fan, "Adenosine Detection by Using Gold Nanoparticles and Designed Aptamer Sequences", *Analyst*, Vol. 134, 2009, pp. 1355–1360.

[63] J. Liu and Y. Lu, "Fast Colorimetric Sensing of Adenosine and Cocaine Based on a General Sensor Design Involving Aptamers and Nanoparticles", *Angew. Chem. Int. Ed.*, Vol. 45, 2006, pp. 90–94.

[64] W. Zhao, W. Chiuman, M. A. Brook, and Y. Li, "Simple and Rapid Colorimetric Biosensors Based on DNA Aptamer and Noncrosslinking Gold Nanoparticle Aggregation", *ChemBioChem*, Vol. 8, 2007, pp. 727–731.

[65] W. Zhao, W. Chiuman, J. C. F. Lam, S. A. McManus, W. Chen, Y. Cui, R.

Pelton, M. A. Brook, and Y. Li, "DNA Aptamer Folding on Gold Nanoparticles: From Colloid Chemistry to Biosensors", *J. Am. Chem. Soc.*, Vol. 130, 2008, pp. 3610–3618.

[66] S.-J. Chen, Y.-F. Huang, C.-C. Huang, K.-H. Lee, Z.-H. Lin, and H.-T. Chang, "Colorimetric Determination of Urinary Adenosine Using Aptamer-Modified Gold Nanoparticles", *Biosens. Bioelectron.*, Vol. 23, 2008, pp. 1749–1753.

[67] Y. Jiang, H. Zhao, N. Zhu, Y. Lin, P. Yu, and L. Mao, "A Simple Assay for Direct Colorimetric Visualization of Trinitrotoluene at Picomolar Levels Using Gold Nanoparticles", *Angew. Chem. Int. Ed.*, Vol. 47, 2008, pp. 8601–8604.

[68] W. L. Daniel, M. S. Han, J.-S. Lee, and C. A. Mirkin, "Colorimetric Nitrite and Nitrate Detection with Gold Nanoparticle Probes and Kinetic End Points", *J. Am. Chem. Soc.*, Vol. 131, 2009, pp. 6362–6363.

[69] B. Kong, A. Zhu, Y. Luo, Y. Tian, Y. Yu, and G. Shi, "Sensitive and Selective Colorimetric Visualization of Cerebral Dopamine Based on Double Molecular Recognition", *Angew. Chem. Int. Ed.*, Vol. 50, 2011, pp. 1837–1840.

[70] C. C. Huang and W. L. Tseng, "Role of Fluorosurfactant-Modified Gold Nanoparticles in Selective Detection of Homocysteine Thiolactone: Remover and Sensor", *Anal. Chem.*, Vol. 80, 2008, pp. 6345–6350.

[71] M. H. Kim, S. S. Lee, S. J. Chung, H. H. Jang, S. Yi, S. Kim, S.-K. Chang, and M. S. Han, "Real-Time Colorimetric Screening of Endopeptidase Inhibitors Using Adenosine Triphosphate (ATP)-Stabilized Gold Nanoparticles", *Tetrahedron Lett.*, Vol. 51, 2010, pp. 2228–2231.

[72] Y. Jiang, H. Zhao, Y. Lin, N. Zhu, Y. Ma, and L. Mao, "Colorimetric Detection of Glucose in Rat Brain Using Gold Nanoparticles", *Angew. Chem. Int. Ed.*, Vol. 49, 2010, pp. 4800–4804.

[73] J. Wang, L. Wang, X. Liu, Z. Liang, S. Song, W. Li, G. Li, and C. Fan, "A Gold Nanoparticle-Based Aptamer Target Binding Readout for ATP Assay", *Adv. Mater.*, Vol. 19, 2007, pp. 3943–3946.

[74] C. C. Huang, Y. F. Huang, Z. Cao, W. Tan, and H. T. Chang, "Aptamer-Modified Gold Nanoparticles for Colorimetric Determination of Platelet-Derived Growth Factors and Their Receptors", *Anal. Chem.*, Vol. 77, 2005, pp. 5735–5741.

[75] L. J. Ou, P. Y. Jin, X. Chu, J. H. Jiang, and R. Q. Yu, "Sensitive and Visual

Detection of Sequence-Specific DNA-Binding Protein via a Gold Nanoparticle-Based Colorimetric Biosensor", *Anal. Chem.,* Vol. 82, 2010, pp. 6015–6024.

[76] C.-K. Chen, C.-C. Huang, and H.-T. Chang, "Label-Free Colorimetric Detection of Picomolar Thrombin in Blood Plasma Using a Gold Nanoparticle-Based Assay", *Biosens. Bioelectron.,* Vol. 25, 2010, pp. 1922–1927.

[77] C. D. Medley, J. E. Smith, Z. Tang, Y. Wu, S. Bamrungsap, and W. Tan, "Gold Nanoparticle-Based Colorimetric Assay for the Direct Detection of Cancerous Cells", *Anal. Chem.,* Vol. 80, 2008, pp. 1067–1072.

[78] C. A. Mirkin, R. L. Letsinger, R. C. Mucic, and J. J. Storhoff, "A DNA-Based Method for Rationally Assembling Nanoparticles into Macroscopic Materials", *Nature,* Vol. 382, 1996, pp. 607–609.

[79] M. S. Han, A. K. R. Lytton-Jean, and C. A. Mirkin, "A Gold Nanoparticle Based Approach for Screening Triplex DNA Binders", *J. Am. Chem. Soc.,* Vol. 128, 2006, pp. 4954–4955.

[80] I.-H. Lee, K.-A. Yang, J.-H. Lee, J.-Y. Park, Y. G. Chai, J.-H. Lee, and B.-T. Zhang, "The Use of Gold Nanoparticle Aggregation for DNA Computing and Logic-Based Biomolecular Detection", *Nanotechnology,* Vol. 19, 2008, p. 395103.

[81] S. Bi, Y. Yan, S. Hao, and S. Zhang, "Colorimetric Logic Gates Based on Supramolecular DNAzyme Structures", *Angew. Chem. Int. Ed.,* Vol. 49, 2010, pp. 4438–4442.

[82] M. S. Han, A. K. R. Lytton-Jean, B. K. Oh, J. Heo, and C. A. Mirkin, "Colorimetric Screening of DNA-Binding Molecules with Gold Nanoparticle Probes", *Angew. Chem. Int. Ed.,* Vol. 45, 2006, pp. 1807–1810.

[83] X. Xu, M. S. Han, and C. A. Mirkin, "A Gold-Nanoparticle-Based Real-Time Colorimetric Screening Method for Endonuclease Activity and Inhibition", *Angew. Chem. Int. Ed.,* Vol. 46, 2007, pp. 3468–3470.

[84] S. J. Hurst, M. S. Han, A. K. R. Lytton-Jean, and C. A. Mirkin, "Screening the Sequence Selectivity of DNA-Binding Molecules Using a Gold Nanoparticle-Based Colorimetric Approach", *Anal. Chem.,* Vol. 79, 2007, pp. 7201–7205.

[85] G. Song, C. Chen, J. Ren, and X. Qu, "A Simple, Universal Colorimetric Assay for Endonuclease/Methyltransferase Activity and Inhibition Based on

an Enzyme-Responsive Nanoparticle System", *ACS Nano,* Vol. 3, 2009, pp. 1183–1189.

[86] C. Chen, C. Zhao, X. Yang, J. Ren, and X. Qu, "Enzymatic Manipulation of DNA-Modified Gold Nanoparticles for Screening G-Quadruplex Ligands and Evaluating Selectivities", *Adv. Mater.,* Vol. 22, 2010, pp. 389–393.

[87] E. Jung, S. Kim, Y. Kim, S. H. Seo, S. S. Lee, M. S. Han, and S. Lee, "A Colorimetric High-Throughput Screening Method for Palladium-Catalyzed Coupling Reactions of Aryl Iodides Using a Gold Nanoparticle-Based Iodide-Selective Probe", *Angew. Chem. Int. Ed.,* Vol. 50, 2011, pp. 4386–4389.

[88] T. Jiang, R. Liu, X. Huang, H. Feng, W. Teo, and B. Xing, "Colorimetric Screening of Bacterial Enzyme Activity and Inhibition Based on the Aggregation of Gold Nanoparticles", *Chem. Commun.,* 2009, pp. 1972–1974.

[89] H. X. Li and L. J. Rothberg, "Label-Free Colorimetric Detection of Specific Sequences in Genomic DNA Amplified by the Polymerase Chain Reaction", *J. Am. Chem. Soc.,* Vol. 126, 2004, pp. 10958–10961.

[90] K. Sato, K. Hosokawa, and M. Maeda, "Non-Cross-Linking Gold Nanoparticle Aggregation as a Detection Method for Single-Base Substitutions", *Nucleic Acids Res.,* Vol. 33, 2005, p. e4.

[91] A. Jyoti, P. Pandey, S. P. Singh, S. K. Jain, and R. Shanker, "Colorimetric Detection of Nucleic Acid Signature of Shiga Toxin Producing Escherichia coli Using Gold Nanoparticles", *J. Nanosci. Nanotechnol.,* Vol. 10, 2010, pp. 4154–4158.

[92] Y. L. Jung, C. Jung, H. Parab, T. Li, and H. G. Park, "Direct Colorimetric Diagnosis of Pathogen Infections by Utilizing Thiol-Labeled PCR Primers and Unmodified Gold Nanoparticles", *Biosens. Bioelectron.,* Vol. 25, 2010, pp. 1941–1946.

[93] E. Tan, J. Wong, D. Nguyen, Y. Zhang, B. Erwin, L. K. Van Ness, S. M. Baker, D. J. Galas, and A. Niemz, "Isothermal DNA Amplification Coupled with DNA Nanosphere-Based Colorimetric Detection", *Anal. Chem.,* Vol. 77, 2005, pp. 7984–7992.

[94] J. Li, T. Deng, X. Chu, R. Yang, J. Jiang, G. Shen, and R. Yu, "Rolling Circle Amplification Combined with Gold Nanoparticle Aggregates for Highly Sensitive Identification of Single-Nucleotide Polymorphisms", *Anal. Chem.,* Vol. 82, 2010, pp. 2811–2816.

[95] W. Xu, X. Xue, T. Li, H. Zeng, and X. Liu, "Ultrasensitive and Selective Colorimetric DNA Detection by Nicking Endonuclease Assisted Nanoparticle Amplification", *Angew. Chem. Int. Ed.*, Vol. 48, 2009, pp. 6849–6852.

[96] A. R. Herdt, S. M. Drawz, Y. Kang, and T. A. Taton, "DNA Dissociation and Degradation at Gold Nanoparticle Surfaces", *Colloids Surf., B*, Vol. 51, 2006, pp. 130–139.

[97] R. L. Letsinger, R. Elghanian, G. Viswanadham, and C. A. Mirkin, "Use of a Steroid Cyclic Disulfide Anchor in Constructing Gold Nanoparticle–Oligonucleotide Conjugates", *Bioconjugate Chem.*, Vol. 11, 2000, pp. 289–291.

[98] Z. Li, R. Jin, C. A. Mirkin, and R. L. Letsinger, "Multiple Thiol-Anchor Capped DNA–Gold Nanoparticle Conjugates", *Nucleic Acids Res.*, Vol. 30, 2002, pp. 1558–1562.

[99] J. A. Dougan, C. Karlsson, W. E. Smith, and D. Graham, "Enhanced Oligonucleotide–Nanoparticle Conjugate Stability Using Thioctic Acid Modified Oligonucleotides", *Nucleic Acids Res.*, Vol. 35, 2007, pp. 3668–3675.

[100] J. Sharma, R. Chhabra, H. Yan, and Y. Liu, "A Facile *in situ* Generation of Dithiocarbamate Ligands for Stable Gold Nanoparticle–Oligonucleotide Conjugates.", *Chem. Commun.*, Vol. 44, 2008, pp. 2140–2142.

[101] L. M. Liz-Marzán, M. Giersig, and P. Mulvaney, "Synthesis of Nanosized Gold–Silica Core–Shell Particles", *Langmuir*, Vol. 12, 1996, pp. 4329–4335.

[102] C. Graf, D. L. J. Vossen, A. Imhof, and A. van Blaaderen, "A General Method To Coat Colloidal Particles with Silica", *Langmuir*, Vol. 19, 2003, pp. 6693–6700.

[103] J. Xu and C. Perry, "A Novel Approach to Au@SiO2 Core-Shell Spheres", *J. Non-Cryst. Solids*, Vol. 353, 2007, pp. 1212–1215.

[104] Y. Han, J. Jiang, S. S. Lee, and J. Y. Ying, "Reverse Microemulsion-Mediated Synthesis of Silica-Coated Gold and Silver Nanoparticles", *Langmuir*, Vol. 24, 2008, pp. 5842–5848.

[105] S. M. Kang, B. S. Lee, S. G. Lee, and I. S. Choi, "Biomimetic Coating of Gold Nanoparticles with Ultrathin Silica Layers", *Colloids Surf., A*, Vol. 313–314, 2008, pp. 150–153.

[106] M. Schulzendorf, C. Cavelius, P. Born, E. Murray, and T. Kraus, "Biphasic Synthesis of Au@SiO2 Core−Shell Particles with Stepwise Ligand

Exchange", *Langmuir,* Vol. 27, 2011, pp. 727−732.

[107] S. H. Liu and M. Y. Han, "Synthesis, Functionalization, and Bioconjugation of Monodisperse, Silica-Coated Gold Nanoparticles: Robust Bioprobes", *Adv. Funct. Mater.,* Vol. 15, 2005, pp. 961−967.

[108] N. R. Jana and J. Y. Ying, "Synthesis of Functionalized Au Nanoparticles for Protein Detection", *Adv. Mater.,* Vol. 20, 2008, pp. 430−434.

[109] K. C. Grabar, R. G. Freeman, M. B. Hommer, and M. J. Natan, "Preparation and Characterization of Au Colloid Monolayers", *Anal. Chem.,* Vol. 67, 1995, pp. 735−743.

[110] W. Haiss, N. T. K. Thanh, J. Aveyard, and D. G. Fernig, "Determination of Size and Concentration of Gold Nanoparticles from UV−Vis Spectra", *Anal. Chem.,* Vol. 79, 2007, pp. 4215−4221.

[111] J. J. Storhoff, R. Elghanian, R. C. Mucic, C. A. Mirkin, and R. L. Letsinger, "One-Pot Colorimetric Differentiation of Polynucleotides with Single Base Imperfections Using Gold Nanoparticle Probes", *J. Am. Chem. Soc.,* Vol. 120, 1998, pp. 1959−1964.

[112] S. K. Ghosh, N. Sarma, M. Mandal, S. Kundu, K. Esumi, and T. Pal, "Evolution of Gold Nanoparticles in Micelle by UV-Irradiation: A Conductometric Study", *Curr. Sci.,* Vol. 84, 2003, pp. 791−795.

[113] S. J. Hurst, A. K. R. Lytton-Jean, and C. A. Mirkin, "Maximizing DNA Loading on a Range of Gold Nanoparticle Sizes", *Anal. Chem.,* Vol. 78, 2006, pp. 8313−8318.

[114] W. Zhao, Y. Gao, S. A. Kandadai, M. A. Brook, and Y. Li, "DNA Polymerization on Gold Nanoparticles through Rolling Circle Amplification: Towards Novel Scaffolds for Three-Dimensional Periodic Nanoassemblies", *Angew. Chem. Int. Ed.,* Vol. 45, 2006, pp. 2409−2413.

[115] G. T. Walker, M. S. Fraiser, J. L. Schram, M. C. Little, J. G. Nadeau, and D. P. Malinowski, "Strand Displacement Amplification—An Isothermal, In Vitro DNA Amplification Technique", *Nucleic Acids Res.,* Vol. 20, 1992, pp. 1691−1696.

[116] D. Liu, S. L. Daubendiek, M. A. Zillman, K. Ryan, and E. T. Kool, "Rolling Circle DNA Synthesis: Small Circular Oligonucleotides as Efficient Templates for DNA Polymerases", *J. Am. Chem. Soc.,* Vol. 118, 1996, pp. 1587−1594.

[117] T. Notomi, H. Okayama, H. Masubuchi, T. Yonekawa, K. Watanabe, N.

Amino, and T. Hase, "Loop-Mediated Isothermal Amplification of DNA", *Nucleic Acids Res.*, Vol. 28, 2000, p. e63.

[118] M. Vincent, Y. Xu, and H. Kong, "Helicase-Dependent Isothermal DNA Amplification", *EMBO Rep.*, Vol. 5, 2004, pp. 795–800.

[119] J. J. Li, Y. Chu, B. Y.-H. Lee, and X. S. Xie, "Enzymatic Signal Amplification of Molecular Beacons for Sensitive DNA Detection", *Nucleic Acids Res.*, Vol. 36, 2008, p. e36.

[120] L. Cui, G. Ke, C. Wang, and C. J. Yang, "A Cyclic Enzymatic Amplification Method for Sensitive and Selective Detection of Nucleic Acids", *Analyst*, Vol. 135, 2010, pp. 2069–2073.

[121] A. K. Bej, M. H. Mahbubani, R. M. Atlas, and R. K. Salkl, "Amplification of Nucleic Acids by Polymerase Chain Reaction (PCR) and Other Methods and their Applications", *Crit. Rev. Biochem. Mol.*, Vol. 26, 1991, pp. 301–334.

[122] P. Anderson. (2011). PCR: Uses, Steps, Purpose. [Online]. Available: http://schoolworkhelper.net/2011/06/pcr-uses-steps-purpose/

[123] V. H. J. van der Velden, A. Hochhaus, G. Cazzaniga, T. Szczepanski, J. Gabert, and J. J. M. van Dongen, "Detection of Minimal Residual Disease in Hematologic Malignancies by Real-Time Quantitative PCR: Principles, Approaches, and Laboratory Aspects", *Leukemia*, Vol. 17, 2003, pp. 1013–1034.

[124] H. Li, J. Huang, J. Lv, H. An, X. Zhang, Z. Zhang, C. Fan, and J. Hu, "Nanoparticle PCR: Nanogold-Assisted PCR with Enhanced Specificity", *Angew. Chem. Int. Ed.*, Vol. 44, 2005, pp. 5100–5103.

[125] M. Li, Y. C. Lin, C. C. Wu, and H. S. Liu, "Enhancing the Efficiency of a PCR Using Gold Nanoparticles", *Nucleic Acids Res.*, Vol. 33, 2005, p. e184.

[126] B. V. Vu, D. Litvinov, and R. C. Willson, "Gold Nanoparticle Effects in Polymerase Chain Reaction: Favoring of Smaller Products by Polymerase Adsorption", *Anal. Chem.*, Vol. 80, 2008, pp. 5462–5467.

[127] W. Wan and J. T. W. Yeow, "The Effects of Gold Nanoparticles with Different Sizes on Polymerase Chain Reaction Efficiency", *Nanotechnology*, Vol. 20, 2009, p. 325702.

[128] D. G. Thompson, A. Enright, K. Faulds, W. E. Smith, and D. Graham, "Ultrasensitive DNA Detection Using Oligonucleotide-Silver Nanoparticle Conjugates", *Anal. Chem.*, Vol. 80, 2008, pp. 2805–2810.

[129] Cao, R. Jin, and C. A. Mirkin, "DNA-Modified Core−Shell Ag/Au

Nanoparticles", *J. Am. Chem. Soc.*, Vol. 123, 2001, pp. 7961–7962.

[130] J. S. Lee, A. K. R. Lytton-Jean, S. J. Hurst, and C. A. Mirkin, "Silver Nanoparticle-Oligonucleotide Conjugates Based on DNA with Triple Cyclic Disulfide Moieties", *Nano Lett.*, Vol. 7, 2007, pp. 2112–2115.

[131] X. Xu, J. Wang, F. Yang, K. Jiao, and X. Yang, "Label-Free Colorimetric Detection of Small Molecules Utilizing DNA Oligonucleotides and Silver Nanoparticles", *Small*, Vol. 5, 2009, pp. 2669–2672.

[132] S. Liu, Z. Zhang, and M. Han, "Gram-Scale Synthesis and Biofunctionalization of Silica-Coated Silver Nanoparticles for Fast Colorimetric DNA Detection", *Anal. Chem.*, Vol. 77, 2005, pp. 2595–2600.

[133] Y. Yin, Z.-Y. Li, Z. Zhong, B. Gates, Y. Xia, and S. Venkateswaran, "Synthesis and Characterization of Stable Aqueous Dispersions of Silver Nanoparticles Through the Tollens Process", *J. Mater. Chem.*, Vol. 12, 2002, pp. 522–527.

[134] K. L. Mittal, *Silanes and Other Coupling Agents*, VSP, 1992.